Kapitza-Dirac Effects of Free Electrons in Two-Color Laser Fields

Inaugural-Dissertation

zur Erlangung des Doktorgrades
der Mathematisch-Naturwissenschaftlichen Fakultät
der Heinrich-Heine-Universität Düsseldorf

vorgelegt von

Matthias Maximilian Dellweg
aus Würzburg

Januar 2017

aus dem Institut für Theoretische Physik I
der Heinrich-Heine-Universität Düsseldorf

Gedruckt mit der Genehmigung der
Mathematisch-Naturwissenschaftlichen Fakultät der
Heinrich-Heine-Universität Düsseldorf

Referent: Prof. Dr. Dr. Carsten Müller

Koreferent: Prof. Dr. Dagmar Bruß

Tag der mündlichen Prüfung: 06.04.2017

Abstract

The Kapitza-Dirac effect is the stimulated version of Compton scattering of free electrons from a standing electromagnetic wave. It can also be understood as the diffraction of the electron matter wave from the light lattice given by the ponderomotive potential of the standing wave. Despite the original idea dating back to the early days of quantum mechanics, a direct experimental proof has been accomplished only recently.

In this thesis, we investigate two generalization schemes of the Kapitza-Dirac effect, both of which deploy bichromatic laser fields to influence the dynamics of the scattering. We show that the combination of two standing light waves with commensurate frequencies leads to distinct quantum interference. The relative phase between the nodes of the two color components plays an important role as a control parameter. On the other hand, we demonstrate that electrons can be scattered resonantly from non-standing, counterpropagating and differently colored laser waves as well. The interaction now comprises the exchange of three photons, and the aforementioned phase becomes immaterial. Instead, the polarization states of the photons gain key importance. We develop various methods to describe the electron scattering from such field configurations and characterize the influence of different laser polarizations on the electron spin. We present diverse configurations therein which allows coherent control of the spin.

By a special sequence of three different Kapitza-Dirac scattering events, we develop the theoretical basis for a spin-polarizing electron beam splitter. It effectively acts as a Stern-Gerlach magnet for free electrons and so provides a possible answer to the longstanding question of the realizability of such a device.

Zusammenfassung

Der Kapitza-Dirac-Effekt ist die stimulierte Version der Compton-Streuung von freien Elektronen an einer stehenden elektromagnetischen Welle. Gleichzeitig lässt er sich als Streuung einer Elektronenwelle an dem Lichtgitter verstehen, welches durch das pondermotorische Potential der stehenden Welle gegeben ist. Obwohl die initiale Idee der Namensgeber zur frühen Geschichte der Quantenmechanik gehört, ist ein direkter experimenteller Nachweis erst vor wenigen Jahren gelungen.

In der vorliegenden theoretischen Arbeit untersuchen wir zwei Verallgemeinerungen des Kapitza-Dirac-Effekts, die zweifarbige Laserfelder verwenden um die Dynamik der Streuung zu beeinflussen. Wir zeigen, dass die Kombination von zwei stehenden Wellen mit kommensurablen Frequenzen zu deutlichen Quanteninterferenzen führt. Die relative Phase zwischen den Knotenpunkten der zwei Farbkomponenten wird dabei zu einem wichtigen Kontrollparameter. Andererseits demonstrieren wir, dass Elektronen auch an nichtstehenden, gegenläufigen und verschiedenfarbigen Laserwellen resonant gestreut werden können. Die Wechselwirkung beinhaltet hier den Austausch von drei Photonen und die oben genannte Phase tritt in den Hintergrund. Dafür erhalten die Polarisationszustände der Photonen eine Schlüsselrolle. Wir entwickeln verschiedene Methoden, die Streuung der Elektronen in diesen Feldern zu beschreiben, und charakterisieren den Einfluss verschiedener Laserpolarisationen auf den Spin der Elektronen. Wir erabeiten darunter verschiedene Konfigurationen, die es erlauben den Spin kohärent zu kontrollieren.

Durch eine spezielle Abfolge von drei verschiedenen Kapitza-Dirac-Streuvorgängen konstruieren wir theoretisch einen spinpolarisierenden Elektronenstrahlteiler. Dieser repräsentiert in seiner Wirkweise einen Stern-Gerlach-Magneten für freie Elektronen und liefert so eine mögliche Antwort auf die seit langem diskutierte Frage der Realisierbarkeit eines solchen.

Eidesstattliche Erklärung

Ich versichere an Eides Statt, dass die Dissertation von mir selbstständig und ohne unzulässige fremde Hilfe unter Beachtung der ,,Grundsätze zur Sicherung guter wissenschaftlicher Praxis an der Heinrich-Heine-Universität Düsseldorf“ erstellt worden ist.

Ich erkläre, dass ich diese Dissertation keiner anderen Fakultät bereits vorgelegt und auch keinen früheren Promotionsversuch unternommen habe.

Düsseldorf,

Contents

Chapter 1

Introduction

The Kapitza-Dirac effect as originally proposed in 1933 [KD33] is the diffraction of a free electron from a grating given by the periodic ponderomotive potential of a standing light wave. Invented in the early days of quantum mechanics by Dirac and Kapitza as a consequence of the wave-particle duality for both light and matter, it resembles the well known diffraction of light from a material lattice, with the roles of light and matter interchanged.

While, beautifully underlining the wave nature of the quantum electron in this wave picture, the effect can simultaneously be seen in a particle picture. A free electron aborbs one photon of one of the counterpropagating light rays, forming the standing wave. In order to fulfill its own vacuum dispersion relation, it must subsequently emit a photon again. Due to the Bose-Einstein statistic of the photons, it may be favorable to emit this photon resonantly back into one of the light rays. In combination, the electron gains two photon momenta and returns to its original kinetic energy. In this picture, the Kapitza-Dirac effect can be viewed as stimulated Thomson or Compton scattering.

In their original paper, the authors concluded, that the experimental realization of this resonant process deemed to be unfeasible with mercury lamps, the brightest continuous light sources available at that time. Consequently, the idea was revived for theoretical investigation after the invention of the laser in the nineteen-sixties [Fed67] and generalized to strong fields including multi-photon interactions.

A first experimental realization of this kind of scattering, however, has been reported for atomic beams instead of electrons [ASM94; Fre+99]. Observations in both the so-called diffraction [Mar+88; EZE14] and the Bragg regime [GRP86] have been made. There, the probability of the constitutive interaction with a single photon can be greatly enhanced by the photon energy being close to an inner atomic resonance. Such a benefit, that increases the number of scattered particles, cannot be expected in the case of a free electron.

As for electrons, the first Kapitza-Dirac scattering has been realized in above threshold ionization of argon or krypton, in a standing wave of high intensity $\sim 10^{14}\ \frac{\mathrm{W}}{\mathrm{cm}^2}$ [BSB88]. The narrow distribution of the emitted electons centered around the polarization direction helped to distiguish the scattering orders in the laser propagation direction.

It took again several years until a convincing experimental realization of the Kapitza-Dirac effect in the originally proposed geometry with free electrons was presented by Freimund, Aflatooni and Batelaan [FAB01]. In 2001, they reported the observation of clear diffraction peaks of an electron beam with 380 eV kinetic energy after travelling through a standing wave. The latter was formed by two beams of a 10 ns Nd:YAG laser pulse with 0.2 J energy focused to a spot size of 125 μm, corresponding to a laser intensity of $5 \times 10^{10}\ \frac{\mathrm{W}}{\mathrm{cm}^2}$.

Meanwhile, the Kapitza-Dirac effect gained also a lot of theoretical attention. The influence of adiabatic switching of the interaction on the final scattering probabilities has been debated in [Fed74]. A relativistic version based on the Klein-Gordon equation for spin-zero particles was developped [HA75; FM80]. The description was adapted to an electron wave packet instead of a plane wave in [EF00].

Besides, the question has been raised whether the Kapitza-Dirac effect can be sensitive to the electron spin. Then this fundamental quantum phenomenon would involve yet another genuine quantum feature. First considerations came to the conclusion, though, that the electron spin is immaterial for Kapitza-Dirac scattering [FB03; Ros04]. However recently, a spin-sensitive relativistic treatment in linear polarization based on the full Dirac equation [Ahr+12; Ahr+13], and in elliptical polarization based on the Foldy-Wouthuysen transformation of the latter [EB15] has been presented. Both setups show distinct involvement of the spin in the diffraction.

In this thesis, we generalize the Kapitza-Dirac effect in two ways using two-color waves with a small integer frequency ratio. In part I the standing wave is augmented to a bichromatic standing wave. The lattice, the electron is diffracted from, is now given a regular but not necessarily symmetric substructure. The influence thereof is examined in both the diffraction and the Bragg regime. In the latter, interference effects of two quantum pathways, comparable to the double-slit experiment, are exposed. In these standing waves, the ponderomotive potential is predominant in a way, that all visible features can be attributed to interference between the effects due to the individual standing waves.
In part II we switch from the standing waves to two counterpropagating waves of different frequencies. There, no ponderomotive potential emenates. We show that, though not obvious, there are still periodic effective potential structures for the electron when the frequency ratio is 1:2 (compare also [Smi+04]). That way, by forcing resonant three-photon scattering, the electron spin gains a crucial role in the interaction. We investigate the influence of several different laser polarization states on the scattering probability, and classify some electron beam splitting techniques based on these principles by their spin dependence and spin-flipping properties.* In this framework we also try to formulate a theoretical answer to the longstanding question of whether a Stern-Gerlach experiment for free electrons can be realized. Being first raised by Bohr and Pauli, who concluded

* We call an interaction *spin-sensitive* if it happens due to the existence of the electron spin. A spin-insensitive effect, on the other hand, could in principle also happen with spin-zero particles. To differentiate further, when the scattering depends on the individual spin state, we call it *spin-dependent*, when the spin has changed after being scattered, we call it *spin-flipping*.

that no such experiment based on classical trajectories in static magnetic fields can succeed [MM65; BGS97; RG98b; RG98a; MBB11], the question was transferred to the framework of Kapitza-Dirac scattering from circular polarized light by [FB03].

To put our studies into a larger context, we briefly mention other quantum effects occuring in two-color laser fields. Commensurate two-color effects, showing similar interference pattern (as in part I) include laser-assisted electron scattering in atomic potentials [VE93; KJE95; MEP97], photoionization [SK92; Yin+92; Sch+94; VTM95; PBW95], coherent control of chemical reactions and molecular dynamics [SB00], Thomson [Spe+11] or Compton scattering [NF00] and high harmonics generation from atoms [TWC95; Ban+97; Mor+99; MBK00; Kim+05; Mau+06].

As for QED effects, the influence of bichromaticity was also theoretically investigated in several pair creation schemes like the Breit-Wheeler process [NF00; JM13], where a strong laser and a gamma photon create matter only from light, or the Bethe-Heitler process [KK12; AM13], where particles are created by a strong laser in the vicinity of a nuclear Coulomb field.

Pair production in purely time-dependent oscillating electric fields with two frequencies was considered in [AVM14]. This is a model for multi-photon pair-production in bichromatic standing waves, if the laser wave length is large compared to the Compton wave length. The process is then assumend to be localized in the wave crests. In this interpretation it is a rather similar laser configuration to what we employ in part I, though not commensurate in the frequencies. But with respect to the electron, we can state, that the former is emitting particle pairs in a continuum of states, whereas the latter scatters an electron resonantly from a defined momentum into a discrete set of momentum states.

Besides, spin effects in monochromatic fields were studied in laser-induced photoionization [FB04; Kla+14], high-harmonic generation [WK01] Compton [KK13; IKS04] and Mott [STM98] scattering and electron-positron pair creation [IKS05; WBK15].

Publications

The studies presented in this thesis have also led to the following publications. The contextual overlap with some of the following chapters will be indicated there.

M. M. Dellweg and C. Müller. "Kapitza-Dirac scattering of electrons from a bichromatic standing laser wave". In: *Phys. Rev. A* 91.6 (June 2015), p. 062102

M. M. Dellweg and C. Müller. "Influence of laser pulse shape and spectral composition on strong-field Kapitza-Dirac scattering". In: *J. Phys.: Conf. Ser.* 594 (Mar. 2015), p. 012015

M. M. Dellweg, H. M. Awwad, and C. Müller. "Spin dynamics in Kapitza-Dirac scattering of electrons from bichromatic laser fields". In: *Phys. Rev. A* 94.2 (Aug. 2016), p. 022122

M. M. Dellweg and C. Müller. "Spin-Polarizing Interferometric Beam Splitter for Free Electrons". In: *Phys. Rev. Lett.* 118.7 (Feb. 2017), p. 070403

M. M. Dellweg and C. Müller. "Controlling electron spin dynamics in bichromatic Kapitza-Dirac scattering by the laser field polarization". In: *Phys. Rev. A* 95 (Apr. 2017), p. 042124

Part I

Standing Waves: Quantum Interference

Chapter 2

Theoretical Framework

The non-relativistic quantum nature of the electron (excluding its spin degree of freedom) in electromagnetic fields is described by Schrödinger's equation

$$i\hbar\partial_t\psi(t,\vec{r}) = \frac{1}{2m}\left(-i\hbar\vec{\nabla} + \frac{e}{c}\vec{A}(t,\vec{r})\right)^2\psi(t,\vec{r}) - e\phi(t,\vec{r})\psi(t,\vec{r})\,. \tag{2.1}$$

Here, ψ is the complex scalar wave function of the electron, $\vec{A}$ and ϕ are the vector and scalar potential of the external electromagnetic field. m is the electron's mass, $-e$ its charge, $\hbar$ is the quantum unit of action and c the speed of light.

A standing wave along the z-axis with wave number k, frequency $\omega = ck$ and amplitude a_0, as considered in this part of the thesis, can be described in radiation gauge ($\phi \equiv 0$, $\vec{\nabla}\cdot\vec{A} \equiv 0$) as

$$\begin{aligned}\vec{A}(t,z) &= \frac{a_0}{2}\vec{\epsilon}(\cos(\omega t - kz) + \cos(\omega t + kz)) \\ &= a_0\vec{\epsilon}\cos(\omega t)\cos(kz)\,.\end{aligned} \tag{2.2}$$

The polarization vector $\vec{\epsilon}$ needs to fulfill $\vec{\epsilon}^{\,2} = 1$ and $\vec{\epsilon}\cdot\vec{e}_z = 0$.

Basically, the Schrödinger equation could be solved with this vector potential, from first principle to investigate the Kapitza-Dirac effect. However, a more intuitive picture can be built up, by following an alternative approach that relies on a time-independent scalar potential. It was shown [Bat07], that the electron motion is dominantly influenced by the ponderomotive potential

$$\begin{aligned}V(z) &= \left\langle\frac{e^2\vec{A}^2}{2mc^2}\right\rangle_t = \frac{e^2a_0^2}{4mc^2}\cos^2(kz) = V_0\cos^2(kz) \\ &= \frac{V_0}{2}\left(1+\cos(2kz)\right) = \frac{V_0}{2} + \frac{V_0}{4}\left(e^{2ikz} + e^{-2ikz}\right)\end{aligned} \tag{2.3}$$

with amplitude $V_0 = \frac{e^2a_0^2}{4mc^2}$. The condition, that this approximation based on temporal averaging the Hamiltonian is valid, is that the laser frequency is substantially larger

than the ponderomotive amplitude (i.e. $\hbar\omega \gg V_0$)[Fed81]. The constant term $\frac{V_0}{2}$ (resulting in a spatially constant complex phase of the wave function) can be removed by a gauge transformation on the electron wave function. It will further be omitted. These approximations result in an effectively time-independent system, where the transverse momentum becomes immaterial. The Schrödinger equation (2.1) consequentially reduces to being time-independent and one-dimensional.

The main goal in this part of the thesis is to investigate the modifications of the Kapitza-Dirac effect caused by adding a second standing wave with commensurate frequency, i.e. using a bichromatic standing wave. The extension of (2.2) to the case of two standing waves with frequency ratio 1:2 is a vector potential of the form

$$\vec{A}(t,z) = a_0 \left[\alpha\vec{\epsilon}_1 \cos(\omega t)\cos(kz) + \frac{\sqrt{1-\alpha^2}}{2}\vec{\epsilon}_2 \cos\left(2\omega t + \frac{\eta}{2}\right)\cos\left(2kz + \frac{\delta}{2}\right)\right] . \quad (2.4)$$

There, four new degrees of freedom were introduced. First, η is a relative phase in the temporal oscillation of the two waves, and second δ the corresponding spatial phase shift. Third, a relative amplitude parameter $\alpha \in [0,1]$ was inserted in a way to keep the overall laser intensity fixed, i.e. independent of α. The last one is hidden in the fact, that the second harmonic standing wave does not need to be polarized in the same direction as the fundamental mode. The two new polarization vectors $\vec{\epsilon}_1$ and $\vec{\epsilon}_2$ were hence introduced. The aforementioned ponderomotive potential now reads

$$\begin{aligned} V(z) &= \frac{V_0}{2}\left(\alpha^2\cos(2kz) + \frac{1-\alpha^2}{4}\cos(4kz+\delta)\right) \\ &= \frac{\alpha^2 V_0}{4}\left(e^{2ikz} + e^{-2ikz}\right) + \frac{\left(1-\alpha^2\right)V_0}{16}\left(e^{4ikz+i\delta} + e^{-4ikz-i\delta}\right) . \end{aligned} \quad (2.5)$$

The generalization of this potential to other commensurate frequency ratios or more involved harmonics is straight forward. Of the above mentioned degrees of freedom only α^2 and δ remain. One can see, that the potential represented in momentum space has the form of a comb with four Dirac peaks lying at wave numbers $\pm 4k, \pm 2k$. Therefore only momenta lying an integer multiple of $2\hbar k$ apart from the discrete incident momentum are accessible to the wave function at any later time. The interpretation of this observation is, that the electron does not obey momentum conservation on its own. Rather, the total momentum including the to be absorbed and the later emitted photon momenta is conserved, in agreement with the particle picture. With the offset p_z of the incident momentum from such an integer multiple of $2\hbar k$, we make the Fourier mode ansatz

$$\psi(t,z) = \sum_{n\in\mathbb{Z}} a_n(t) e^{i(2nk + p_z/\hbar)z} . \quad (2.6)$$

By plugging (2.6) into the Schrödinger equation with the time-independent bichromatic potential (2.5), we arrive at

$$\begin{aligned} i\hbar\dot{a}_n(t) = E_n a_n(t) &+ f(t)\frac{\alpha^2 V_0}{4}\left(a_{n-1}(t) + a_{n+1}(t)\right) \\ &+ f(t)\frac{\left(1-\alpha^2\right)V_0}{16}\left(e^{i\delta}a_{n-2}(t) + e^{-i\delta}a_{n+2}(t)\right) \qquad \forall n \in \mathbb{Z} \end{aligned} \quad (2.7)$$

where the kinetic energy of the momentum eigenstate with index n is given by $E_n = \frac{\hbar^2 k^2}{2m}(2n+q)^2$ with the abbreviation $q = \frac{p_z}{\hbar k}$ for the relative momentum offset. Additionally we have introduced an envelop or switching function $f(t)$ at this stage. Its purpose is to model that the electron's interaction with the laser field does not start or end instantaneously, but is ramped up and down over several laser cycles. This reduces nonphysical behaviour and phase dependence on the exact switching time to practically zero. For most of the analytical derivations, however we will assume this function to be identically unity and impose its influence by other means. Whenever used in numerical simulations, we use a flat-top function with $\sin^2$-slopes, such that $\int f(t)dt = T$ is the effective interaction time.

In the following we will investigate Eq. (2.7) both analytically as well as numerically in different parameter regimes. Note that the original single color Kapitza-Dirac effect is included in this formulation, and can be recovered by setting $\alpha^2 = 1$ (or 0 for the second harmonic).

Chapter 3

Diffraction Regime

The motivational analogy of the Kapitza-Dirac effect with the diffraction of light from a grating becomes particularly clear in the so-called diffraction or Ramam-Nath regime. It is characterized by the fact that the mean kinetic energy of the electron is negligibly small compared to the ponderomotive interaction potential $V_0 \gg \frac{\hbar^2 k^2}{m}$ [Fed81]. In this situation, the accessible momentum modes are much closer, than the absolute value of the transient momentum given to the electron by the field ($\hbar k \ll \frac{e a_0}{c}$). While still only momenta lying a multiple of two photon momenta apart are allowed by the overall momentum conservation in the interaction, the energy conservation does no longer impose a limit on which of these modes may be occupied. By this simple consideration, after some interaction time, the electron probability gets diluted into equidistant states in a big portion of momentum space. An illustration is provided in the upper two panels of Fig. 3.1. The resulting broad but discrete distribution of final electron momenta manifests in a fan like structure of the electron beam in position space [Fed81]. Diffractive Kapitza-Dirac scattering from monochromatic waves has been successfully observed for the first time in 2001 [FAB01]. In this chapter we want to study the effects of a second harmonic standing wave on the process. We shall demonstrate distinct qualitative modifications, that can arise depending on the relative intensities and relative spatial phase of the two frequency modes. Up to a few additions, the results presented in this chapter have been originally published in [DM15a].

3.1 First Approximation

A good approximation in the diffractive regime is to neglect the kinetic term altogether. To ease the calculation, we first define a new time scale* with $\tau := \frac{V_0 t}{2\hbar}$ and adjust the expansion coefficients to $b_n(\tau) := i^n a_n(t)$. The Schrödinger equation (2.7) can then be

*Keep in mind, that the typical time $\frac{2\hbar}{V_0}$ for the here described Kapitza-Dirac effects implies, that the swiftness of their dynamic depends proportionally on the ponderomotive potential strength.

recast to

$$\begin{aligned}\partial_\tau b_n(\tau) = -i\epsilon\left(n+\frac{q}{2}\right)^2 b_n(\tau) + \frac{\alpha^2}{2}\left(b_{n-1}(\tau) - b_{n+1}(\tau)\right) \\ + \frac{1-\alpha^2}{8}\left(ie^{i\delta}b_{n-2}(\tau) + ie^{-i\delta}b_{n+2}(\tau)\right).\end{aligned} \tag{3.1}$$

Here, $\epsilon = \frac{4\hbar^2k^2}{mV_0} \ll 1$ was introduced, to treat the kinetic energy as a small parameter. Without loss of generality we can choose the initial condition as $b_n(0) = \delta_{n,0}$, corresponding to an electron with longitudinal momentum $p_z = \hbar kq$. It is a well established result [Bat07], that in the monochromatic case ($\alpha^2 = 1$) Eq. (3.1) is solved to zeroth order in ϵ by ordinary Bessel functions of the first kind. In the bichromatic case a similar analytically exact solution can be found. We present this by switching to generating functions, a method that could be generalized to other commensurate frequency ratios and more frequencies in an obvious way. To this end, we define the generating function for the expansion coefficients[†]

$$B(\tau,\zeta) := \sum_{n\in\mathbb{Z}} b_n(\tau)\zeta^n \tag{3.2}$$

and the differential operator that corresponds to the unperturbed ($\epsilon = 0$) version of (3.1)

$$\mathcal{D} := \frac{\partial}{\partial\tau} - \frac{\alpha^2}{2}\left(\zeta - \zeta^{-1}\right) - \frac{1-\alpha^2}{8}\left(ie^{i\delta}\zeta^2 + ie^{-i\delta}\zeta^{-2}\right) \tag{3.3}$$

With the help of another differential operator

$$\mathcal{N} := \zeta\frac{\partial}{\partial\zeta} \tag{3.4}$$

we arrive at

$$\mathcal{D}B(\tau,\zeta) = -i\epsilon\left(\frac{q}{2}+\mathcal{N}\right)^2 B(\tau,\zeta) \tag{3.5}$$

while the boundary condition reads $B(0,\zeta) = 1$. The zeroth order solution to (3.5) which satisfies $\mathcal{D}B^0(\tau,\zeta) = 0$, can be readily derived as

$$\begin{aligned}B^0(\tau,\zeta) &= \exp\left[\frac{\alpha^2\tau}{2}\left(\zeta-\zeta^{-1}\right)\right]\exp\left[\frac{\left(1-\alpha^2\right)\tau}{8}\left(ie^{i\delta}\zeta^2 + ie^{-i\delta}\zeta^{-2}\right)\right] \\ &= J\left(\alpha^2\tau,\zeta\right)J\left(\frac{1-\alpha^2}{4}\tau, ie^{i\delta}\zeta^2\right).\end{aligned} \tag{3.6}$$

In the second step we used $J(\rho,\zeta) = \exp\left(\frac{\rho}{2}(\zeta-\zeta^{-1})\right) = \sum_{n\in\mathbb{Z}} J_n(\rho)\zeta^n$, the generating function for ordinary Bessel functions of the first kind. From there we can extract the

[†] Note that the generating function (which is formally a Laurent series) is closely related to the wave function by $\psi(t,z) = (i\zeta)^{q/2}B(\tau,\zeta)$, when $\tau = \frac{V_0 t}{2\hbar}$ and $\zeta = -ie^{2ikz}$. In this context, $\mathcal{N}$ is related to the momentum operator.

expansion coefficients to zeroth order

$$b_n^0(\tau) = \sum_{\ell\in\mathbb{Z}} J_{n-2\ell}\left(\alpha^2\tau\right) i^\ell e^{i\ell\delta} J_\ell\left(\frac{1-\alpha^2}{4}\tau\right) = J_n^{(2)}\left(\alpha^2\tau, \frac{1-\alpha^2}{4}\tau; ie^{i\delta}\right) \tag{3.7}$$

that turn out to be generalized Bessel functions[‡] (see Eq. (1.15) in [Dat+91]).

At this point we can already note two observations. For $\alpha^2 = 1$ or 0 the solution reduces expectedly to the well known single-color version, whose probabilities $|b_n|^2$ are symmetric under the exchange $n \leftrightarrow -n$. On the other hand for $0 < \alpha^2 < 1$, we arrive at scattering probabilities, which depend on δ and can in general be asymmetric. This is illustrated in Fig. 3.1. In panels (a) and (b) a typical behaviour of ordinary Bessel functions of the first kind can be observed. Symmetrically in momentum space, a wall of excitation moves outwards, while the states already swiped over oscillate. Due to the second harmonic standing wave, every second momentum state is completely omitted in panel (b). Panel (c) shows that combining both waves without relative phase, preserves the symmetry, but a larger portion of momentum space is covered by the outwards moving excitation. Also the momentum states in the central part appear more chaotically distributed. Finally in panel (d) when introducing an asymmetric potential (having $\delta = \frac{\pi}{2}$), the momentum distribution looses its symmetry as well, and additionally moves a bit sideways.

It has been proposed, that this asymmetry can be exploited to scatter the electron in a specific direction similar to a blazed grating [VC15], and that this might be enhanced by combining even more harmonics.

3.2 Corrections to First Approximation

Despite being the unperturbed solution, B^0 can be seen as the Green's function of the linear operator $\mathcal{D}$, since

$$\mathcal{D}\theta(\tau)B^0(\tau,\zeta) = \theta'(\tau)B^0(\tau,\zeta) = \delta(\tau)B^0(0,\zeta) = \delta(\tau)\,. \tag{3.8}$$

By Green's theorem this leads to the Dyson relation for the full differential equation (3.5)

$$B(\tau,\zeta) = B^0(\tau,\zeta) - i\epsilon\int_0^\tau d\,\sigma B^0(\tau-\sigma,\zeta)\left(\frac{q}{2}+\mathcal{N}\right)^2 B(\sigma,\zeta)\,. \tag{3.9}$$

Here, the Heaviside step function $\theta(\tau)$ and the Dirac delta $\delta(\tau) = \theta'(\tau)$ have been used.[§] In turn, this allows us to expand the full solution into the corresponding Dyson series, sorted by powers of ϵ:

$$B(\tau,\zeta) = B^0(\tau,\zeta) + \epsilon B^1(\tau,\zeta) + \epsilon^2 B^2(\tau,\zeta)\ldots \tag{3.10}$$

[‡] $J_n^{(k)}(u,v;s) := \sum_{\ell\in\mathbb{Z}} J_{n-k\ell}(u)s^\ell J_\ell(v)$ are an even more generalised version of the Bessel functions as presented in appendix B of [Rei80]. The latter can be recovered by setting the argument after the semicolon to unity.

[§] Both θ and δ are not functions in the traditional sense, but rather tempered distributions. The prime is therefore understood as the distributional derivative.

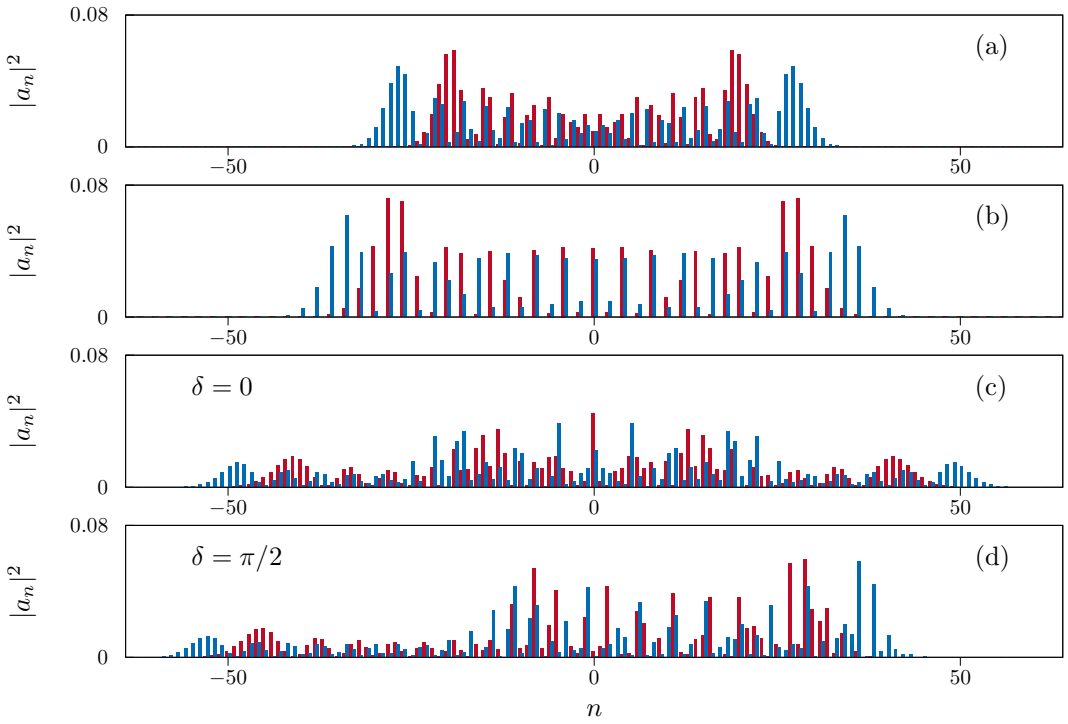

Figure 3.1: Scattering probabilities for Kapitza-Dirac scattering in the diffraction regime. After an interaction time of 0.8×10^{-12} s (left red bars) and 1.1×10^{-12} s (blue right bars) the occupation probabilities in momentum space are shown. A single color standing wave with frequency $\hbar\omega_1 = 2$ eV and intensity $I_1 = 5 \times 10^{11}\ \frac{\mathrm{W}}{\mathrm{cm}^2}$ was employed in panel (a). The doubled frequency $\hbar\omega_2 = 4$ eV with intensity $I_2 = 1.5 \times 10^{12}\ \frac{\mathrm{W}}{\mathrm{cm}^2}$ results in panel (b). In panels (c) and (d) the probabilities for the interaction with the combined laser fields of relative phase $\delta = 0$ and $\frac{\pi}{2}$ respectively are displayed. One can clearly see the asymmetry in the momentum distribution introduced by the asymmetric potential via interference.

Their calculation is based on the following identities (where $[,]$ indicates a commutator):

$$B^0(\rho+\sigma,\zeta) = B^0(\rho,\zeta)B^0(\sigma,\zeta) \tag{3.11a}$$

$$\mathcal{M} := [\mathcal{D},\mathcal{N}] = \frac{\alpha^2}{2}\left(\zeta+\zeta^{-1}\right) + \frac{1-\alpha^2}{4}\left(ie^{i\delta}\zeta^2 - ie^{-i\delta}\zeta^{-2}\right) \tag{3.11b}$$

$$\mathcal{N}B^0(\sigma,\zeta) = \sigma\left[\mathcal{D},\mathcal{N}\right]B^0(\sigma,\zeta) = \sigma\mathcal{M}B^0(\sigma,\zeta) \tag{3.11c}$$

For the first order correction we obtain

$$\begin{aligned}
B^1(\tau,\zeta) &= -i\int_0^\tau d\,\sigma B^0(\tau-\sigma,\zeta)\left(\frac{q}{2}+\mathcal{N}\right)^2 B^0(\sigma,\zeta)\\
&= -i\int_0^\tau d\,\sigma B^0(\tau-\sigma,\zeta)\left(\frac{q}{2}+\mathcal{N}\right)\left(\frac{q}{2}+\sigma\mathcal{M}\right) B^0(\sigma,\zeta)\\
&= -i\int_0^\tau d\,\sigma B^0(\tau-\sigma,\zeta)\left(\left(\frac{q}{2}+\sigma\mathcal{M}\right)^2 + \sigma\left[\mathcal{N},\mathcal{M}\right]\right) B^0(\sigma,\zeta)\\
&= -i\int_0^\tau d\,\sigma\left(\frac{q^2}{4}+\sigma q\mathcal{M}+\sigma^2\mathcal{M}^2+\sigma\left[\mathcal{N},\mathcal{M}\right]\right) B^0(\tau,\zeta)\\
&= -i\left(\frac{\tau}{4}q^2+\frac{\tau^2}{2}q\mathcal{M}+\frac{\tau^3}{3}\mathcal{M}^2+\frac{\tau^2}{2}\left[\mathcal{N},\mathcal{M}\right]\right) B^0(\tau,\zeta)\\
&= -i\left(\frac{\tau}{4}q^2+\frac{\tau}{2}q\mathcal{N}+\frac{\tau^2}{3}\mathcal{N}^2+\frac{\tau^2}{6}\left[\mathcal{N},\mathcal{M}\right]\right) B^0(\tau,\zeta)
\end{aligned} \tag{3.12}$$

which, for the individual coefficients b_n, reads

$$\begin{aligned}
b_n(\tau) = &\left(1 - i\epsilon\frac{\tau}{4}q^2 - i\epsilon\frac{\tau}{2}nq - i\epsilon\frac{\tau}{3}n^2\right) b_n^0(\tau)\\
&- i\epsilon\frac{\alpha^2\tau^2}{12}\left(b_{n-1}^0(\tau) - b_{n+1}^0(\tau)\right)\\
&+ \epsilon\frac{\left(1-\alpha^2\right)\tau^2}{12}\left(e^{i\delta}b_{n-2}^0(\tau) + e^{-i\delta}b_{n+2}^0(\tau)\right) + o(\epsilon)\,.
\end{aligned} \tag{3.13}$$

With the Taylor series of the generalizes Bessel functions

$$b_0^0(\tau) = 1 - \left(\alpha^2 + \frac{\left(1-\alpha^2\right)^2}{16}\right)\left(\frac{\tau}{2}\right)^2 + o\left(\tau^2\right) \tag{3.14a}$$

$$b_{\pm1}^0(\tau) = \pm\,\alpha^2\frac{\tau}{2} \mp ie^{\pm i\delta}\frac{\alpha^2\left(1-\alpha^2\right)}{4}\left(\frac{\tau}{2}\right)^2 + o\left(\tau^2\right) \tag{3.14b}$$

$$b_{\pm2}^0(\tau) = ie^{\pm i\delta}\frac{1-\alpha^2}{4}\frac{\tau}{2} + \frac{1}{2}\left(\frac{\tau}{2}\right)^2 + o\left(\tau^2\right) \tag{3.14c}$$

we can now estimate the relative error in the intensity of the zeroth diffraction peak

$$\frac{|b_0(\tau)|^2}{|b_0^0(\tau)|^2} - 1 = \epsilon\tau^4\frac{1}{4}\alpha^4\frac{1-\alpha^2}{4}\cos\delta + o\left(\epsilon\tau^4\right)\,. \tag{3.15}$$

We emphasize, that to this order the error is only non-vanishing for the bichromatic case where $\alpha^2 \notin \{0,1\}$ and $\delta \neq \frac{\pi}{2}$. For the second order in ϵ, by a very similar but much longer calculation, we arrive at

$$\begin{aligned} B^2(\tau,\zeta) &= -i\int_0^\tau d\,\sigma B^0(\tau-\sigma,\zeta)\left(\frac{q}{2}+\mathcal{N}\right)^2 B^1(\sigma,\zeta) \\ &= -\Bigg(\frac{\tau^2}{32}q^4+\frac{\tau^2}{8}q^3\mathcal{N}+\frac{5\tau^2}{24}q^2\mathcal{N}^2+\frac{\tau^3}{12}q^2[\mathcal{N},\mathcal{M}] \\ &\quad+\frac{\tau^2}{6}q\mathcal{N}^3+\frac{\tau^3}{6}q[\mathcal{N},\mathcal{M}]\mathcal{N}+\frac{\tau^3}{6}q[\mathcal{N},[\mathcal{N},\mathcal{M}]] \\ &\quad+\frac{\tau^2}{18}\mathcal{N}^4+\frac{\tau^3}{10}[\mathcal{N},\mathcal{M}]\mathcal{N}^2+\frac{7\tau^3}{36}[\mathcal{N},[\mathcal{N},\mathcal{M}]]\mathcal{N} \\ &\quad+\frac{\tau^3}{9}[\mathcal{N},[\mathcal{N},[\mathcal{N},\mathcal{M}]]]+\frac{\tau^4}{40}[\mathcal{N},\mathcal{M}]^2\Bigg)B^0(\tau,\zeta) \end{aligned} \tag{3.16}$$

giving the second order correction

$$\begin{aligned} b_n^2(\tau) =& -\left[\frac{\tau^2}{32}q^4+\frac{\tau^2}{8}nq^3+\frac{5\tau^2}{24}n^2q^2+\frac{\tau^2}{6}n^3q+\frac{\tau^2}{18}n^4-\frac{\tau^4}{80}\left(1-2\alpha^2+2\alpha^4\right)\right]b_n^0(\tau) \\ &-\left[\frac{\tau^3}{24}q^2+\frac{\tau^3}{12}nq+\frac{\tau^3}{20}n^2+\frac{\tau^3}{120}\right]\alpha^2\left(b_{n-1}^0(\tau)-b_{n+1}^0(\tau)\right) \\ &+\frac{\tau^3}{360}n\alpha^2\left(b_{n-1}^0(\tau)+b_{n+1}^0(\tau)\right) \\ &+\frac{\tau^4}{80}\alpha^2\left(1-\alpha^2\right)\left(ie^{i\delta}b_{n-1}^0(\tau)-ie^{-i\delta}b_{n+1}^0(\tau)\right) \\ &-\left[\frac{\tau^3}{24}q^2+\frac{\tau^3}{12}nq+\frac{\tau^3}{20}n^2+\frac{\tau^3}{30}\right]\left(1-\alpha^2\right)\left(ie^{i\delta}b_{n-2}^0(\tau)+ie^{-i\delta}b_{n+2}^0(\tau)\right) \\ &+\frac{\tau^3}{180}\left(1-\alpha^2\right)\left(ie^{i\delta}b_{n-2}^0(\tau)-ie^{-i\delta}b_{n+2}^0(\tau)\right) \\ &-\frac{\tau^4}{160}\alpha^4\left(b_{n-2}^0(\tau)+b_{n+2}^0(\tau)\right) \\ &-\frac{\tau^4}{80}\alpha^2\left(1-\alpha^2\right)\left(ie^{i\delta}b_{n-3}^0(\tau)-ie^{-i\delta}b_{n+3}^0(\tau)\right) \\ &+\frac{\tau^4}{160}\left(1-\alpha^2\right)^2\left(e^{2i\delta}b_{n-4}^0(\tau)+e^{-2i\delta}b_{n+4}^0(\tau)\right) \end{aligned} \tag{3.17}$$

for the coefficients $b_n(\tau)$.

3.3 Numerical Treatment

To see how good an approximation (3.12) and (3.16) are, we show a comparison of the Bessel-solution (3.7), the first and the second approximation with a numerically obtained solution from (2.7) in Fig. 3.2. Looking closely at Fig. 3.2 we can see, that the validity

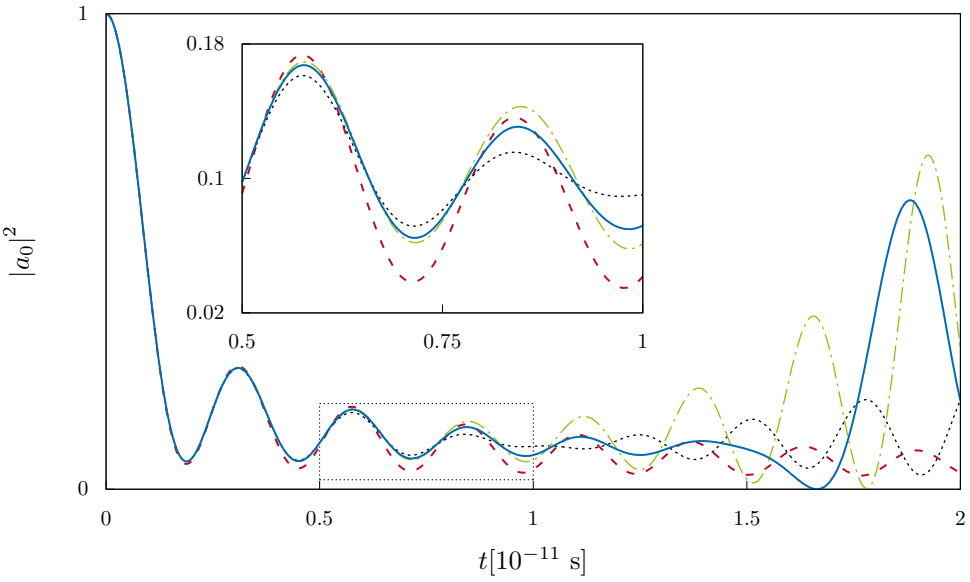

Figure 3.2: Probability $|a_0|^2$ of the incident electron mode in diffractive two-color Kapitza-Dirac scattering. The combined laser Intensity is $I = 4.363 \times 10^{10}\ \frac{\mathrm{W}}{\mathrm{cm}^2}$, and its fundamental frequency is $\hbar\omega = 2$ eV corresponding to $\epsilon = \frac{1}{100}$. The mixing parameters are $\alpha^2 = \frac{1}{2}$ and $\delta = 0$. The full numeric solution is shown in solid blue. The zeroth, first and second order approximations are plotted in dashed red, dotted black and dash dotted green respectively. The region magnified in the inset is marked in the main window.

of the three approximations cease in the predicted order, but that they are altogether longer valid than estimated.

To investigate this further, we performed simulations of the bichromatic Kapitza-Dirac effect in the transitional parameter region between the diffraction and the Bragg regime. For that purpose, we solved the Schrödinger equation with the ponderomotive potential (2.5) by Fourier split-step methods. In Fig. 3.3 four different simulations show the influence of ϵ and δ on the temporal evolution of a Gaussian wave packet in a bichromatic wave.[¶] The simulation in the upper left two panels shows a wave packet, that is focused symmetrically into the valleys of the symmetrically chosen, strong ($\epsilon = \frac{1}{100}$) potential. In momentum space, higher momentum modes are excited one after another. After reaching the highest degree of focusing, the spots start to broaden again, basically starting the whole process from the beginning. In the upper right panels, the more shallow potential ($\epsilon = \frac{1}{10}$) induces less sharp focusing, and less momentum modes are excited. Apart from that, the simulation shows qualitatively the same behaviour. In the two simulations below, that differ from their upper counterpart only by the asymmetrically chosen potential ($\delta = \frac{\pi}{2}$), an asymmetry is introduced in the focusing as well as the momentum distribution. While the distributions in the symmetric potentials

[¶] By using the universality of the reduced Planck constant $\hbar$, time can be measured electively in seconds or inverse electron volts. The equivalence $1\ \mathrm{s} \mathrel{\widehat{=}} 1.519 \times 10^{15}\ \mathrm{eV}^{-1}$ applies.

defocus to almost their original state, the asymmetry stops this from happening. Note, that the time scale in the right panels is much slower, because the promptitude of the dynamic is determined by the strength of the ponderomotive potential.

One can see, that the deviation from the Bessel-solution (3.7) becomes important, as soon as the excitation reaches an out-most momentum mode $\pm n_{\max}$. The latter has kinetic energy $E_{n_{\max}}$ comparable to the amplitude of the ponderomotive potential V_0. With the definition of ϵ, we can see that $n_{\max} \propto \frac{1}{\sqrt{\epsilon}}$ in agreement with the results of Fig. 3.3.

From this we can conclude, that, even in the monochromatic case, no set of parameters is adequately described by the Bessel-solution for all times, because by nature of the Bessel functions momentum mode $n_{\max}$ will be excited after $t \approx \frac{n_{\max}}{V_0}$. At the same time higher momentum modes will never be excited. That way, the fan like structure emerging in position space after leaving the interaction region, is always finite.

By going from the diffraction regime with small ϵ to the other extreme, i.e. making the kinetic energy dominant, we can limit the accessible momentum modes further. As soon as only two modes participate in the interaction, this is called the Bragg regime which will be the topic of the following chapter.

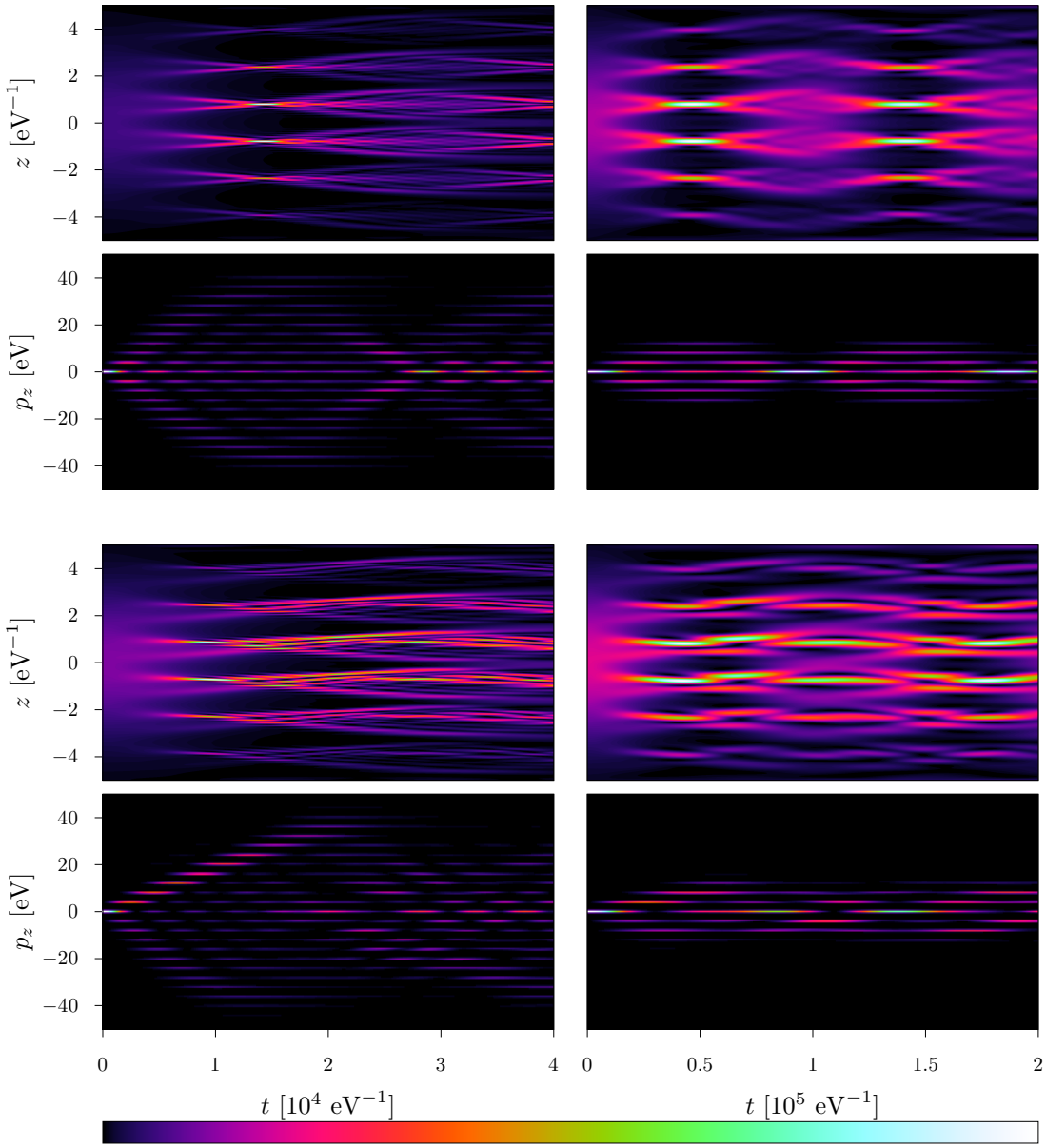

Figure 3.3: Wave packet with initial width 2 eV^{-1} in Kapitza-Dirac scattering both in one-dimensional position and momentum space. In the two upper left panels, the simulation parameters are chosen as in Fig. 3.2, especially $\epsilon = \frac{1}{100}$ and $\delta = 0$. In the second row, the ponderomotive potential is made asymmetric by $\delta = \frac{\pi}{2}$, leaving all other parameters intact. Finally, in the right column, the potential amplitude is lowered to meet $\epsilon = \frac{1}{10}$. One can see, that the symmetry of the ponderomotive potential is somehow translated to the symmetry of the probability distribution in both position and momentum space. It is also visible, that after starting in a way compatible to the Bessel functions, there is a maximum momentum state whose number scales with $\epsilon^{-\frac{1}{2}}$.

Chapter 4

Bragg Regime

The Bragg regime of Kapitza-Dirac scattering is, as shortly indicated in the last chapter, characterized by the fact, that the kinetic energy (i.e. the difference in kinetic energy of neighbouring momentum modes) is large compared to the amplitude of the ponderomotive potential [Bat07] (or in Part II its generalized version). The single-color version of this Bragg scattering has been experimentally achieved in [FB02]. They used a frequency doubled Nd:YAG laser that produced 6 ns pulses which were focused only perpendicular to the electron beam by cylindrical optics. That way an intensity of $3 \times 10^8 \ \frac{\mathrm{W}}{\mathrm{cm}^2}$ over the height of 200 μm was achieved.

The combined electron-photon momentum balance is now accompanied by stricter energy conservation, allowing only two momentum states to be accessible. In the non-relativistic regime for monochromatic standing laser waves, these states are always an even number of photon momenta apart, and have longitudinal momenta on equal sides of the electron dispersion relation. That is, an incident electron with longitudinal momentum $-\ell\hbar k$ is scattered into the mirrored state with longitudinal momentum $+\ell\hbar k$ by interacting with 2ℓ photons. An effective resonant two-state quantum dynamic develops, which exhibits typical Rabi flopping. This is also known as Pendellösung, owed to the similarity with a slow swinging pendulum [Bat07]. For possible combinations with three photons of the same frequency, at least one involved momentum needs to be relativistic (see also Part II and [Ahr+13]).

In the following, we focus on bichromatic standing waves with a frequency ratio of 1:2, together with the lowest order transition, that can be accomplished by both waves individually: The incident electron with longitudinal momentum $-2\hbar k$ (mode $n = -1$) is scattered into mode $n = 1$ by either absorbing and emitting two lower frequency photons, or absorbing and emitting one of the higher frequency as pictured in Fig. 4.1. In principle, various other transitions are possible as well, for example, the electron may absorb one high-frequency photon and emit two low-frequency ones or vice versa. Such processes involving an odd number of photons, however, comprise at least one interaction with a single photon, which are not part of the ponderomotive model. Besides, their scattering probability includes an additional scaling factor of $\sim \frac{p_x}{mc}$ or $\sim \frac{\hbar\omega}{mc^2}$, suppressing their contribution significantly in the non-relativistic regime. Such 3-photon interactions

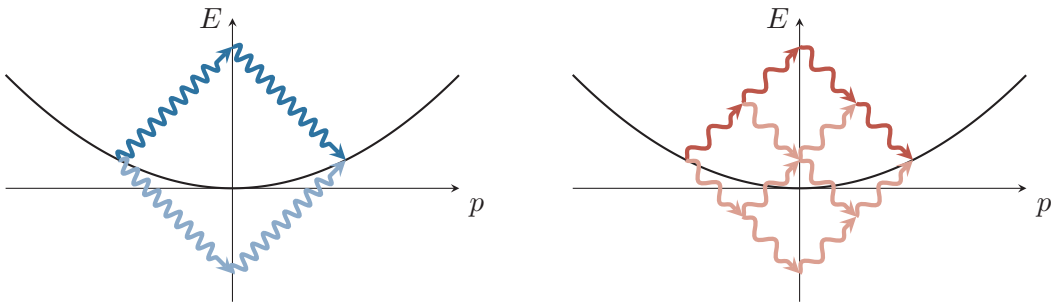

Figure 4.1: Sketch of the two predominant, concurrent processes of Kapitza-Dirac scattering from a bichromatic wave in the non-relativistic dispersion relation of the electron. Every wiggly arrow reflects the combined change in the electrons momentum and energy. An upwards tilted arrow describes an increase in energy and therefore the absorption of one photon. Accordingly, the downwards arrows describe emission. The arrows in the lighter color indicate, that the absorption and emission can happen in any given order. Only if the whole transition starts and ends precisely on the dispersion relation, it is realized in the Bragg regime.

will be discussed in Part II, in a different setup where they contribute isolated to the leading order. Also quantum pathways like absorbing two high-frequency photons with the same direction and emitting them with opposite directions back into the standing wave are imaginable. They are suppressed by being processes of higher order in the vector potential. All in all, the fact, that two dominant processes compete, enriches the quantum dynamics in a way, that two-pathway interference becomes possible. In this chapter, we want to investigate the influence of the mixing parameters on the latter.

4.1 Numerical Experiments

Numerical simulations by solving (2.7) with Runge-Kutta methods in this Bragg regime have been performed. Fig. 4.2 presents the typical behaviour of a single interaction. Shown are the occupation probabilities of the electron in the incident (blue solid line), as well as the resonantly scattered, momentum state (red dashed line). While switching on the field, some probability is transferred into intermediate states, which are in total plotted by the black dotted line. As long as the interaction with the field is active, an oscillation between the corresponding states takes place. Switching the fields off, returns all probability back to the two kinematically allowed states, not necessarily completely to one of them.

To characterize the oscillation described above as a Rabi oscillation, we look at only the final states after interactions of different durations took place. Having the otherwise same parameters as in Fig. 4.2, Fig. 4.3 shows the resulting occupation probabilities for various interaction durations. A clear Rabi oscillation, where the initial probability of being in a state with momentum $-2\hbar k$ is transferred completely to the state with $+2\hbar k$,

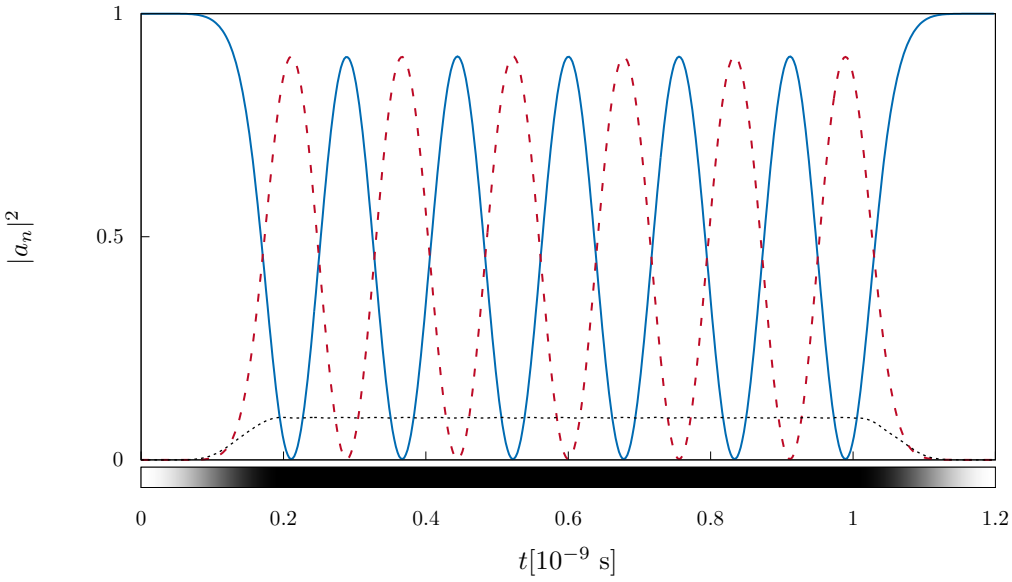

Figure 4.2: Kapitza-Dirac scattering in the Bragg regime. An incident electron with longitudinal momentum $p_z = -2\hbar k$ is scattered by a bichromatic wave with frequency $\hbar\omega = 4$ eV, total intensity $I = 1.117 \times 10^{10}\ \frac{\mathrm{W}}{\mathrm{cm}^2}$, mixing parameter $\alpha^2 = \frac{1}{2}$ and mixing phase $\delta = 0$. The incident electron mode ($n = -1$) is plotted with the solid blue line and the mirrored mode ($n = 1$) in dashed red. The dotted black line combines the probability of all remaining modes ($1 - |a_{-1}|^2 - |a_1|^2$). The switching function f, and with it the potential strength, is presented in the bar at the bottom.

and then back and forth again, can be seen. The duration ΔT of one full cycle defines the Rabi frequency via $\Omega_R := \frac{2\pi}{\Delta T}$. The total interaction time is chosen as $T = \int f(t)dt$ because the transition dynamics is not completely stopped while switching on and off. That way the probabilities plotted at $T = 10^{-9}$ s in Fig. 4.3 are exactly the final values of Fig. 4.2 at $t = 1.2 \times 10^{-9}$ s.

4.2 Interference Effects

The natural question to ask at this point is, how does this result change for different combinations of the two standing waves. Since we can expect clear Rabi oscillations in these idealized numerical conditions (see Fig. 4.3), the Rabi frequency Ω_R remains as a single parameter to adequately describe the output. In Figs. 4.4-4.6 this Rabi frequency is shown for fixed total laser intensity, but depending on the specific mixing characterized by α^2 and δ. In Fig. 4.4 we see, that for $\delta = 0$ (symmetric potential) the Rabi frequency Ω_R passes smoothly through a shallow minimum on its way from the monochromatic setup with $\alpha^2 = 0$ over the combined waves to the other monochromatic standing wave at $\alpha^2 = 1$. On the other hand for the relative phase $\delta = \pi$ with the most asymmetric potential, Ω_R starts at the same value, drops down to zero for a certain

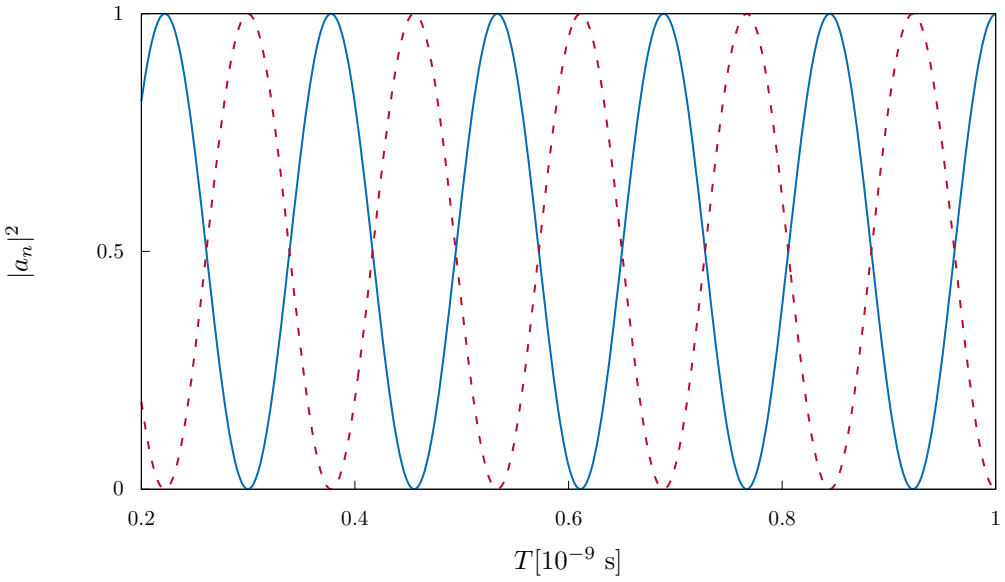

Figure 4.3: Occupation probabilities of the momentum states fulfilling a Bragg condition after interactions of different durations T. The parameters are chosen as in Fig. 4.2. Every plotted data point corresponds to a full interaction including switching on and off the laser field. Due to energy conservation and the resonant character of the process, a clear Rabi oscillation emerges.

α^2 and then rises again to meet at $\alpha^2 = 1$. Fig. 4.5 shows, that the dependence on the relative phase δ is qualitatively different for different mixing ratios α^2. Especially the solid blue line for $\alpha^2 = 0.4$ indicates significant destructive interference. The global dependence of Ω_R on both mixing parameters is shown in Fig. 4.6. As in Chap. 3, for $\alpha^2 \in \{0, 1\}$, which correspond to the monochromatic corner cases, Ω_R does not depend on the phase parameter δ. On the other hand, for the bichromatic setups in between, there is a strong dependence on this phase parameter showing constructive and destructive interference. That way, the two elementary processes sketched in Fig. 4.1 are considered to be competing quantum pathways for the transition from momentum $-2\hbar k$ to $2\hbar k$. In combination, they show distinct interference.

4.3 Dimensionally Reduced Model

To shed some more light on the interference pattern in Fig. 4.6, we analyze (2.7) in a dimensionally reduced model (see also [DM15a; EB15]). By restricting the ansatz (2.6) to the modes with $n = 0, \pm 1$, with their coefficients combined in a tuple, we can rewrite

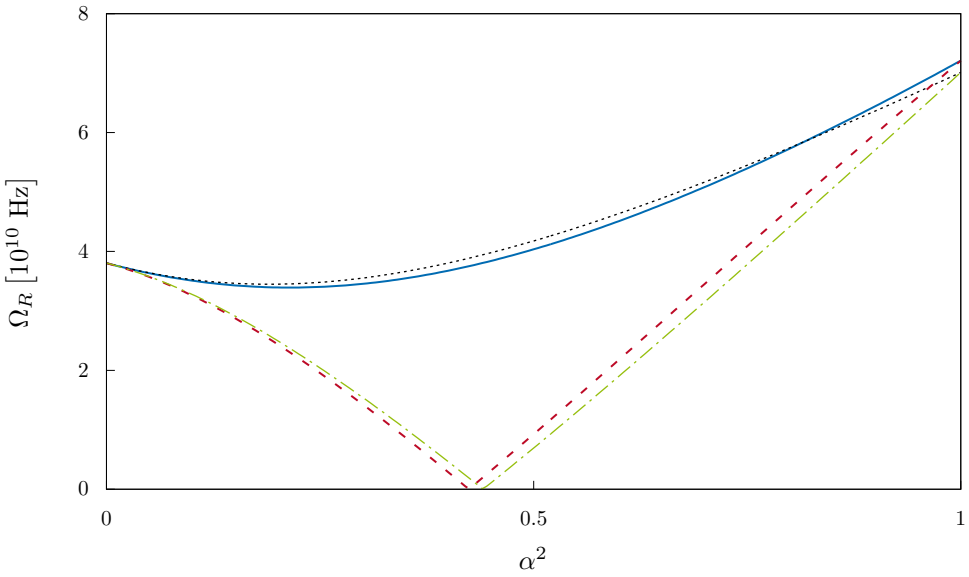

Figure 4.4: Rabi frequency Ω_R of Kapitza-Dirac scattering from bichromatic waves in the Bragg regime. Ω_R is plotted as a function of the mixing parameter α^2 for fixed $\delta = 0$ (solid blue) and compared with its analytical prediction from (4.7) (dotted black). In the same way, the numerical results for $\delta = \pi$ (dashed red) are compared with the prediction (dash dotted green). The summed laser intensity is 1.117×10^{10} $\frac{\mathrm{W}}{\mathrm{cm}^2}$ and its fundamental frequency $\hbar\omega = 4$ eV. The electron is incident with momentum $2\hbar k$ along the laser propagation direction.

(2.7) in the form

$$i\hbar\frac{\partial}{\partial t}a = Ma\,; \qquad M = \begin{pmatrix} A & B & D \\ B & 0 & B \\ D^* & B & A \end{pmatrix}\,; \qquad a = \begin{pmatrix} a_{-1} \\ a_0 \\ a_1 \end{pmatrix} \tag{4.1}$$

where $A = \frac{2\hbar^2k^2}{m}$ denotes the kinetic energy of the incident and scattered electron. $B = V_0\frac{\alpha^2}{4}$ and $D = V_0\frac{1-\alpha^2}{16}e^{-i\delta}$ are the interaction strengths to the neighboring momentum modes due to the fundamental and the harmonic laser modes respectively. The intermediate state $n = 0$ needs to be carried along, because the scattering by the low frequency standing wave is a two-step process. The characteristic polynomial of M reads

$$\chi_M(\lambda) = \lambda^3 - 2A\lambda^2 + \left(A^2 - 2B^2 - |D|^2\right)\lambda + 2B^2\left(A - \Re D\right)\,. \tag{4.2}$$

The roots λ_j of (4.2) are the eigenenergies of the eigenstates v_j with $j \in \{-1, 0, 1\}$. They are given by

$$\lambda_j = \frac{2}{3}A + \sqrt{\frac{4}{9}A^2 + \frac{8}{3}B^2 + \frac{4}{3}|D|^2}\cos\left(\Phi + \frac{2}{3}j\pi\right) \tag{4.3}$$

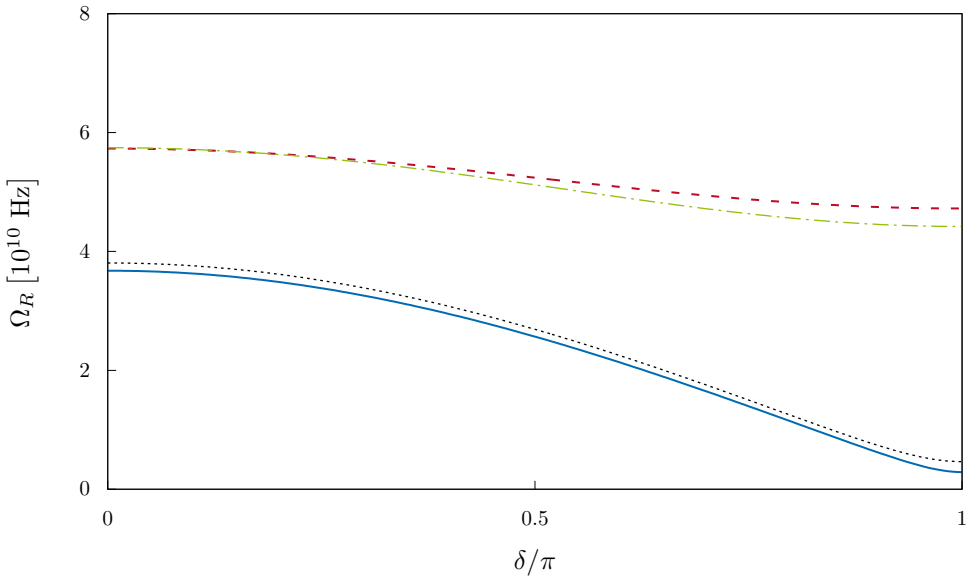

Figure 4.5: Rabi frequency Ω_R plotted as a function of the mixing phase δ for fixed $\alpha^2 = 0.4$ (solid blue / dotted black) and for $\alpha^2 = 0.8$ (dashed red / dash dotted green). All other parameters coincide with the choice in Fig. 4.4.

with

$$\begin{aligned}\Phi =& \frac{1}{3}\arccos\left[\left(-\frac{1}{27}A^3 - \frac{1}{3}AB^2 + \frac{1}{3}A|D|^2 + B^2\Re D\right)\left(\frac{1}{9}A^2 + \frac{2}{3}B^2 + \frac{1}{3}|D|^2\right)^{-\frac{2}{3}}\right] \\ =& \frac{1}{3}\arccos\left\{\frac{-\frac{8\hbar^6k^6}{27m^3} + \frac{\hbar^2k^2V_0^2\left(\left(1-\alpha^2\right)^2-16\alpha^2\right)}{384m} + \frac{V_0^3\alpha^4\left(1-\alpha^2\right)\cos(\delta)}{256}}{\left[\frac{4\hbar^4k^4}{9m^2} + \frac{1}{24}V_0^2\alpha^4 + \frac{1}{768}V_0^2\left(1-\alpha^2\right)^2\right]^{3/2}}\right\}\end{aligned} \tag{4.4}$$

and visualized in Fig. 4.7.

In the limit $V_0 \to 0$, they converge to $\lambda_{-1,0} \to A = E_1$ and $\lambda_1 \to 0 = E_0$. The corresponding eigenstates in this limit are

$$v_{-1} = \begin{pmatrix}1\\0\\e^{i\delta}\end{pmatrix} \qquad v_0 = \begin{pmatrix}1\\0\\-e^{i\delta}\end{pmatrix} \qquad v_1 = \begin{pmatrix}0\\1\\0\end{pmatrix} \tag{4.5}$$

where v_{-1} and v_0 span the degenerate eigenspace containing the initial momentum state as the linear combination

$$a = \begin{pmatrix}1\\0\\0\end{pmatrix} = \frac{1}{2}\left(v_{-1} + v_0\right). \tag{4.6}$$

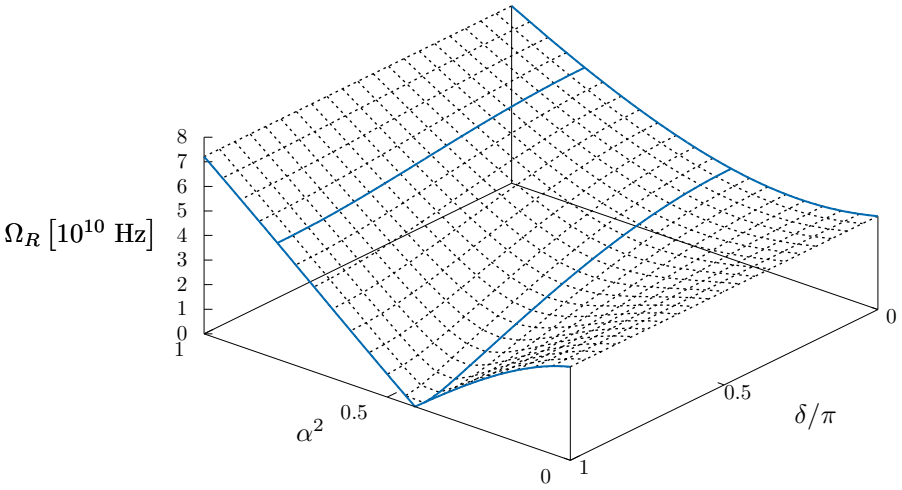

Figure 4.6: Rabi frequency on the full α^2, δ – landscape. The parameters are chosen as in Figures 4.4 and 4.5. Their results are embedded by the solid blue lines.

By virtue of the smooth switching on and off of the laser field, the final state also returns to that subspace, thereby obeying energy conservation. The Rabi cycle results as a beat oscillation between those two eigenstates. Its Rabi frequency, as plotted in Figures 4.4, 4.5 and 4.6, is the difference of the corresponding eigenvalues consequentially:

$$\begin{aligned}\Omega_R =& \frac{1}{\hbar}\left(\lambda_0 - \lambda_{-1}\right) \\ =& \frac{1}{\hbar}\sqrt{\frac{16\hbar^4k^4}{9m^2} + \frac{1}{6}V_0^2\alpha^4 + \frac{1}{192}V_0^2\left(1-\alpha^2\right)^2}\left[\cos\Phi - \cos\left(\Phi - \frac{2\pi}{3}\right)\right] .\end{aligned} \tag{4.7}$$

Fig. 4.4 and 4.5, additionally to showing numerical results, compare them to this analytical result. While slightly different in detail, the predicted general behaviour is reproduced nicely. Specifically in (4.7), the frequency Ω_R vanishes completely when $\delta = \pi$ and the mixing parameter fulfills

$$\alpha^2 = \frac{4\sqrt{1 + 32\frac{\hbar^2k^2}{mV_0} + 16\frac{\hbar^4k^4}{m^2V_0^2}} - 16\frac{\hbar^2k^2}{mV_0} - 1}{15} . \tag{4.8}$$

We conclude, that the quantum interference can fully suppress the interaction in our dimensionally reduced model. Although our numerical results show slight deviations, they are qualitatively consistent with this conclusion.

Numerical investigations of this bichromatic setup with frequency ratio of 1:3 have shown comparable, though less pronounced results (see [DM15b]). In principle, Kapitza-Dirac scattering from a bichromatic standing wave could also proceed in a mixed regime, where the parameters of the first mode lie in the diffraction regime, whereas those of the second mode are Bragg-like (or vice versa). However, as a comparison of Fig. 3.3

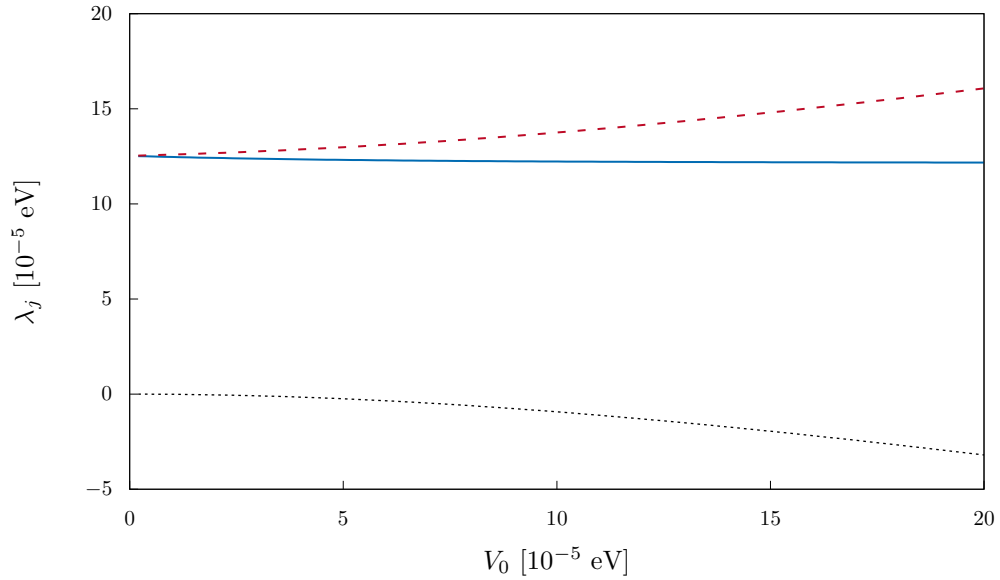

Figure 4.7: Roots λ_j of the characteristic polynomial $\chi_M(\lambda)$ depending on the amplitude V_0 of the ponderomotive potential. The fundamental laser frequency is $\hbar\omega = 4\text{eV}$ and the mixing is $\alpha^2 = \frac{1}{2}$ and $\delta = \frac{\pi}{2}$. The solid blue line shows λ_{-1}, the dashed red line λ_0 and the dotted black one λ_1.

with Fig. 4.2 reveals, diffraction and Bragg regime of the Kapitza-Dirac effect are largely different with respect to the relevant timescales, with diffractive Kapitza-Dirac scattering being much faster, in general. Therefore, this mixed regime is irrelevant in practice.

Part II

Travelling Waves: Spin Effects

Chapter 5

Preliminaries

Not only electrons, the smallest elementary charged particles within the standard model, carry angular momentum in form of spin, but also photons, the elementary particles of light, exhibit spin. It has therefore been proposed [FB03], that the controlled interaction of photons and electrons within the Kapitza-Dirac setup could be used to control the electron spin. We remember, that the interaction of a free electron with only one photon is kinematically forbidden ($[p + \hbar k]^2 \neq m^2c^2$). By further noting, that the electron has spin $\frac{1}{2}$ while photons have spin 1, it seems unlikely to find dominant spin effects in a two-photon process. However spin-involving Kapitza-Dirac scattering in an elliptically polarized standing wave has been predicted [EB15]. Still these spin flips are in competition with the much stronger normal monochromatic Kapitza-Dirac effect, which does not involve spin. With this in mind it seems natural to think about three-photon processes. An appropriate selection rule might only allow $\Delta S = \pm 1, \pm 3$ for the three photons, which means, that the electron could only interact with an included spin-flip ($\Delta S = \pm 1$). This consideration is pictured in Fig. 5.1.

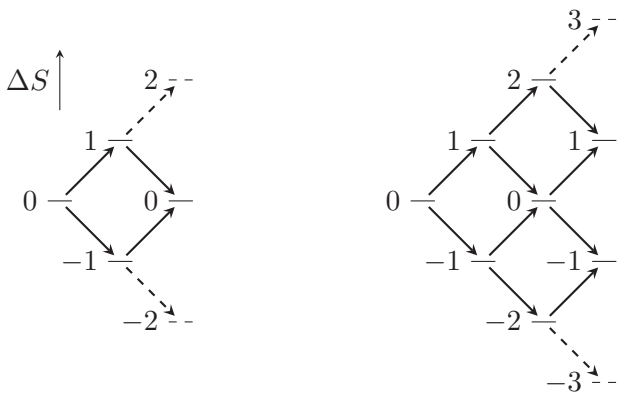

Figure 5.1: Illustration of the possible spin transitions in two- and three-photon interactions. The dashed transitions are inaccessible to interactions with the spin of a single electron.

A three-photon process cannot be induced by the $\vec{A}^2$-term alone, which the Kapitza-Dirac effect in part I relied upon. An interaction term linear in the external field is required in addition. Within the framework of non-relativistic quantum mechanics, there are $\vec{p}\cdot\vec{A}$ and $\vec{\sigma}\cdot\vec{B}$. An interaction via the latter could lead to $\Delta S = \pm 1$, as argued above. However, when constraints from energy and momentum conservation are taken into account, it turns out, that to force a 3-photon interaction in a standing wave configuration, relativistic parameters (for at least one involved electron momentum) are required [Ahr+12; Ahr+13]. Even for optical to UV photons, the electron momenta would need to be centered around $\frac{mc}{\sqrt{8}}$.

A Lorentz-boost of this setup can render the electron's incident and scattered momentum symmetric, while Doppler shifting the frequencies of the counterpropagating waves to a ratio of 1:2 (a boost with $\beta = \frac{\sqrt{2}-1}{\sqrt{2}+1} \approx 0.17$ would be necessary). That way the process can be mapped to all non-relativistic parameters in a bichromatic non-standing wave configuration (see also Fig. 5.2).

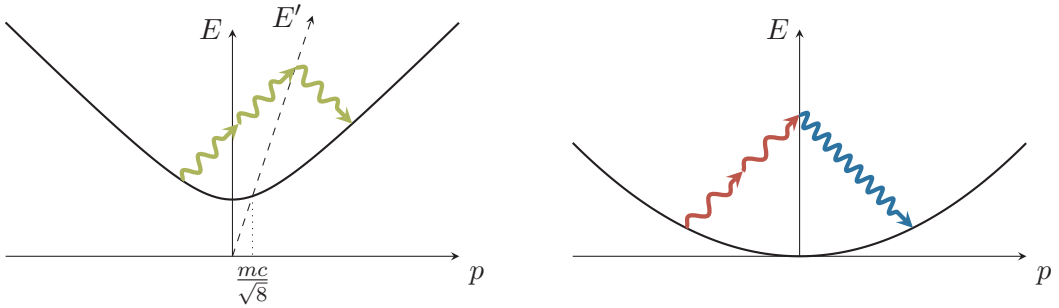

Figure 5.2: Sketches of the 3-photon Kapitza-Dirac diffraction in the electron dispersion relation. On the left side, the relativistic 3-photon interaction in a standing γ-ray wave is shown. On the right side, one can see the Lorentz-boosted version, where the electron momenta are non-relativistic and symmetric, but the lasers have a frequency ratio of 1:2. The energy axis in this frame of reference coincides with the dashed one labeled E' in the left picture. Besides, the boost parameter is independent of the laser wave lengths.

In the original proposal [FB03] usage of circularly polarized light was preferred over linearly polarized one, because it has a defined spin angular momentum. But the problem remains, that the $\vec{p}\cdot\vec{A}$-term in the interaction Hamiltonian can hardly be suppressed here. Therefore, and also for easier analytical treatment, the investigations began with linearly polarized light [Smi+04].

We want to follow that path and start with a closer look at a spin-sensitive 3-photon Kapitza-Dirac effect with two beams of linear polarization in Chap. 6. To this end, we derive an analytical expression for the involved Rabi frequency by means of time dependent perturbation theory, being the naïve and conceptually easiest approach. We then rediscover that Rabi frequency in the effective ponderomotive potential of this setup. Within this framework, we arrive at a system of differential equations that describes the actual Rabi cycle.

With this spin-flipping interaction in the toolbox, we demonstrate theoretically the construction of a spin polarizing beam splitter for free electrons in Chap. 7. The latter is a multi-step polarizer based on an interferometric setup. Its mirrors and semi-reflective mirrors are mimicked by successive Kapitza-Dirac deflections, one of them being spin-flipping.

We follow up by considerations of the asymmetric Kapitza-Dirac effect in arbitrary laser polarizations in Chap. 8. In particular, the setups with purely circular polarization and combined from one linear and one circular polarized wave will be investigated. As higher order corrections to the Pauli equation are necessary there (for discussion see [EB15]), we base our analytical model, as well as the numerical simulations, on the full Dirac equation.

In this context we would like to mention, that considerations of this spin-sensitive two-color Kapitza-Dirac effect in circularly polarized light have been made in [McG+15] based on the Pauli-equation. Because they neglected in this setup important terms, their conclusions disagree with some of our findings. Their numerical simulations, that have been made with linearly polarized light only, are however compliant with our results.

Chapter 6

Linear Polarization

In this chapter, we take a closer look on the simplest asymmetric setup of two linearly polarized counterpropagating laser waves with frequency ratio 1:2. At the same time, we choose the electron momentum to be perpendicular to the polarization direction of both laser waves. In this manner, any effect arising from $\vec{p}\cdot\vec{A}$, for example the spin-insensitive three-photon Kapitza-Dirac scattering predicted in [Smi+04], can be suppressed, and the derivations become easier.

To this end, we employ two different analytical methods, that are easy enough to be applied in this special setup, to calculate the Rabi frequency for this process. A third one, based on relativistic Dirac-Volkov states, will be deferred to Chap. 8 in a more general framework, including arbitrary polarization and the $\vec{p}\cdot\vec{A}$-interaction. That way we emphasize the mutual validity of these methods and motivate the use of the third one to obtain the Rabi frequency in setups with arbitrary polarizations.

The question of experimental realizability will be briefly discussed in Chap. 7 in relation to the parameters chosen there. However, as we shall already see in the present chapter, the analytical model of this 3-photon process is valid for a wide range of parameters.

6.1 Time-Dependent Perturbation Theory

The conceptually easiest way to understand the induced transition of the electron from the incident to the scattered momentum state is by time-dependent perturbation theory. This calculation has been carried out in [DAM16]; see also [Aww16] for a basically equivalent treatment.

Since we want to capture the influence of the electron spin in the non-relativistic limit, we start our derivation with Pauli's equation

$$i\hbar\frac{\partial}{\partial t}\psi = \frac{1}{2m}\left[\vec{\sigma}\cdot\left(-i\hbar\vec{\nabla}+\frac{e}{c}\vec{A}\right)\right]^2\psi \tag{6.1}$$

that emerges as the lowest order in the Foldy-Wouthuysen expansion to the Dirac equation [FW50]. It should be noted, that using the Pauli equation is sufficient in this setup,

because the next higher order corrections of this expansion ($\sim \vec{E} \times \vec{A}$) are only substantial in circularly polarized light. Compare also [EB15; DAM16]. By exploiting the algebraic identity $\sigma_j \sigma_k = \delta_{jk} + i\varepsilon_{jkl}\sigma_l$ of the Pauli matrices, (6.1) reduces to a more common representation

$$i\hbar \frac{\partial}{\partial t}\psi = \left[\frac{1}{2m}\left(-i\hbar\vec{\nabla} + \frac{e}{c}\vec{A}\right)^2 + \mu_\mathrm{B}\,\vec{\sigma}\cdot\vec{B}\right]\psi \tag{6.2}$$

that equals the Schrödinger equation (2.1) with an additional spin-sensitive interaction term. Here $\mu_\mathrm{B} = \frac{\hbar e}{2mc}$ is the absolute value of the electron's magnetic moment, also known as Bohr magneton. The specific setup of two counterpropagating waves with frequency ratio 1:2 is encoded by the vector potential

$$\vec{A}(z,t) = f(t)\left[\vec{A}_1(z,t) + \vec{A}_2(z,t)\right] \tag{6.3}$$

consisting of a right-travelling part of frequency ω

$$\vec{A}_1(z,t) = a_1\vec{e}_x\cos(\omega t - kz) \tag{6.4}$$

and a left-moving part of frequency 2ω

$$\vec{A}_2(z,t) = a_2\vec{e}_x\cos(2\omega t + 2kz)\ . \tag{6.5}$$

with amplitudes a_1 and a_2 respectively.* Since the vector potential is taken in Coulomb-gauge, $\vec{\nabla}\cdot\vec{A} = 0$ and $\vec{A}\cdot\vec{p} = 0$, we can split the potential into a spin-independent $V(t) = \frac{e^2}{2mc^2}\vec{A}^2$ and a spin-sensitive part $W(t) = \mu_\mathrm{B}\vec{\sigma}\cdot\vec{B}$. As in Chap. 2 we make a Fourier mode ansatz†

$$\psi(t,z) = \sum_{n\in\mathbb{Z}} c_n(t)e^{inkz + \frac{i}{\hbar}p_z z} = \sum_{n\in\mathbb{Z}} c_n(t)\,|n\rangle\ . \tag{6.6}$$

As we want to handle resonant scattering, we set $p_z = 0$ in favor of encoding the incident electron momentum with a suitable integer n. At the same time we have $p_x = 0$ by assumption, and by a suitable gauge transformation may further assume $p_y = 0$. It should be noted, that in contrast to (2.6) this ansatz contains momentum modes $|n\rangle$ which are equidistantly spaced by a *single* photon momentum. This reflects the nature of the interaction terms needed to be taken into account. The time dependent coefficients are Pauli spinors, encoding the spin degree of freedom by virtue of $c_n = \begin{pmatrix} c_n^\uparrow \\ c_n^\downarrow \end{pmatrix}$. Using this ansatz, the Pauli equation (6.2) transforms into the coupled system of differential equations

$$i\hbar\dot{c}_n(t) = E'_n c_n(t) + \mathcal{V}_n(t) + \mathcal{W}_n(t) \tag{6.7}$$

*It turns out that it is not beneficial here to encode the amplitudes with the mixing parameter α, that controlled the interference in part I, because the two waves render the interaction possible only in combination, obstructing interference.

† The ket-states $|n\rangle = e^{inkz + \frac{i}{\hbar}p_z z}$ form a Hilbert basis in the Hilbert space of $\frac{2\pi}{k}$-periodic functions equipped with the inner product $\langle\phi|\psi\rangle = \frac{k}{2\pi}\int_0^{\frac{2\pi}{k}} dz\,\phi^*(z)\psi(z)$.

which govern the temporal evolution of the coefficients c_n. The kinetic energy of state $|n\rangle$ is $E'_n = \frac{\hbar^2 k^2}{2m} n^2$. The potential energy terms can be categorized by the spin-independent part

$$\begin{aligned}\mathcal{V}_n(t) =& \frac{e^2}{8mc^2} f(t)^2 \Big[a_2^2 e^{4i\omega t} c_{n-4}(t) + 2a_1 a_2 e^{i\omega t} c_{n-3}(t) \\ &+ a_1^2 e^{-2i\omega t} c_{n-2}(t) + 2a_1 a_2 e^{3i\omega t} c_{n-1}(t) \\ &+ 2\left(a_1^2 + a_2^2\right) c_n(t) \\ &+ 2a_1 a_2 e^{-3i\omega t} c_{n+1}(t) + a_1^2 e^{2i\omega t} c_{n+2}(t) \\ &+ 2a_1 a_2 e^{-i\omega t} c_{n+3}(t) + a_2^2 e^{-4i\omega t} c_{n+4}(t) \Big] \end{aligned} \tag{6.8a}$$

and the spin-sensitive part

$$\begin{aligned}\mathcal{W}_n(t) =& \frac{i\hbar e\omega}{4mc^2} \sigma_y f(t) \Big[2a_2 e^{2i\omega t} c_{n-2}(t) + a_1 e^{-i\omega t} c_{n-1}(t) \\ &- a_1 e^{i\omega t} c_{n+1}(t) - 2a_2 e^{-2i\omega t} c_{n+2}(t) \Big] . \end{aligned} \tag{6.8b}$$

As before, the switching function $f(t)$ is set to one for this derivation.

To construct the Dyson-expansion of the amplitude for the transition from momentum mode $|-2\rangle$ to $|2\rangle$, we need the free propagator

$$U_0(t - t') = \sum_{n \in \mathbb{Z}} e^{-\frac{i}{\hbar} E'_n (t - t')} |n\rangle \langle n| \tag{6.9}$$

as well as the terms of (6.8) that allow for a combined momentum transfer of $4\hbar k$ without a change in energy. In other words, we need the summands which may be combined to a time independent product proportional to $e^{4ikz} = \sum_{n \in \mathbb{Z}} |n\rangle \langle n - 4|$.[‡] In this setup, those are

$$V_1(t) = \frac{e^2}{8mc^2} a_1^2 e^{-2i\omega t} \sum_{n \in \mathbb{Z}} |n\rangle \langle n - 2| , \tag{6.10a}$$

$$V_2(t) = \frac{e^2}{4mc^2} a_1 a_2 e^{i\omega t} \sum_{n \in \mathbb{Z}} |n\rangle \langle n - 3| , \tag{6.10b}$$

$$W_1(t) = \frac{i\hbar e\omega}{4mc^2} a_1 \sigma_y e^{-i\omega t} \sum_{n \in \mathbb{Z}} |n\rangle \langle n - 1| , \tag{6.10c}$$

$$W_2(t) = \frac{i\hbar e\omega}{2mc^2} a_2 \sigma_y e^{2i\omega t} \sum_{n \in \mathbb{Z}} |n\rangle \langle n - 2| . \tag{6.10d}$$

[‡] To be more precise, the correspondence between the state-vector operator and its position space representation is $\sum_{n \in \mathbb{Z}} \langle z|n\rangle \langle n|z'\rangle = e^{4ikz} \delta(z - z')$.

Emphasizing, that neither the zeroth nor the first order contribute to the desired transition, we calculate the Dyson expansion of the transition amplitude in second and third order as

$$\begin{aligned}
\langle 2|\, U(T)\, |-2\rangle \approx & -\frac{1}{\hbar^2}\int_0^T dt_1 \int_0^{t_1} dt_2\, \langle 2|\, U_0(T-t_1)[V(t_1)+W(t_1)] \\
& \times U_0(t_1-t_2)[V(t_2)+W(t_2)]U_0(t_2)\,|-2\rangle \\
& + \frac{i}{\hbar^3}\int_0^T dt_1 \int_0^{t_1} dt_2 \int_0^{t_2} dt_3\, \langle 2|\, U_0(T-t_1)[V(t_1)+W(t_1)] \\
& \times U_0(t_1-t_2)[V(t_2)+W(t_2)]U_0(t_2-t_3)[V(t_3)+W(t_3)]U_0(t_3)\,|-2\rangle \\
\approx & -\frac{ie^3\omega}{16\hbar m^2c^4} a_1^2 a_2 \sigma_y \left(I_+ + I_- + J_+ + J_-\right) \\
& + \frac{e^3\omega^3}{32m^3c^6} a_1^2 a_2 \sigma_y \left(K_1 + K_2 + K_3\right) .
\end{aligned} \tag{6.11}$$

In the last and in the next step, terms that do not grow, but only oscillate in the interaction time T are being neglected (see also App. A for the connection to the switching time). Besides, we have introduced abbreviations for the integrals with the time-dependent parts of the relevant processes. For example

$$\begin{aligned}
I_\pm &= \int_0^T dt_1 \int_0^{t_1} dt_2 e^{-\frac{i}{\hbar}E_2' T} e^{-\frac{i}{\hbar}\left(-E_2' \pm 2\hbar\omega\right)t_1} e^{-\frac{i}{\hbar}\left(E_2' \mp 2\hbar\omega\right)t_2} \\
&\approx \frac{i\hbar T e^{-\frac{i}{\hbar}E_2' T}}{E_2' \mp 2\hbar\omega}
\end{aligned} \tag{6.12}$$

for first emitting one 2ω-photon at t_2 via W_2 and then absorbing two ω-photons at t_1 via V_1 (I_+) or vice versa (I_-). Accordingly,

$$\begin{aligned}
J_\pm &= \int_0^T dt_1 \int_0^{t_1} dt_2 e^{-\frac{i}{\hbar}E_2' T} e^{-\frac{i}{\hbar}\left(-E_2' + E_1' \pm \hbar\omega\right)t_1} e^{-\frac{i}{\hbar}\left(E_2' - E_1' \mp \hbar\omega\right)t_2} \\
&\approx \frac{i\hbar T e^{-\frac{i}{\hbar}E_2' T}}{E_2' - E_1' \mp \hbar\omega}
\end{aligned} \tag{6.13}$$

describes the combined emission of one 2ω-photon with the absorption of one ω-photon at t_2 via V_2 and the consecutive absorption of another ω-photon at t_1 via W_1 (J_+) or vice versa (J_-). The sequential interaction with all three photons (twice via W_1, once

W_2) at times t_3, t_2, t_1 in three different orders results in the terms

$$\begin{aligned} K_1 &= \int_0^T dt_1 \int_0^{t_1} dt_2 \int_0^{t_2} dt_3 \\ &\qquad e^{-\frac{i}{\hbar}E_2' T} e^{-\frac{i}{\hbar}(-E_2'-2\hbar\omega)t_1} e^{-\frac{i}{\hbar}(E_1'+\hbar\omega)t_2} e^{-\frac{i}{\hbar}(E_2'-E_1'+\hbar\omega)t_1} \\ &\approx \frac{-\hbar^2 T e^{-\frac{i}{\hbar}E_2' T}}{(E_2' - E_1' + \hbar\omega)(E_2' + 2\hbar\omega)}, \end{aligned} \tag{6.14a}$$

$$K_2 \approx \frac{-\hbar^2 T e^{-\frac{i}{\hbar}E_2' T}}{(E_2' - E_1' + \hbar\omega)(E_2' - E_1' - \hbar\omega)}, \tag{6.14b}$$

$$K_3 \approx \frac{-\hbar^2 T e^{-\frac{i}{\hbar}E_2' T}}{(E_2' - 2\hbar\omega)(E_2' - E_1' - \hbar\omega)}. \tag{6.14c}$$

With these approximations in place, the transition amplitude is

$$\begin{aligned} &\langle 2| U(T) |-2\rangle \\ &\approx \frac{e^3\omega}{16m^2c^4} a_1^2 a_2 \sigma_y T e^{-\frac{i}{\hbar}E_2' T} \left[\frac{mc^2}{\hbar^2\omega^2 - m^2c^4} + \frac{3mc^2}{\frac{9}{4}\hbar^2\omega^2 - m^2c^4} \right] \\ &- \frac{\hbar^2 e^3 \omega^3}{32m^3c^6} a_1^2 a_2 \sigma_y T e^{-\frac{i}{\hbar}E_2' T} \frac{5m^2c^4}{2\left(\frac{9}{4}\hbar^2\omega^2 - m^2c^4\right)(\hbar^2\omega^2 - m^2c^4)} \\ &= \frac{e^3\omega}{4m^3c^6} a_1^2 a_2 \sigma_y T e^{-\frac{i}{\hbar}E_2' T} \frac{m^2c^4}{\frac{9}{4}\hbar^2\omega^2 - m^2c^4} \\ &\approx -\frac{e^3\omega}{4m^3c^6} a_1^2 a_2 \sigma_y T e^{-\frac{i}{\hbar}E_2' T} \end{aligned} \tag{6.15}$$

where we can deduce the Rabi frequency

$$\Omega_R' = \frac{e^3\omega}{2m^3c^6} a_1^2 a_2 \tag{6.16}$$

for this resonant process which involves a spin flip via σ_y. This result is obtained with the premise that the population probability for the scattered momentum state, as in Chap. 4, follows a Rabi oscillation. This adopts the form

$$|c_2^{\downarrow}(T)|^2 = \sin^2\left(\frac{1}{2}\Omega_R' T\right) \tag{6.17}$$

when starting with an electron of momentum $-2\hbar k$ and spin up, as described by the initial condition $c_{-2}^{\uparrow}(0) = 1$ (and vanishing amplitude for all other states).

6.2 Magnus Expansion and Effective Potentials

In [Smi+04], the authors raised the question, whether 3-photon Kapitza-Dirac diffraction in bichromatic counterpropagating laser waves can take place without a grating. Their

considerations involved the $\vec{p} \cdot \vec{a}$-term instead of $\vec{\sigma} \cdot \vec{B}$, but they concluded, that by averaging the classical trajectories over one laser period, a magnetic grating could be identified. In this section we ask a similar question for the $\vec{\sigma} \cdot \vec{B}$-Term. Our approach however is purely quantum mechanical and follows the ideas in [EB15]. By means of averaging the leading terms in a Magnus-expansion [Mag54] of the time-dependent Hamilton operator, we identify generalized versions of the ponderomotive potential used throughout Part I.

The complete solution to a Schrödinger equation with time-dependent Hamilton operator $H(t)$ can be given as the unitary time evolution operator $U(t, t_0)$. It is an ordered exponential defined by

$$\frac{\partial}{\partial t} U(t, t_0) = -\frac{i}{\hbar} H(t)\, U(t, t_0) \qquad \text{and} \qquad U(t_0, t_0) = 1 \tag{6.18}$$

and often colloquially written in the form

$$U(t, t_0) = \mathcal{T} \exp\left(-\frac{i}{\hbar} \int_{t_0}^{t} H(t')\, d\, t' \right) \tag{6.19}$$

with the time-ordering operator $\mathcal{T}$. A word of caution with the right-hand side of this formula needs to be spelled out, because the time ordering is to be done on the integrands inside the exponential power series, as can be seen in its expansion

$$\begin{aligned} U(t, t_0) = 1 &- \frac{i}{\hbar} \int_{t_0}^{t} d\, t_1 H(t_1) - \frac{1}{2\hbar^2} \int_{t_0}^{t} d\, t_1 \int_{t_0}^{t} d\, t_2 \mathcal{T}\left[H(t_1) H(t_2) \right] \\ &+ \frac{i}{6\hbar^3} \int_{t_0}^{t} d\, t_1 \int_{t_0}^{t} d\, t_2 \int_{t_0}^{t} d\, t_3 \mathcal{T}\left[H(t_1) H(t_2) H(t_3) \right] + \dots . \end{aligned} \tag{6.20}$$

Besides, the factors $H(t)$ in the products are always ordered by descending time from left to right. Because $U(T, 0)$, given fixed start $t_0 = 0$ and end times $t = T$, is a specific unitary operator, one could ask which time-independent Hamilton operator would have led to the same result without the complication of time ordering. This is more rigorously formulated by finding $\mathcal{M}(T)$ so that[§]

$$\exp\left(-\frac{i}{\hbar} \mathcal{M}(T) \right) = U(T, 0) = \mathcal{T} \exp\left(-\frac{i}{\hbar} \int_{0}^{T} H(t')\, d\, t' \right) . \tag{6.21}$$

By taking the logarithm of the recursive expansion of (6.20), an expansion series for $\mathcal{M}(T)$ emerges, which is called Magnus expansion. Sorted by powers of H one obtains

[§]This definition is made unique by the requirements that $\mathcal{M}(0) = 1$ and that it is continuous.

$\mathcal{M}(T) = \sum_{n\geq 1} \mathcal{M}_n(T)$, where the first three orders are given by

$$\mathcal{M}_1(T) = \int_0^T d\,t_1 H(t_1)\,, \tag{6.22a}$$

$$\mathcal{M}_2(T) = -\frac{i}{2\hbar}\int_0^T d\,t_1 \int_0^{t_1} d\,t_2\,[H(t_1), H(t_2)]\;, \tag{6.22b}$$

$$\begin{aligned}\mathcal{M}_3(T) = &-\frac{1}{6\hbar^2}\int_0^T d\,t_1 \int_0^{t_1} d\,t_2 \int_0^{t_2} d\,t_3 \\ &([H(t_1), [H(t_2), H(t_3)]] + [[H(t_1), H(t_2)]\, H(t_3)])\;.\end{aligned} \tag{6.22c}$$

In a way, the time ordering of (6.20) has been translated into the commutators here. A convenient property of these summands is, that they are all Hermitian, given that H had this property in the first place. We like to emphasize, that the ponderomotive potential in the traditional meaning (as used in chapter 2) together with the kinetic term can be recovered from the first order expression, by virtue of

$$\lim_{T\to\infty} \frac{\mathcal{M}_1(T)}{T} = \langle H(t)\rangle_t \tag{6.23}$$

whenever these limits and averages exist. In this specific case, it does not change the result, if we first average $\mathcal{M}_1(T)$ over the start and end time by one laser period, denoted by $\tilde{\mathcal{M}}_1(T)$. This corresponds in effect to smoothly switching on and off the interaction.

When applicable to higher orders of $\mathcal{M}(T)$ we interpret the result of this method as a generalized ponderomotive potential. In the following, it will be employed especially to identify these generalized ponderomotive potentials for linearly polarized bichromatic counterpropagating laser waves. Now by using the Pauli Hamiltonian with the vector potential (6.3), we find, after averaging over one laser period of the initial and final time,

$$\lim_{T\to\infty} \frac{\tilde{\mathcal{M}}_1(T)}{T} = -\frac{\hbar^2}{2m}\frac{\partial^2}{\partial z^2} + \frac{e^2\left(a_1^2 + a_2^2\right)}{4mc^2}\,, \tag{6.24a}$$

$$\lim_{T\to\infty} \frac{\tilde{\mathcal{M}}_2(T)}{T} = 0\,, \tag{6.24b}$$

$$\lim_{T\to\infty} \frac{\tilde{\mathcal{M}}_3(T)}{T} = -\frac{\hbar e^3 a_1^2 a_2 \omega}{2m^3c^6}\sigma_y \sin(4kz) + \frac{e^4\left(a_1^4 + a_2^4\right)}{64m^3c^6} + \frac{41e^4 a_1^2 a_2^2}{72m^3c^6} + \frac{e^2\left(a_1^2 + 4a_2^2\right)\omega^2}{16m^3c^6}\,. \tag{6.24c}$$

As the constant terms can be removed by a gauge transformation, we can identify a time independent effective Hamiltonian (compare the Hamiltonian with the ponderomotive potential in the standing wave case)

$$H_{\text{eff}} = \frac{\hbar^2}{2m}\frac{\partial^2}{\partial z^2} - \frac{\hbar e^3 a_1^2 a_2 \omega}{2m^3c^6}\sigma_y \sin(4kz)\,. \tag{6.25}$$

Employing the assumption, that only the coefficients $c_{\pm 2}$ can become substantial, the latter leads to

$$i\hbar\dot{c}_2(t) = E_2' c_2(t) + \frac{i\hbar}{2}\Omega_R' \sigma_y c_{-2}(t)\,, \tag{6.26a}$$

$$i\hbar\dot{c}_{-2}(t) = E_2' c_{-2}(t) - \frac{i\hbar}{2}\Omega_R' \sigma_y c_2(t)\,. \tag{6.26b}$$

This pair of coupled differential equations describes a resonant coupling between the two momentum states, resulting in well-understood Rabi cycles (compare (6.17)) [see also SZ97, Chap. 5.2.1].

6.3 Numerical Results

To underpin the results of the previous sections, we performed numerical simulations of the electron scattering with the Pauli equation in momentum space. The simulations have been carried out with a Runge-Kutta algorithm[¶] of (6.7) for the spinor coefficients c_n. The final scattering probability depending on the interaction time T for the fields described by (6.3) can be seen in Fig. 6.1. In the upper panel, the incident spin-up electron is partly scattered into the reflected spin-down state. After reaching a saturation, the probability is transferred back to the original state, starting the process over from the beginning. Especially, the probabilities of the spin-down state with the original momentum and the spin-up state with the reflected momentum are confined very close to zero. The lower panel shows, that this process is indeed symmetric under exchanging the spin states. In total, it is spin-independent and spin-flipping, leaving the electron in a state, where its spin and momentum are entangled.

Even though we originally expected nice Rabi cycles, we see cycles with reduced amplitude C and an increased oscillation frequency $\Omega > \Omega_R'$, hinting, that the process is not exactly resonant during the interaction. We account this to a field-induced detuning of the momentum states within the strong laser field. More details shall be presented in Sec. 6.4.

Although we stated earlier, that in this linearly polarized setup the Pauli equation is sufficiently accurate to predict the Rabi frequency, it might be that the results calculated with Dirac's equation differ sightly. For example, we have calculated the simulation in Fig. 6.1 again with Dirac's equation. The results, shown in Fig. 6.2, are qualitatively the same, but the oscillation amplitude is a bit larger and, at the same time, the oscillation frequency is slightly diminished. In the framework of the field induced detuning from the next section, both results at least agree on the Rabi frequency calculated before. They do however quantitatively abberate in the amount of detuning.

[¶] Specifically, we used a Runge-Kutta scheme with Dormand-Prince coefficients [DP80] of order 5 with automatic step size control in forth order.

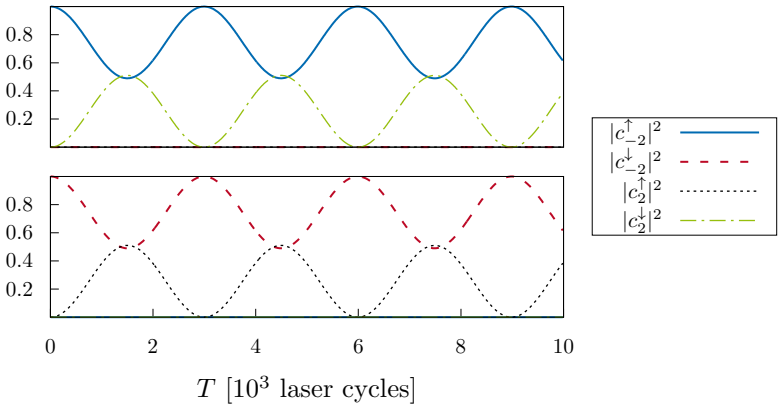

Figure 6.1: Dynamics of the Kapitza-Dirac effect with the Pauli-equation in bichromatic, linearly polarized, counterpropagating laser waves. The laser parameters are $\hbar\omega_1 = 2 \times 10^3$ eV, $\omega_2 = 2\omega_1$, $ea_1 = 5.656 \times 10^4$eV and $ea_2 = 2 \times 10^4$eV, giving a combined intensity of 6.543×10^{22} $\frac{\mathrm{W}}{\mathrm{cm}^2}$. The switching on and off takes place over 5 laser cycles each. The initial electron momentum is $-2\hbar k_1$ along the laser propagation direction and has no component parallel to the polarization direction. In the upper panel the electron is injected with spin up ($\uparrow$), and in the lower panel with spin down ($\downarrow$). Plotted are the occupation probabilities after an interaction of time T of the four momentum states fulfilling the Bragg condition in both panels. The interaction is independent of the initial electron spin, but it is always spin-flipping at the same time. The expected Rabi oscillation is not fully developed (here to an amplitude of approximately 0.510).

6.4 Field-Induced Detuning

In the last section it was shown, that the Rabi cycles of the three-photon Kapitza-Dirac effect are not always fully developed. Still the scattering probability has a nice oscillating behaviour, that can be mimicked by

$$|c_2^{\downarrow}(T)|^2 = C \sin^2\left(\frac{1}{2}\Omega T\right) \tag{6.27}$$

replacing (6.17). The Rabi-amplitude C and the measured oscillation frequency Ω have been introduced as new parameters.

A parameter scan where the amplitude C is measured depending on the laser frequency ω in the range 10 eV to 3×10^3 eV and $a_1^2 a_2$ (ranging from $ea_{1,2} = 2 \times 10^3$ eV to 4×10^4 eV) shows, that for small laser amplitudes the value of C is at least very close to 1 and decreases with higher $a_1^2 a_2$ but independent of k. Then a dyke-like structure emerges, where the amplitude reaches one again and then drops rapidly down to zero. The summit of this dyke can approximately be described by $e^3 a_1^2 a_2 \approx \hbar^2 \omega^2 10^6$ eV. To illustrate this result, a sketch of this dyke is given in Fig. 6.3.

While having a reduced amplitude C, the actual oscillation frequency Ω is increased

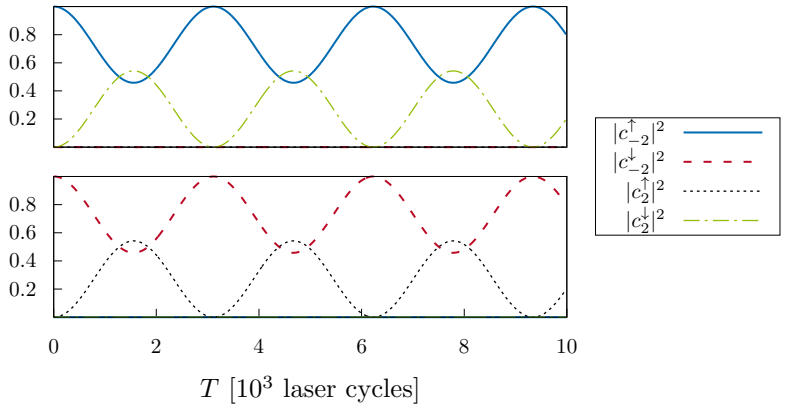

Figure 6.2: The same simulation as in Fig. 6.1, but instead calculated with the Dirac equation. One can see the qualitatively same behaviour, only the oscillation amplitude (here 0.542) and frequency differ slightly. The Dirac-spinors in the initial condition as well as for the projection of the final states are chosen as in (8.15) with $s = 0, 1$ for spin up or down respectively.

compared to the predicted Rabi frequency Ω'_R by

$$\Omega = \frac{1}{\sqrt{C}}\Omega'_R \,. \tag{6.28}$$

That way, the transition probability $|c_2^{\downarrow}(T)|^2 = \frac{C}{4}\Omega^2 T^2 + o(\Omega^3 T^3) = \frac{1}{4}{\Omega'_R}^2 T^2 + o(\Omega^3 T^3)$ for small interaction times ($T \ll \frac{1}{\Omega}$) still coincides, because the factor C drops out in the first relevant order of the expansion.

This behaviour indicates a detuning of the quantum two state system at hand, as can be seen in a very simple model of this interaction [compare SZ97, Chap. 5.2.1]. Assuming we only need to account for the states $|-2\ \uparrow\rangle$ and $|2\ \downarrow\rangle$, we take them as the orthonormal basis in the reduced Hilbert space. By reintroducing the small momentum offset p_z of the incident (and thereby every involved) momentum state (see Eq. (6.6)), we get an artificial relative detuning in the kinetic energy of the two states by $\frac{4\hbar k}{m}p_z$. Together with the yet undetermined detuning Δ, we can describe the reduced system with a Hamilton operator

$$H = \frac{1}{2}\begin{pmatrix} \delta & \Omega'_R \\ \Omega'_R & -\delta \end{pmatrix} \qquad \text{where} \qquad \delta = \Delta - \frac{4\hbar k}{m}p_z \,. \tag{6.29}$$

The time evolution operator of this Hamiltonian is

$$\begin{aligned} U(T) &= \exp\left(-\frac{i}{\hbar}HT\right) = \cos\left(\frac{\Omega}{2}T\right) - \frac{2i}{\hbar\Omega}\sin\left(\frac{\Omega}{2}T\right)H \\ &= \begin{pmatrix} \cos\left(\frac{\Omega}{2}T\right) - \frac{i\delta}{\hbar\Omega}\sin\left(\frac{\Omega}{2}T\right) & -\frac{i\Omega'_R}{\Omega}\sin\left(\frac{\Omega}{2}T\right) \\ -\frac{i\Omega'_R}{\Omega}\sin\left(\frac{\Omega}{2}T\right) & \cos\left(\frac{\Omega}{2}T\right) + \frac{i\delta}{\hbar\Omega}\sin\left(\frac{\Omega}{2}T\right) \end{pmatrix} \end{aligned} \tag{6.30}$$

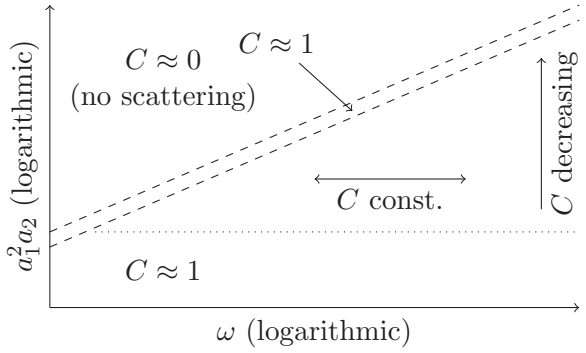

Figure 6.3: Sketch of the C dependence on ω and $a_1^2 a_2$. Various parameter regimes are indicated. The position of the dyke summit (dashed lines) is roughly described by $e^3 a_1^2 a_2 \approx \hbar^2 \omega^2 10^6$ eV (order of magnitude).

and its characteristic frequency manifests as

$$\Omega = \sqrt{{\Omega'_R}^2 + \frac{\delta^2}{\hbar^2}} = \sqrt{{\Omega'_R}^2 + \left(\frac{\Delta}{\hbar} - \frac{4kp_z}{m}\right)^2}\,. \tag{6.31}$$

With the off-diagonal terms of (6.30) we can predict the scattering probability

$$|\langle 2\ \downarrow|\, U(T)\,|-2\ \uparrow\rangle|^2 = \frac{{\Omega'_R}^2}{\Omega^2} \sin^2\left(\frac{\Omega}{2}T\right) \tag{6.32}$$

and derive the dependence of the effective Rabi amplitude on the detuning parameters to be

$$C = \frac{{\Omega'_R}^2}{\Omega^2} = \frac{1}{1 + \left(\frac{\Delta/\hbar - 4kp_z/m}{\Omega'_R}\right)^2}\,. \tag{6.33}$$

By scanning over the parameter p_z we can now determine the field induced detuning Δ numerically. This is exemplified in Fig. 6.4. A Lorentz-shaped resonance peak that is shifted by Δ, together with an equally shifted hyperbola for the oscillating frequency can be seen. A very similar description of the detuning effects in the relativistic 3-photon scattering from a standing wave can be found in [Ahr+13].

While having no real model for this detuning, it can be attributed to the phenomenon, that the presence of the laser field changes the electron momentum to a so-called dressed momentum (see also Sec.8.1). In Part I, this dressing effect happens symmetrically on both involved momentum states, due to the symmetric setup. Therefore the relative detuning in this case was immaterial. In the case of two counterpropagating waves of different frequencies, however, this symmetry is broken, and the originally equal energies of the momentum states may be detuned differently.

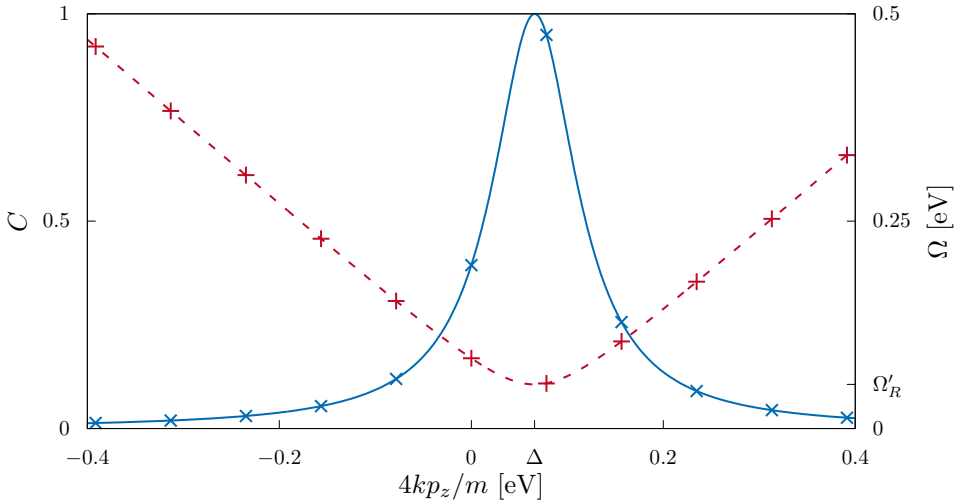

Figure 6.4: Resonance peak for spin-flipping 3-photon Kapitza-Dirac scattering. The laser frequency is $\hbar\omega = 1$ keV and the amplitudes are $ea_1 = ea_2 = 2.422 \times 10^4$ eV. The numerical data (blue crosses) is fitted with (6.33) (solid blue line) over Ω'_R and Δ. Simultaneously the numerical frequency (red pluses) is compared to (6.31) (dashed red line) with the same fit parameters. For convenience, the fit parameters are marked on the respective axis.

Chapter 7

Spin-Polarizing Beam Splitter

In this chapter we discuss the possibility to create a Stern-Gerlach device for free electrons. In their famous experiment [GS22], Stern and Gerlach have shown that a beam of silver atoms can be spatially separated by an inhomogeneous magnetic field depending on the total spin of the individual atom. However, for charged particles, the relatively small force introduced by the divergence of the magnetic field in their spin magnetic moment, is always significantly less important than the Lorentz force. Thus, in combination with Heisenberg's uncertainty principle, Bohr and Pauli concluded [MM65; BGS97; RG98b; RG98a; MBB11], it was impossible to separate electrons by their spin with considerations based on classical trajectories. This statement has since become part of textbooks paradigmatically denying the possibility to create a Stern-Gerlach device for free electrons.

In recent years, other attempts to tackle this assertion theoretically have been underway. For example a Wien filter for electron vortex beams has been proposed in [Kar+12], that couples spin angular momentum to orbital angular momentum. Other suggestions involve solid state nanostructures to create spin-polarized Talbot carpets [TPW12] or microscopic current loops [MBB11]. A Mach-Zehnder interferometer, where magnetic coils implement different phase shifts depending on the spin states in the two interferometer arms is envisaged in [MBB11]. Finally, a splitting of electrons propagating on axis by their spin state in circularly polarized standing waves has been proposed in [Ahr16]. There, a slight difference in the oscillation frequency for the two spin orientations along the beam axis can be exploited. By tailoring the interaction time, the electrons can be extracted polarized. Despite these efforts, the Bohr-Pauli conjecture still represents an open problem, as a clear analogy for the Stern-Gerlach effect with free electrons has not been realized yet.

The electron in the 3-photon Kapitza-Dirac process described in Chap. 6 is scattered in a quantum coherent way. We can now exploit this fact to construct a spin-polarizing beam splitter for free electrons based solely on Kapitza-Dirac like interactions in an interferometric setup. This proposal was first published in [DM17b]. The schematic construction of this beam splitter as shown in Fig. 7.1 consists of three stages. The first involves a spin-flipping bichromatic Kapitza-Dirac scattering. The interaction here is

ideally tuned to a quarter of a Rabi cycle, in order to split the beam in two halves of opposing z-polarization. The second and third stage on the other hand are composed by half and then another quarter of a Rabi cycle of the monochromatic spin-independent and non-flipping interaction described in Chap. 4. For simplicity we chose the second harmonic of the laser for the later stages, so that they are two-photon processes. That way, the second stage reflects both emerging beams back on themselves, and the third stage acts as the final beam splitting mirror in the interferometer recombining their halves coherently into the two outgoing beams. The fact, that the two resulting beams are linear superpositions, allows their spin state to be predetermined, as we shall see.

We point out that a spin-insensitive interferometer based on Kapitza-Dirac diffraction has been proposed in [Mar13] for electrons. For ions, a similar setup has been implemented for gravitational studies in the GAIN project [Sch+15].

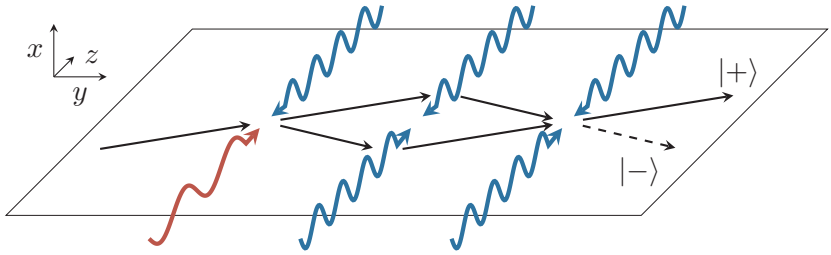

Figure 7.1: Schematic setup of the spin-polarizing beam splitter. The electron beam while travelling from left to right experiences three stages of Kapitza-Dirac scattering. It is first split in two portions by the bichromatic setup with frequencies ω (red) and 2ω (blue). Afterwards both partial beams are reflected into a diamond shape and coherently superposed by scattering from standing laser waves with frequency 2ω (blue). The outgoing beam leaves this interferometer on the right side separated by its spin component measured along the laser magnetic field direction. In analogy to the Stern-Gerlach experiment, we obtain a clear spatial separation of the beams.

7.1 Analytical Considerations

As all three stages are working in the Bragg regime on the same momentum states, we can restrict our analysis to the four-dimensional subspace spanned by the two momentum states $|\mp 2\rangle$ in both spin states. We will use the notation of a vector with two Pauli-spinors. Shifted down by the kinetic energy E_2', to enter the interaction picture, the effective Hamiltonian (6.25) for the bichromatic interaction takes the form

$$H_\mathrm{b} = \frac{\hbar\Omega_R'}{2}\begin{pmatrix} \mathbf{0} & -i\sigma_y \\ i\sigma_y & \mathbf{0} \end{pmatrix} \tag{7.1}$$

This leads to the time evolution operator

$$U_{\mathrm{I}} = \begin{pmatrix} \cos\left(\frac{\Omega_R' T_{\mathrm{b}}}{2}\right)\mathbf{1} & -\sin\left(\frac{\Omega_R' T_{\mathrm{b}}}{2}\right)\sigma_y \\ \sin\left(\frac{\Omega_R' T_{\mathrm{b}}}{2}\right)\sigma_y & \cos\left(\frac{\Omega_R' T_{\mathrm{b}}}{2}\right)\mathbf{1} \end{pmatrix} = \frac{1}{\sqrt{2}}\begin{pmatrix} \mathbf{1} & -\sigma_y \\ \sigma_y & \mathbf{1} \end{pmatrix} \tag{7.2}$$

for the first stage, when substituting the interaction time $T_{\mathrm{b}} = \frac{\pi}{2\Omega_R'}$ for a quarter of a Rabi cycle.

The monochromatic standing wave of the second harmonic is described by setting $\alpha^2 = 0$ in (2.4). The parameter δ now helps to position the nodes of this standing wave relative to the effective ponderomotive potential of the first stage.* In the same way as before, the effective Hamiltonian to this standing wave is reduced to

$$H_{\mathrm{m}} = \frac{\hbar\Omega_R}{2}\begin{pmatrix} \mathbf{0} & e^{-i\delta}\mathbf{1} \\ e^{i\delta}\mathbf{1} & \mathbf{0} \end{pmatrix} \tag{7.3}$$

with its corresponding Rabi frequency Ω_R (compare (4.1)). The time evolution operators for the second and third stage with the appropriate timings are

$$U_{\mathrm{II}} = \begin{pmatrix} \mathbf{0} & -ie^{-i\delta}\mathbf{1} \\ -ie^{i\delta}\mathbf{1} & \mathbf{0} \end{pmatrix} \tag{7.4}$$

and

$$U_{\mathrm{III}} = \frac{1}{\sqrt{2}}\begin{pmatrix} \mathbf{1} & -ie^{-i\delta}\mathbf{1} \\ -ie^{i\delta}\mathbf{1} & \mathbf{1} \end{pmatrix} \tag{7.5}$$

respectively. Combining the time evolution operators in the order described earlier†, results in the total time evolution operator

$$U = U_{\mathrm{III}}U_{\mathrm{II}}U_{\mathrm{I}} = \frac{1}{2}\begin{pmatrix} -\mathbf{1} - ie^{-i\delta}\sigma_y & -ie^{-i\delta}\mathbf{1} + \sigma_y \\ -ie^{i\delta}\mathbf{1} - \sigma_y & -\mathbf{1} + ie^{i\delta}\sigma_y \end{pmatrix}. \tag{7.6}$$

The spin filtering effect can be achieved for $\delta = \frac{\pi}{2}$, where we have

$$U = \frac{1}{2}\begin{pmatrix} -\mathbf{1} - \sigma_y & -\mathbf{1} + \sigma_y \\ \mathbf{1} - \sigma_y & -\mathbf{1} - \sigma_y \end{pmatrix}. \tag{7.7}$$

To ease the discussion, we introduce the spin-basis $|\pm\rangle := \frac{1}{\sqrt{2}}(|\uparrow\rangle \pm i\,|\downarrow\rangle)$ of σ_y-eigenstates. When starting with an electron ensemble of momentum $2k$ and arbitrary spin distribution described by a vector $\vec{n} = (n_x, n_y, n_z)$ in the Bloch sphere, applying the beam splitting procedure to the initial density matrix results in

$$\rho = U\begin{pmatrix} \mathbf{0} & \mathbf{0} \\ \mathbf{0} & \frac{1}{2}(\mathbf{1} + \vec{n}\cdot\vec{\sigma}) \end{pmatrix}U^\dagger = \frac{1}{4}\begin{pmatrix} (1-n_y)(\mathbf{1}-\sigma_y) & \left(n^\perp - i\vec{e}_y\times\vec{n}\right)\cdot\vec{\sigma} \\ \left(n^\perp + i\vec{e}_y\times\vec{n}\right)\cdot\vec{\sigma} & (1+n_y)(\mathbf{1}+\sigma_y) \end{pmatrix}. \tag{7.8}$$

*In [DM17b] the parameter δ is called χ.

†The operators are multiplied in descending order, so that U_{I} acts first on a state. This rule is known by the mnemonic 'later left'.

Here the parallel projection of $\vec{n}$ onto the x-z-plane along $\vec{e}_y$ has been called $n^\perp$. The upper left component implies, that the electron is prepared in the spin state $|-\rangle$ if scattered into momentum mode $|-2\rangle$. On the other hand, if not scattered (see the lower right component), the spin state is purely $|+\rangle$. Their probabilities coincide with the probabilities of having been in the same spin state beforehand. To exemplify this statement, we like to take a closer look at some corner cases of y-polarized spin. For an unpolarized electron beam ($\vec{n} = 0$) the density matrix ρ reduces to

$$\rho_{\text{unpol}} = \frac{1}{4}\begin{pmatrix} \mathbf{1} - \sigma_y & \mathbf{0} \\ \mathbf{0} & \mathbf{1} + \sigma_y \end{pmatrix} . \tag{7.9}$$

This corresponds to an equally distributed probability over the two states $|2, +\rangle$ and $|-2, -\rangle$. It can be interpreted, that the uncertainty of the incident spin is translated into momentum uncertainty. At the same time, the knowledge of the incident momentum is transferred to the knowledge of a specific spin state in every final momentum state. Further, if starting with a pure, y-polarized electron state ($\vec{n} = \pm\vec{e}_y$), the resulting density matrices read

$$\rho_+ = \frac{1}{2}\begin{pmatrix} \mathbf{0} & \mathbf{0} \\ \mathbf{0} & \mathbf{1} + \sigma_y \end{pmatrix} , \qquad \rho_- = \frac{1}{2}\begin{pmatrix} \mathbf{1} - \sigma_y & \mathbf{0} \\ \mathbf{0} & \mathbf{0} \end{pmatrix} . \tag{7.10}$$

Here, the electron remains in its initial spin state, and it is scattered into the mirrored momentum state if and only if previously it was in state $|2, -\rangle$.

Combining these results, we can state, that the action of the device described above is spin-dependent and non-flipping, when quantising the spin along the magnetic field direction. With these properties, we are confident to call this setup a spin-polarizing beam splitter for free electrons, or a Stern-Gerlach device.

7.2 Numerical Simulation

To present some resilient arguments, we performed real-space numerical simulations of the beam splitter. To this end, Pauli's equation was solved by Fourier split step methods in $z - t$-coordinates. A Gaussian wave packet with central momentum $p_z = 400\ \frac{\text{eV}}{c}$ and width 39.4 nm has been subject to the laser fields described as the three stages before. The laser parameters are $\hbar\omega = 200$ eV for the fundamental mode, and $ea_1 = ea_2 = 2.35 \times 10^4$ eV in the first stage. The chosen interaction time is $T_\text{b} = 106$ fs. The second and third stage have frequency $400\ \frac{\text{eV}}{\hbar}$, and amplitude 200 V. They can, alternatively, be represented by the vector potential (2.4) when using the parameters $\hbar\omega = 200$ eV, $ea_0 = 4 \times 10^2$ eV, $\alpha^2 = 0$ and $\delta = \frac{\pi}{2}$. Their interaction durations are 212 fs and 106 fs respectively. Switching on and off the fields takes 5 fs every time.

As can be seen in the projection on the σ_z-eigenstates in Fig. 7.2, the electron is partly scattered by the first stage, while the spin of the scattered part is opposite to the incident one. At the second stage both outwards moving beams are almost completely reflected, and then, at the third stage, after closing the diamond shape, they are crossed over and

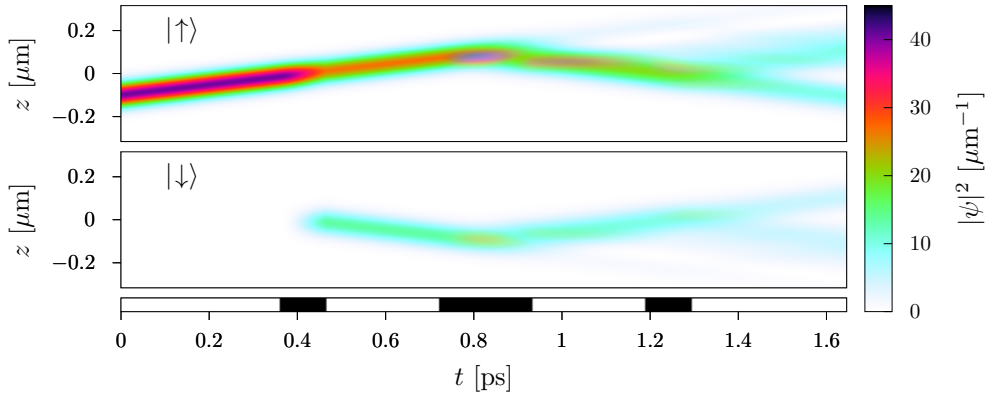

Figure 7.2: Simulation of the beam splitter with a wave packet of central momentum $p_z = 400\ \frac{\text{eV}}{c}$ and width 39.4 nm. The fundamental laser frequency is $\hbar\omega = 200$ eV. In the first stage, the bichromatic lasers with $ea_1 = ea_2 = 2.35 \times 10^4$ eV are switched on for 106 fs. The second and third stage have $ea_0 = 200$ eV for 212 fs or 106 fs, respectively. Plotted is the spatial probability density projected on σ_z-eigenstates $|\uparrow\rangle$ and $|\downarrow\rangle$. Additionally, the interaction time of the three stages is marked in the bottom part.

thereby brought to interference. The actual beam splitting impact on the electron can be seen, when looking at the same simulation in the projection on σ_y-eigenstates $|\pm\rangle$ in Fig. 7.3. The originally z-polarized state now appears distributed to equal parts on both spin states. So do the reflected parts after the first stage, and since the second stage is indifferent with respect to spin, nothing changes until the third stage. After the latter, the two beams are brought to interference, and the tight coupling between momentum and spin, as predicted, is revealed. The coupling is, however, less tight, than expected, but can be substantially improved, as shown in the next section.

7.3 Discussion

At this point, the experimental realizability of this beam splitter shall be discussed representatively for all the processes described within this part. We focus our attention on the bichromatic first stage, since it is deemed to be the most challenging. Also due to the lower intensity needed, the second and third stage might be realized by coupling out a small portion of the second harmonic laser beam. The intensity of the XUV beams used in our numerical simulation is $I_1 = 7.56 \times 10^{19}\ \frac{\text{W}}{\text{cm}^2}$ for the fundamental mode and $I_2 = 4I_1$ for the second harmonic. This corresponds to small values of the relativistic parameter $\xi_{1,2} = \frac{ea_{1,2}}{mc^2} \approx 0.05$. Note, that it is not necessarily only the beam intensity whose requirements are demanding, but also the total beam energy. The Rabi frequency $\Omega'_R = \frac{1}{2}\xi_1^2\xi_2\omega \approx 10\ \frac{\text{meV}}{\hbar}$ (1.5×10^{13} Hz) requires the interaction duration $T_\text{b} \approx 0.1$ ps which is a lower bound on the laser pulse duration $\Delta\tau \gtrsim T_\text{b}$. On the other hand it poses a constraint on the focal width $\Delta y \gtrsim vT_\text{b} \approx 0.3\ \mu$m. An electron velocity $v = 0.01\ c$ was

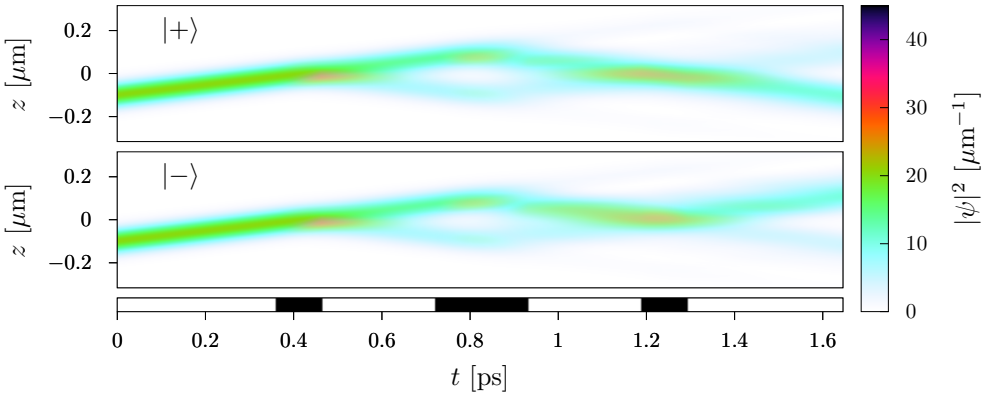

Figure 7.3: The same simulation as in Fig. 7.2. This time the wave function is projected on σ_y eigenstates $|\pm\rangle$. One can see, that the two spin states are heavily weighted in the two momentum modes. A polarization degree of $\kappa \approx -0.33$ is reached.

assumed resulting from a kinetic energy of 30 eV. Assuming, a spherical beam waist for the laser ($\Delta x = \Delta y$), a total pulse energy of 50 mJ seems to be a plausible requirement. This lies rather close to the performance of modern X-Ray free electron laser facilities such as the LCLS (Stanford/ California). XUV pulses with up to 10^{18} $\frac{\mathrm{W}}{\mathrm{cm}^2}$ over about 0.1 ps and pulse energies of a few mJ are available there [LCLS]. Advanced techniques for focusing X-Ray beams to sub μm spot sizes, based on adiabatically focusing refractive lenses or wave guides, as proposed in [Cor+04; SL05; Jar+05] may also be very helpful.

To realize a proper beam splitter, some parameters need to be carefully adjusted. For example the transverse momentum needs to fulfill the Bragg condition $p_z = 2\hbar k$. Judging from the width of the Lorentz-shaped resonance curve (6.33), the relative uncertainty should satisfy $\frac{\Delta p_z}{p_z} \lesssim \frac{m\Omega'_R}{4\hbar k} = \frac{mc\xi_1^2\xi_2}{8\hbar k}$. For the parameters chosen in the simulations above, this translates to $\frac{\Delta p_z}{p_z} \lesssim 0.04$, which is fulfilled with ease by the wave packet's relative momentum width $\frac{\Delta p_z}{p_z} = 0.003$.

The scattering probability $P_{\mathrm{scatt}} = \sin^2\left(\frac{\Omega'_R}{2}T\right)$ of the first stage, whose ideal value is $\frac{1}{2}$, depends on the actual interaction time $T = \frac{mL}{p_y}$ as a function of the transverse momentum p_y and the spatial transverse beam width L. For the uncertainty in this probability one finds

$$\frac{\Delta P_{\mathrm{scatt}}}{P_{\mathrm{scatt}}} = \frac{\pi}{2}\frac{\Delta T}{T} = \frac{\pi}{2}\left(\frac{\Delta p_y}{p_y} + \frac{\Delta L}{L}\right). \tag{7.11}$$

Also, the momentum component p_x along the laser polarization direction can vary from being exactly zero. This can lead to spin-insensitive (and therefore non-flipping) scattering events in the first stage due to the interaction term $\vec{p}\cdot\vec{A}$. As will be shown in Chap. 8, the relative scattering probability of this undesired side effect is $\frac{\Omega_{\mathrm{no-flip}}}{\Omega'_R} = \frac{5\Delta p_x}{2\hbar k}$. We conclude, that $\Delta p_x \ll \hbar k$ must be fulfilled, in order to keep the influence from this momentum component negligible.

Finally, the field induced detuning in the first step has two mechanisms that impose a negative impact on the performance of the beam splitter. First, the reduced oscillation amplitude leads to an uneven splitting of the beam in the first stage. This results in improper polarization because the destructive interference in the last step for either spin states cannot be complete. It might be enhanced by choosing parameters with an oscillation amplitude of at least one half and a correspondingly adjusted interaction time in stage one. Second, the different in-field energy levels of the two momentum states conducts them to build up a relative phase. The latter can however be counteracted by adjusting δ. The final polarization degree $\kappa = \frac{\rho_{|+\rangle} - \rho_{|-\rangle}}{\rho_{|+\rangle} + \rho_{|-\rangle}}$ measured over the portion of the resulting beam with positive momentum, as a function of δ can be seen in Fig. 7.4.

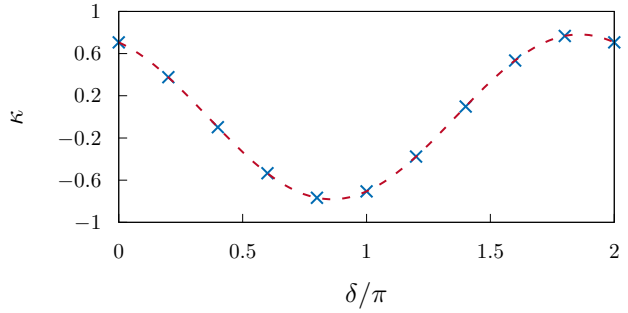

Figure 7.4: δ-dependency of the final polarization degree κ in the positive-momentum part of the split wave packet. The blue crosses represent numerically obtained values, while the dashed red line is a fit of $C_0 \sin(\delta + \Delta)$ over C_0 and Δ.

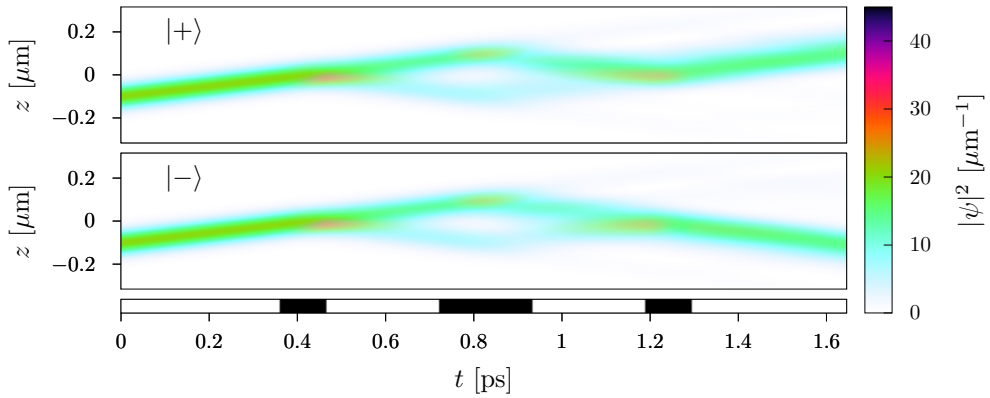

Figure 7.5: Simulation of the spin-polarizing beam splitter with $\delta = -\frac{\pi}{10}$ and otherwise the same parameters as in Fig. 7.3. The separation of the spin states is dramatically improved ($\kappa \approx 0.78$).

It supports our previous statement, and tells us, that the best polarization can be achieved with the special choice $\delta = -\frac{\pi}{10}$. A corresponding simulation has been carried

out and is presented in Fig. 7.5. Indeed, the polarization degree is largely augmented to $\kappa \approx 0.78$.

Additionally, Fig. 7.4 suggests, that we can invert the polarization. The result of choosing $\delta = \frac{9\pi}{10}$ can be seen in Fig. 7.6. There, the clear visible effect of exchanging the output channels is in aggreement with the measured value $\kappa \approx -0.78$.

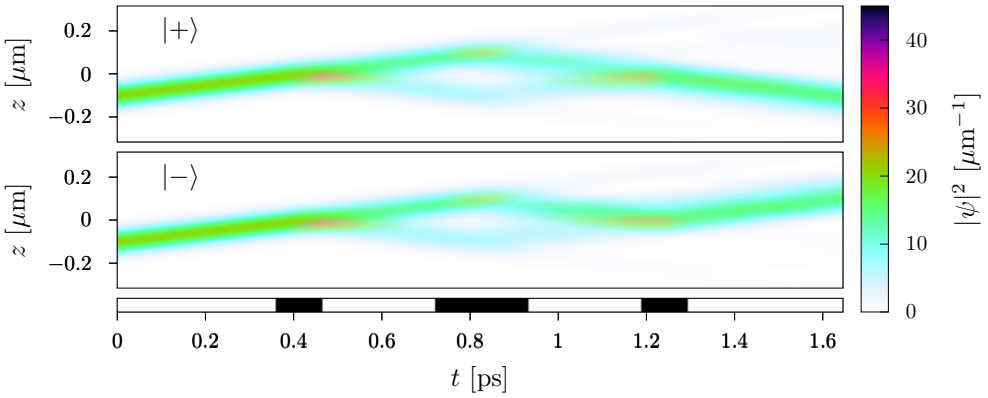

Figure 7.6: Simulation of the spin-polarizing beam splitter with $\delta = \frac{9\pi}{10}$ and otherwise the same parameters as in Fig. 7.3. The correlation of spin and momentum is inverted compared to Fig. 7.5 ($\kappa \approx -0.78$).

As a final remark, we conclude, that a Stern-Gerlach magnet for free electrons has been realized. Especially, electrons, that are already spin-polarized along the y-axis, are deflected accordingly without spin-flip in this device. The analogy, however, is only to be understood regarding the outcome, two spatially separated spin-polarized beams.

Chapter 8

Other Polarizations

In this chapter, we generalize the setup investigated in Chap. 6 in two ways. We keep the general scheme of two counterpropagating laser waves with a frequency ratio of 1:2, and scatter an electron with longitudinal momentum of $-2\hbar k$. But on the one hand, we introduce the transverse electron momentum into the considerations. This allows us to account for the influence of the interaction term $\propto \vec{p} \cdot \vec{A}$. On the other hand, we generalize the polarization of both laser beams to arbitrary directions and circular or elliptical modes. By attributing a definite spin of $+1$ (or -1 for the opposite rotation) to the helicity of circularly polarized photons, we can refine the picture of adding spin angular momentum in the non-relativistic limit delineated in Chap. 5.

Despite keeping the involved frequencies and momenta non-relativistic, it has been pointed out in [EB15], that the interaction with elliptically polarized light cannot be appropriately described within the Pauli equation. To include the spin density cropping up there, either the full Dirac equation itself, or more orders of the Foldy-Wouthuysen transformation [FW50] thereof must be employed. Both the time-dependent perturbation theory of Sec. 6.1 as well as the generalized ponderomotive potential approach of Sec. 6.2 should in principle lead to useful results here. But, being third-order approximations, they both promise to require too much complexity even for computer algebra. A third approach, involving techniques known as strong-field approximation, can however be gainfully utilized. By treating the fundamental laser mode within Volkov states for the incident, as well as the scattered electron, the 3-photon process can be represented within a dressed S-matrix approach, thereby limiting its complexity to the first order in a_2 (see Eq. (8.12) below).

A simpler version of this calculation for linearly polarized light can be found in App. B of [DAM16], and the full calculation with its conclusions also in [DM17a].

8.1 Dirac-Volkov S-Matrix Approach

The evolution of the quantum wave function of a possibly relativistic electron in the presence of a given external electromagnetic 4-potential* $A = (\phi, \vec{A})$ is described by the Dirac equation

$$\left(i\hbar\partial\!\!\!/ + \frac{e}{c}A\!\!\!/(x) - m\right)\psi(x) = 0\,. \tag{8.1}$$

In this formulation the pairwise anti-commuting, trace-free Dirac-gamma matrices

$$\gamma^0 = \begin{pmatrix} \mathbf{1} & \mathbf{0} \\ \mathbf{0} & -\mathbf{1} \end{pmatrix} \qquad \vec{\gamma} = \begin{pmatrix} \mathbf{0} & \vec{\sigma} \\ -\vec{\sigma} & \mathbf{0} \end{pmatrix} \tag{8.2}$$

have been introduced, and the inner product with their 4-vector is denoted by the Feynman slash notation $A\!\!\!/ = \gamma \cdot A$.

For a special class of 4-potentials, there exists a family of closed solutions to the Dirac equation (8.1) called Volkov states [BLP96]:

$$\psi_{p,s}(x) = \sqrt{\frac{mc}{Vp^0}}\left(1 - \frac{ek\!\!\!/A\!\!\!/_1(k\cdot x)}{2ck\cdot p}\right)u_{p,s}e^{-\frac{i}{\hbar}p\cdot x + \frac{i}{\hbar}\Lambda_p}\,. \tag{8.3}$$

The condition on the 4-potential is, that it involves only wave 4-vectors of a common direction ($\propto k = \left(\frac{\omega}{c}, \frac{\omega}{c}\vec{e}_z\right)$ without loss of generality).† This potential enters (8.3) in the form $\mathcal{A}_1(k\cdot x) = A_1(x)$ taken in radiation gauge (here $k \cdot A_1 = 0$). The existence of these solutions is closely related to the kinematically forbidden absorption of any number of photons from that wave without the possibility to deposit the excess 4-momentum, e.g. on a nearby nucleus or into a Compton-photon. Here $p = (p^0 = \sqrt{m^2c^2 + \vec{p}^2}, \vec{p})$ is the canonical 4-momentum of the electron in the limit $\vec{A} \to 0$. The index $s \in \{0, 1\}$ denotes one of two possible spin states and $u_{p,s}$ is the corresponding Dirac-spinor to a plane wave. The additional term in the exponent is

$$\Lambda_p = \frac{1}{ck\cdot p}\int^{k\cdot x}\left[ep\cdot\mathcal{A}_1(\Phi) + \frac{e^2}{2c}\mathcal{A}_1^2(\Phi)\right]d\Phi \tag{8.4}$$

and resembles in classical, non-quantum terms the extra action, imbued on the point-like electron equivalent by the presence of the field, compared to the usual free motion action $p \cdot x$.

In case of a single plane wave

$$A_1(x) = \Re\left(\epsilon_1 a_1 e^{-ik\cdot x}\right) \tag{8.5}$$

with a complex polarization 4-vector $\epsilon_1 = (0, \vec{\epsilon})$ satisfying $\epsilon_1^* \cdot \epsilon_1 = -1$ and $\epsilon_1 \cdot k = 0$, the extra phase factor given by the Volkov action can be further simplified. Let us consider

*In this chapter we use 4-vectors in Minkowski space. Their inner product is denoted by $A \cdot B$ and the metric is chosen with the signature $(+ - - -)$.

†This also precludes any additional electro- or magnetostatic potential, like a Coulomb field of a nucleus or a static field from a plate capacitor or a coil.

the two corner cases of a linearly and a circularly polarized plane wave respectively. The electron canonical momentum shall remain fixed in the x-z-plane. Without loss of generality, we can choose $\epsilon_1 \cdot p$ to be real, but note, that $\epsilon_1^2 = -\rho e^{i\delta}$ might still be a complex number with absolute value ρ ranging from one for linear polarization to zero for circular polarization. Then,

$$\begin{aligned} e^{\frac{i}{\hbar}\Lambda_p} &= \exp\left[i\frac{ea_1 p\cdot\epsilon_1}{\hbar ck\cdot p}\sin(k\cdot x) + i\frac{e^2a_1^2}{8\hbar c^2 k\cdot p}\Re\left(i\epsilon_1^2 e^{-2ik\cdot x}\right) - i\frac{e^2a_1^2}{4\hbar c^2 k\cdot p}k\cdot x\right] \\ &= \exp\left[-i\alpha_p\sin(k\cdot x) - i\rho\beta_p\Re\left(ie^{i\delta}e^{-2ik\cdot x}\right) - 2i\beta_p k\cdot x\right] \\ &= \sum_{n\in\mathbb{Z}} J_n^{(2)}(\alpha_p, \rho\beta_p; e^{i\delta})e^{-ink\cdot x - 2i\beta_p k\cdot x} \end{aligned} \tag{8.6}$$

where the generalized Bessel functions $J_n^{(2)}(u,v;s) = \sum_\ell J_{n-2\ell}(u)s^\ell J_\ell(v)$ and the abbreviations

$$\alpha_p = -\frac{ea_1}{\hbar c}\frac{p\cdot\epsilon_1}{k\cdot p}\,, \qquad \beta_p = \frac{e^2a_1^2}{8\hbar c^2}\frac{1}{k\cdot p} \tag{8.7}$$

have been used. First, for the linear polarization ($\rho = 1, \delta = 0$), we obtain

$$e^{\frac{i}{\hbar}\Lambda_p} = \sum_{n\in\mathbb{Z}} J_n^{(2)}(\alpha_p, \beta_p; 1)e^{-ink\cdot x - 2i\beta_p k\cdot x}\,. \tag{8.8}$$

At this point the Volkov state can be interpreted as a linear combination of plane waves. Especially, assuming for a moment $p\cdot\epsilon_1 = 0$ and henceforth $\alpha_p = 0$ they read

$$\begin{aligned} \psi_{p,s}(x) &= \sqrt{\frac{mc}{Vp^0}}\left(1 - \frac{e\not{k}\not{A}_1(k\cdot x)}{2ck\cdot p}\right)u_{p,s}e^{-i(\frac{p}{\hbar}+2\beta_p k)\cdot x}\sum_{\ell\in\mathbb{Z}} J_\ell(\beta_p)e^{-2i\ell k\cdot x} \\ &= \sqrt{\frac{mc}{Vp^0}}\sum_{\ell\in\mathbb{Z}}\left(J_\ell(\beta_p)e^{-2i\ell k\cdot x} - \frac{ea_1\not{k}\not{\epsilon}_1}{4ck\cdot p}\left(J_\ell(\beta_p) + J_{\ell+1}(\beta_p)\right)e^{-i(2\ell+1)k\cdot x}\right)u_{p,s}e^{-\frac{i}{\hbar}q\cdot x}\,. \end{aligned} \tag{8.9}$$

Each term in the sum represents now the projection of the complete Volkov state (8.3) on a plane wave with virtually absorbed photons. Note, that the components with an even photon number exhibit the same spin state s as the original electron. On the other hand, for an odd photon number, there is the factor $\not{k}\not{\epsilon}_1$ involved. This forces, at least in the low-energy limit, a flip of the spin when measured along the optical axis. Additionally, the common canonical momentum of the electron is changed to $q = p + 2\hbar\beta_p k$, the dressed version.

In case of circular polarization we can chose the explicit polarization 4-vector $\epsilon_1 = \frac{1}{\sqrt{2}}(0,1,i,0)$, leading to $\rho = 0$ and δ being immaterial. The extra phase factor is now

$$e^{\frac{i}{\hbar}\Lambda_p} = \sum_{n\in\mathbb{Z}} J_n(\alpha_p)e^{-ink\cdot x - 2i\beta_p k\cdot x}\,. \tag{8.10}$$

Therefore we arrive at the following decomposition of virtually absorbed photons

$$\begin{aligned}\psi_{p,s}(x) &= \sqrt{\frac{mc}{Vp^0}}\left(1-\frac{e\not{k}\not{A}_1(k\cdot x)}{2ck\cdot p}\right)u_{p,s}e^{-i(\frac{p}{\hbar}+2\beta_p k)\cdot x}\sum_{n\in\mathbb{Z}}J_n(\alpha_p)e^{-ink\cdot x}\\ &= \sqrt{\frac{mc}{Vp^0}}\sum_{n\in\mathbb{Z}}\left(J_n(\alpha_p)-\frac{ea_1\not{k}\not{\epsilon}_1}{4ck\cdot p}J_{n-1}(\alpha_p)-\frac{ea_1\not{k}\bar{\not{\epsilon}}_1}{4ck\cdot p}J_{n+1}(\alpha_p)\right)e^{-ink\cdot x}u_{p,s}e^{-\frac{i}{\hbar}q\cdot x}\end{aligned} \tag{8.11}$$

for arbitrary values of α_p. Here, we can see that, in the low energy limit, the electron can only ever absorb or emit a single photon at a time. Furthermore, in that limit, or for vanishing $\vec{p}\cdot\vec{A}$ (i.e. $\alpha_p = 0$), only $n = 0, \pm 1$ contribute, because all other Bessel functions vanish identically. The electron can therefore only enter intermediate states with at most one absorbed or emitted photon at a time. Additionally the latter is necessarily accompanied by the spinor being multiplied by $\not{k}\not{\epsilon}_1$ or $\not{k}\bar{\not{\epsilon}}_1$ respectively.[‡] Those operators not only induce a spin flip, but are also sensitive to the original spin (Given a spin polarized in z-direction, only one of them has a non-vanishing result.).

It is possible to describe the two-color Kapitza-Dirac effect in a low-energy limit of this strong-field approximation. Unfortunately, a full high-energy treatment is impossible in this way, because A_2 can only be treated perturbatively. To investigate the transition probability from the incident electron state to the scattered state, we start at the S-matrix as used for multi-photon Compton-scattering [IKS04; BDF12; KK13]

$$\mathcal{S} = \frac{ie}{\hbar c}\int d^4x\,\bar{\psi}_{p',s'}\not{A}_2\psi_{p,s}\,. \tag{8.12}$$

The influence of A_1 is encoded in the Volkov-states and therefore we need only one interaction vertex with A_2.

We do not consider the dressing of the momentum by the global factor $e^{-\frac{i}{\hbar}q\cdot x}$ at this point, since we cannot account for the possibly compensating corresponding effect imposed by A_2. The best approach might be, to treat the combined dressing as an arbitrary field induced detuning in the same way as in Sec. 6.4. We can than infer the Rabi frequency from the short time scattering behaviour.

A similar consideration as done for the Volkov states individually can be done for the combined extra phase factor in the S-matrix. In this case,

$$\begin{aligned}e^{\frac{i}{\hbar}\Lambda_p-\frac{i}{\hbar}\Lambda_{p'}} &= \exp\left[-i\left(\alpha_p-\alpha_{p'}\right)\sin(k\cdot x)-i\rho\left(\beta_p-\beta_{p'}\right)\Re\left(ie^{i\delta}e^{-2ik\cdot x}\right)\right]\\ &\quad\times\exp\left[-2i\left(\beta_p-\beta_{p'}\right)k\cdot x\right]\\ &= \sum_{n\in\mathbb{Z}}J_n^{(2)}\left(\alpha_p-\alpha_{p'},\rho\left(\beta_p-\beta_{p'}\right);e^{i\delta}\right)e^{-ink\cdot x-2i\left(\beta_p-\beta_{p'}\right)k\cdot x}\,.\end{aligned} \tag{8.13}$$

[‡]For a complex 4-vector ϵ, it is unclear how the complex conjugate $\not{\epsilon}^*$ would be defined, as it can depend on the chosen representation of the γ-matrices. We use $\bar{\not{\epsilon}} = \gamma^0\not{\epsilon}^\dagger\gamma^0 = \epsilon^*\cdot\gamma^0\gamma^\dagger\gamma^0 = \epsilon^*\cdot\gamma$ as the well defined version.

The S-matrix for the transition from p to p' by absorbing two photons from A_1 and emitting one into A_2 is then given by

$$\begin{aligned}\mathcal{S} \approx & \frac{ie}{\hbar c V}\int d^4x \\ & \times \bar{u}_{p',s'}\left(\not{A}_2^{(+)}\tilde{J}_2 e^{i\left(\frac{p'}{\hbar}-\frac{p}{\hbar}-2k\right)\cdot x} - \frac{e}{2c}\left[\frac{\not{A}_1^{(-)}\not{k}\not{A}_2^{(+)}}{k\cdot p'}+\frac{\not{A}_2^{(+)}\not{k}\not{A}_1^{(-)}}{k\cdot p}\right]\tilde{J}_1 e^{i\left(\frac{p'}{\hbar}-\frac{p}{\hbar}-k\right)\cdot x}\right)u_{p,s} \\ \approx & \frac{ie}{\hbar}T\bar{u}_{p',s'}\left(\frac{1}{2}a_2\tilde{J}_2\bar{\not{\epsilon}}_2 - \frac{ea_1a_2}{8c}\tilde{J}_1\left(\frac{\not{\epsilon}_1\not{k}\bar{\not{\epsilon}}_2}{k\cdot p'}+\frac{\bar{\not{\epsilon}}_2\not{k}\not{\epsilon}_1}{k\cdot p}\right)\right)u_{p,s}\,.\end{aligned} \tag{8.14}$$

Here $\not{A}_1^{(-)} = \frac{1}{2}a_1\not{\epsilon}_1 e^{-ik\cdot x}$ is the component that describes absorption of one photon from A_1, and $\not{A}_2^{(+)} = \frac{1}{2}a_2\bar{\not{\epsilon}}_2 e^{ik'\cdot x}$ is the component that describes emission of one photon into A_2, respectively. Also $\tilde{J}_{1,2}$ were introduced for the generalized Bessel functions including their corresponding arguments. It is worth noting, that this calculation describes a resonant scattering process, where the initial and final state are discrete and not part of a continuum. Therefore, the d^4x-integration does result in the factor cVT instead of the usual energy-momentum conserving Dirac delta-functions. The arguments of the latter vanish in our case automatically due to the fulfilled Bragg condition.

To be specific, we set the initial electron momentum to $p = (p^0, p_x, 0, -2\hbar k)$, while the scattered one reads $p' = (p^0, p_x, 0, 2\hbar k)$ where $p^0 = \sqrt{m^2c^2 + p_x^2 + 4\hbar^2k^2} \approx mc$. The Dirac bispinors for these momenta are constructed from the corresponding Pauli spinors χ_s by [BD64]

$$u_{p,s} = \frac{\not{p}+mc}{\sqrt{2mc\,(p^0+mc)}}\begin{pmatrix}\chi_s\\0\end{pmatrix} = \frac{1}{\sqrt{2mc\,(p^0+mc)}}\begin{pmatrix}\left(p^0+mc\right)\chi_s\\ \vec{p}\cdot\vec{\sigma}\chi_s\end{pmatrix}. \tag{8.15}$$

Please note that, when reading s, s' as indices of a new 2-by-2 matrix, the sigma matrices are reproduced by their matrix elements in

$$\left(\chi^\dagger_{s'}\vec{\sigma}\chi_s\right)_{s',s} = \vec{\sigma}\,. \tag{8.16}$$

With this in mind, we can calculate the parts of (8.14) as

$$\begin{aligned}\left(\bar{u}_{p',s'}\bar{\not{\epsilon}}_2 u_{p,s}\right)_{s',s} &= -\frac{1}{2mc\,(p^0+mc)}\left(\left(p^0+mc\right),\quad -\vec{p}'\cdot\vec{\sigma}\right)\vec{\epsilon}_2^{\,*}\cdot\vec{\gamma}\begin{pmatrix}\left(p^0+mc\right)\\ \vec{p}\cdot\vec{\sigma}\end{pmatrix} \\ &= -\frac{1}{2mc}\left(\vec{p}'\cdot\vec{\sigma}\vec{\epsilon}_2^{\,*}\cdot\vec{\sigma}+\vec{\epsilon}_2^{\,*}\cdot\vec{\sigma}\vec{p}\cdot\vec{\sigma}\right) \\ &= -\vec{\epsilon}_2^{\,*}\cdot\frac{\vec{p}+\vec{p}'}{2mc} - i\left(\vec{\epsilon}_2^{\,*}\times\frac{\vec{p}-\vec{p}'}{2mc}\right)\cdot\vec{\sigma} \\ &= -\frac{p_x}{mc}\vec{\epsilon}_2^{\,*}\cdot\vec{e}_x + i\frac{2\hbar\omega}{mc^2}\left(\vec{\epsilon}_2^{\,*}\times\vec{e}_z\right)\cdot\vec{\sigma}\,.\end{aligned} \tag{8.17}$$

And in a similar way

$$\left(\bar{u}_{p',s'}\left(\frac{\not{\epsilon}_1\not{k}\bar{\not{\epsilon}}_2}{k\cdot p'}+\frac{\bar{\not{\epsilon}}_2\not{k}\not{\epsilon}_1}{k\cdot p}\right)u_{p,s}\right)_{s',s}\approx\frac{2\vec{\epsilon}_1\cdot\vec{\epsilon}_2^*}{mc}+\frac{4i\hbar\omega}{m^2c^3}\left(\vec{\epsilon}_1\times\vec{\epsilon}_2^*\right)\cdot\vec{\sigma}\,. \tag{8.18}$$

From the Taylor series of the generalized Bessel functions, we can estimate

$$\begin{aligned}\tilde{J}_1=J_1^{(2)}\left(\alpha_p-\alpha_{p'},\rho\left(\beta_p-\beta_{p'}\right);e^{i\delta}\right)&\approx\frac{\alpha_p-\alpha_{p'}}{2}\\&\approx-2\frac{ea_1}{mc^2}\frac{p_x}{mc}\vec{\epsilon}_1\cdot\vec{e}_x\,,\end{aligned} \tag{8.19}$$

$$\begin{aligned}\tilde{J}_2=J_2^{(2)}\left(\alpha_p-\alpha_{p'},\rho\left(\beta_p-\beta_{p'}\right);e^{i\delta}\right)&\approx\frac{\left(\alpha_p-\alpha_{p'}\right)^2}{8}+{\vec{\epsilon}_1}^2\frac{\beta_p-\beta_{p'}}{2}\\&\approx\frac{e^2a_1^2}{m^2c^4}\left(2\frac{p_x^2}{m^2c^2}\left(\vec{\epsilon}_1\cdot\vec{e}_x\right)^2-\frac{1}{4}{\vec{\epsilon}_1}^2\right)\,.\end{aligned} \tag{8.20}$$

Putting all this together, we see that the leading order in m^{-1} of the S-matrix for small transverse momentum is

$$\begin{aligned}\mathcal{S}\approx&\frac{i}{2}T\frac{e^3a_1^2a_2}{m^3c^6}\left[\frac{1}{4\hbar}p_xc\,{\vec{\epsilon}_1}^2\vec{\epsilon}_2^*\cdot\vec{e}_x+\frac{1}{\hbar}p_xc\,\vec{\epsilon}_1\cdot\vec{e}_x\vec{\epsilon}_1\cdot\vec{\epsilon}_2^*-\frac{i}{2}\omega{\vec{\epsilon}_1}^2\left(\vec{\epsilon}_2^*\times\vec{e}_z\right)\cdot\vec{\sigma}\right]\\=&\frac{i}{2}T\xi_1^2\xi_2\hat{\Omega}\,.\end{aligned} \tag{8.21}$$

As before, the abbreviations $\xi_{1,2}:=\frac{ea_{1,2}}{mc^2}$ are the usual dimensionless field amplitudes used in atom physics. Some of the polarization dependent terms, as well as the whole polarization dependent part $\hat{\Omega}$ (the square bracket in (8.21)) of the S matrix, are summarized in table 8.1.

First of all, we can see in the first row, that the result from (6.16) for both beams linearly polarized is nicely reproduced within this formalism. The Rabi frequency $\Omega'_R=\frac{1}{2}\xi_1^2\xi_2\omega$, as well as the fact that the interaction involves σ_y can be seen in its last column. Additionally we have included the interaction via $\vec{p}\cdot\vec{A}$ in this derivation. Its relative scattering probability is $\frac{P_{\mathrm{no-flip}}}{P_{\mathrm{flip}}}=\frac{5p_xc}{2\hbar\omega}$. The consequences of the competition introduced by this extra interaction channel is analogous to what will be argued in Sec. 8.3. When discussing the other polarization configurations in the following, we assume, that we can decode these characteristics in the same way.

8.2 Circular Setup

As mentioned before, the first idea of a spin-dependent Kapitza-Dirac effect in a two-color setup was with circularly polarized light beams in mind [FB03]. As we can already read off from Tab. 8.1 in the row labelled *"circ. circ."*, the spin-induced part of the Rabi frequency for this effect vanishes to the order $o\left(m^{-3}\right)$. This is mainly because $\vec{\epsilon}_1^{\,2}=0$, hindering the virtual absorption of two $\vec{A}_1$-photons via $\vec{\sigma}\cdot\vec{B}$.

$\vec{A}_1$	$\vec{A}_2$	$\vec{\epsilon}_1$	$\vec{\epsilon}_2$	$\vec{\epsilon}_1 \cdot \vec{e}_x$	$\vec{\epsilon}_2^* \cdot \vec{e}_x$	$\vec{\epsilon}_1{}^2$
lin.	lin.	$\vec{e}_x$	$\vec{e}_x$	1	1	1
circ.	lin.	$\frac{1}{\sqrt{2}}(\vec{e}_x + i\vec{e}_y)$	$\vec{e}_x$	$\frac{1}{\sqrt{2}}$	1	0
circ.	circ.	$\frac{1}{\sqrt{2}}(\vec{e}_x + i\vec{e}_y)$	$\frac{1}{\sqrt{2}}(\vec{e}_x + i\vec{e}_y)$	$\frac{1}{\sqrt{2}}$	$\frac{1}{\sqrt{2}}$	0
circ.	rcirc.	$\frac{1}{\sqrt{2}}(\vec{e}_x + i\vec{e}_y)$	$\frac{1}{\sqrt{2}}(\vec{e}_x - i\vec{e}_y)$	$\frac{1}{\sqrt{2}}$	$\frac{1}{\sqrt{2}}$	0
lin.	circ.	$\vec{e}_x$	$\frac{1}{\sqrt{2}}(\vec{e}_x + i\vec{e}_y)$	1	$\frac{1}{\sqrt{2}}$	1
ell.	circ.	$\frac{1}{\sqrt{26}}(\vec{e}_x + 5i\vec{e}_y)$	$\frac{1}{\sqrt{2}}(\vec{e}_x + i\vec{e}_y)$	$\frac{1}{\sqrt{26}}$	$\frac{1}{\sqrt{2}}$	$-\frac{12}{13}$

$\vec{A}_1$	$\vec{A}_2$	$\vec{\epsilon}_1 \cdot \vec{\epsilon}_2^*$	$\vec{\epsilon}_2^* \times \vec{e}_z$	$\hat{\Omega}$
lin.	lin.	1	$-\vec{e}_y$	$\frac{5}{4\hbar}p_x c + \frac{i}{2}\omega\sigma_y$
circ.	lin.	$\frac{1}{\sqrt{2}}$	$-\vec{e}_y$	$\frac{1}{2\hbar}p_x c$
circ.	circ.	1	$\frac{1}{\sqrt{2}}(-\vec{e}_y - i\vec{e}_x)$	$\frac{1}{\sqrt{2}\hbar}p_x c$
circ.	rcirc.	0	$\frac{1}{\sqrt{2}}(-\vec{e}_y + i\vec{e}_x)$	0
lin.	circ.	$\frac{1}{\sqrt{2}}$	$\frac{1}{\sqrt{2}}(-\vec{e}_y - i\vec{e}_x)$	$\frac{5}{4\sqrt{2}\hbar}p_x c - \frac{\omega}{2\sqrt{2}}\sigma_-$
ell.	circ.	$\frac{3}{\sqrt{13}}$	$\frac{1}{\sqrt{2}}(-\vec{e}_y - i\vec{e}_x)$	$\frac{6}{13\sqrt{2}}\omega\sigma_-$

Table 8.1: Special terms in the S-matrix (8.21) and their values on polarization corner cases. The definition $\sigma_\pm := \sigma_x \pm i\sigma_y$ was introduced. The polarization of the counter-propagating laser waves are denoted by the abbreviations *"lin."* for linear in x-direction, *"circ."* for circular, *"rcirc."* also for circular but counterrotating, and *"ell."* for a special choice of elliptic polarization.

This result was numerically confirmed in the perturbative regime. But our numerical simulations also show, that in the region just above the dyke (see Chap. 6), some effect can still be found. The scattering that takes place, does not only flip the spin of the electron, but it is also highly sensitive to its initial spin state. An example is given in Fig. 8.1. As before in Fig. 6.2 and in the following simulations based on the Dirac equation, the spinors used in the initial condition as well as for the projection of the final state, are taken from (8.15) with $s = 0, 1$ denoting the spin state as $|\uparrow\rangle$ or $|\downarrow\rangle$, respectively. The electrons are only scattered, when initially in state $|\downarrow\rangle$. The effective scattering term must therefore be proportional to σ_+. The measured Rabi frequencies do not follow the proportionality of Eq. (6.16). We therefore believe, that the scattering is driven highly non-linear, and that, due to immense detuning, the number of involved photons cannot be discriminated easily as before.

8.3 Hybrid Setup

To improve on the result of the last section, we like to focus on another polarization setup, in which one of the beams is linearly polarized and the other one circularly. Tab. 8.1 predicts in the line *"circ. lin."*, that the setup where the small frequency is circularly and the high frequency laser linearly polarized can only scatter the electron via the spin independent and spin preserving term $\hat{\Omega} = \frac{1}{2\hbar}p_x c$.

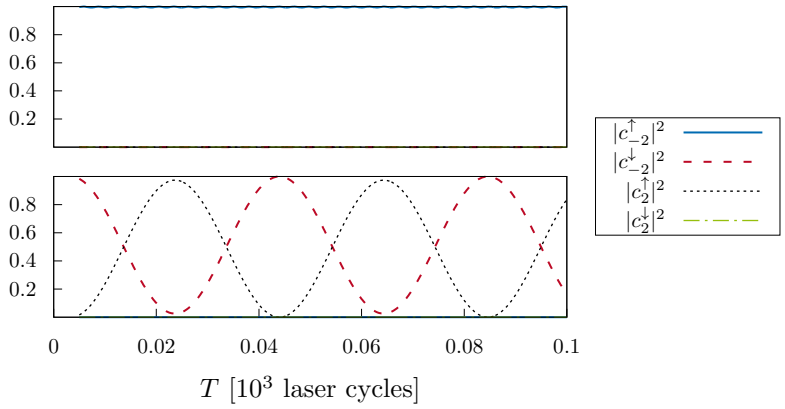

Figure 8.1: Rabi oscillations in nonlinear regime of the Kapitza-Dirac scattering from circular bichromatic counterpropagating but corotating waves. The laser parameters are $\hbar\omega_1 = 2 \times 10^3$ eV, $\omega_2 = 2\omega_1$ and $ea_1 = ea_2 = 8 \times 10^4$eV. The combined intensity of $I = 4.36 \times 10^{23}\ \frac{\mathrm{W}}{\mathrm{cm}^2}$ is much higher than in Fig. 6.2. The switching on and off takes place over 5 laser cycles each. The initial electron momentum is $-2\hbar k_1$ along the laser propagation direction and has no component within the polarization plane. The figure is organized in the same layout as Fig. 6.2 for comparability. An almost fully developed Rabi oscillation with spin flipping can be seen, if the initial state was spin down. For a spin-up electron, no scattering takes place at all, rendering the process spin-dependent.

On the other hand (see line *"lin. circ."*), by choosing the high frequency laser to be the circular one, we have $\hat{\Omega} = \frac{5}{4\sqrt{2}\hbar} p_x c - \frac{\omega}{2\sqrt{2}}\sigma_-$. Three possible interactions[§] between the four quantum states, that share the same energy and thereby fulfill the Bragg condition, emerge from that matrix. They are sketched in Fig. 8.2.

It seems natural to first look at the case, where the $\vec{p}\cdot\vec{A}$-term is suppressed. But we note, that this is only possible if the electron momentum is entirely on axis with the lasers ($p_x = p_y = 0$). In this special case, we are left with the single spin-dependent and spin-flipping Rabi matrix $\hat{\Omega} = -\frac{\omega}{2\sqrt{2}}\sigma_-$. We expect a clear Rabi oscillation that may have a reduced oscillation amplitude as is presented in Fig. 8.3.

While this result looks similar to what was achieved in Chap. 7 with linearly polarized light only, here, the spin of the scattered electron is flipped. This might be suitable for a source of polarized electrons, and for a spin detector, but it does not resemble the spin polarizing beam splitter as a Stern-Gerlach device for electrons.

In experiment, it might be impossible or impractical to inject the electron parallel to the beam axis. In that case, the influence of $\vec{p}\cdot\vec{A}$ cannot be ignored and all four energetically allowed states take part in the interaction, which becomes very complicated. The numerically found behaviour under these circumstances is shown in Fig. 8.4.

Still the simulation supports our interpretation in Fig. 8.2 quite nicely. Looking at

[§]These interactions are drawn with bilateral arrows, because the effective Hamiltonian describing them is necessarily Hermitian. This can be seen as a quantum version of actio = reactio.

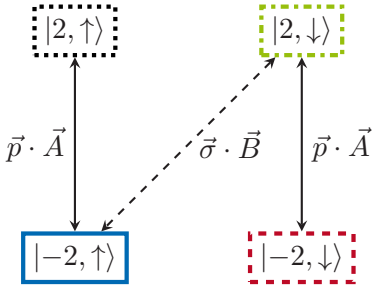

Figure 8.2: Sketch of $\hat{\Omega}$ for the linear – circular hybrid setup. The four involved states are shown, as well as the possible interactions between them. The colors and patterns of the boxes resemble the line-styles used by the plots in this chapter.

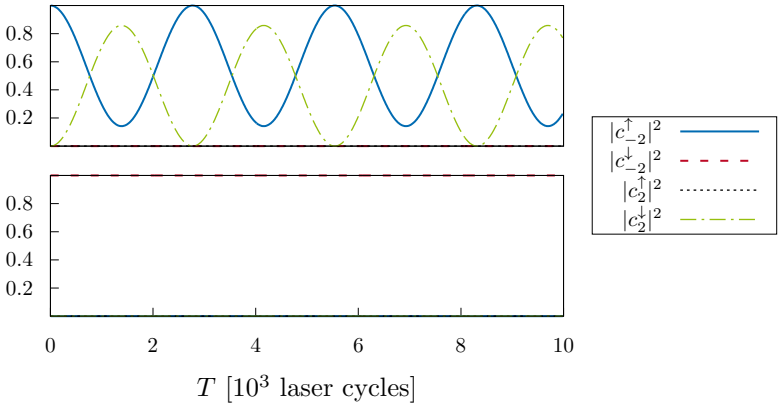

Figure 8.3: Rabi oscillations in the hybrid polarization setup. The laser and incident electron parameters are chosen as in Fig. 6.2, only the polarization of $\vec{A}_2$ was changed to circular. A clear spin-dependent and spin-flipping Rabi oscillation emerges.

the very beginning of the interactions, we see that, starting from $|-2,\uparrow\rangle$ (solid blue) in the upper panel, the electron state can transition directly to $|2,\uparrow\rangle$ (dotted black) or to $|2,\downarrow\rangle$ (dash dotted green). The dashed red line ($|-2,\downarrow\rangle$) enters the picture only after a significant amount of probability has been transferred to $|2,\downarrow\rangle$. Contrasting to that, the probability starting from $|-2,\downarrow\rangle$ needs to travel through both other states to reach $|2,\uparrow\rangle$. This is exactly reproduced by the order in which the lines acquire significance in the lower panel of the plot. A very similar competition of interacting terms in Kapitza-Dirac scattering has been found for single-colored circular standing laser waves [EB15]. There, the spin-sensitive term is accompanied by the much stronger single-color Kapitza-Dirac effect. In such an experiment, it may be possible to find a combination of field strength and interaction time, in order to recover the electron in a spin-polarized beam [Ahr16]. But the interaction time would need to be rather long and the parameters very precise.

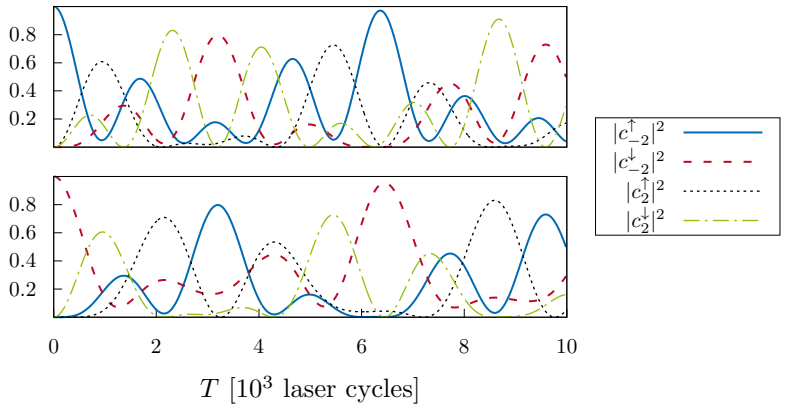

Figure 8.4: Dynamics of the occupation probabilities in the hybrid polarization setup. The influence of $\vec{A} \cdot \vec{p}$ has been introduced by choosing $p_x = \hbar k_1$ in contrast to the otherwise unchanged parameters from Fig. 8.3. Due to the increased number of involved quantum states, the Rabi oscillation is no longer recognizable.

For a spin filter, it seems desirable to suppress the term proportional to p_x without forcing the electron momentum to be on axis with the lasers. Equation (8.21) supports this for a very special elliptical polarization, independent of p_x as well as a_1 and a_2. According to the last line of table 8.1, if the polarization of the low energy photons is elliptical with an eccentricity of 5, the interaction term is proportional to $\hat{\Omega} = \frac{6\omega}{13\sqrt{2}}\sigma_-$. There is no spin-independent contribution then. Fig. 8.5 confirms this result, and we verified numerically, that the interaction in this field configuration is indeed independent of p_x, at least for $p_x < 30\hbar k$ with the parameters chosen in Fig. 8.5. We believe, that this is the most promising of the here proposed experimental setups to achieve short spin-polarized electron beams. This is owed to the independence of the transverse momentum, and the fact that, even for imperfect timing, the scattered portion of the beam is fully polarized.

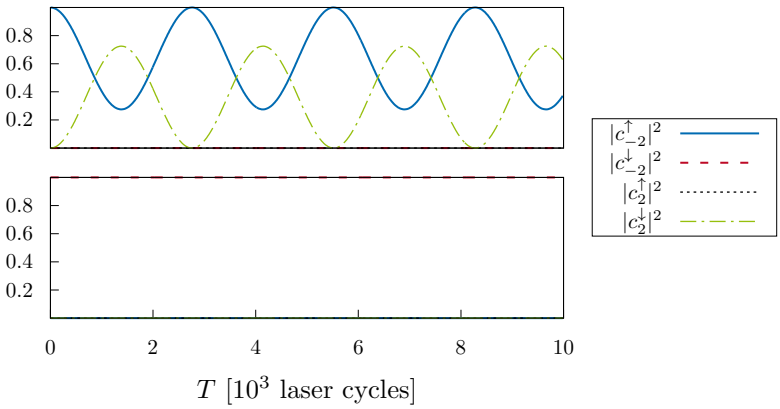

Figure 8.5: Rabi oscillations in elliptically tuned hybrid polarization setup. In contrast to Fig. 8.4 the polarization for $\vec{A}_1$ was changed to elliptic with eccentricity 5. All other laser and electron parameters remain unchanged. The spin-dependent and spin-flipping Rabi process of Fig. 8.3 is qualitatively reproduced.

Chapter 9

Conclusion

The principle ideas of the Kapitza-Dirac effect are based on the wave-particle duality that rocketed the development of quantum mechanics in the early days. It is not surprising, that it is a pure quantum effect, relying on the diffraction and interference of the electron wave after passing through a regular structure constituted by a standing light wave. In this thesis, we studied two further quantum aspects to the Kapitza-Dirac effect by developping two respective generalization schemes involving bichromatic light of commensurate frequencies. That way, two-pathway interference and the involvement of the electron spin were highlighted for non-relativistic parameters.

In the first part, two standing waves were postulated from which electrons were diffracted. Since the most pronounced impact is to be expected for small integer frequency ratios, we focussed on the fundamental frequency combined with its second harmonic, but we anticipate, that further generalization to other combinations of harmonics is straightforward. In the diffraction regime, where the number of accessible equidistant momentum states is (in principle) unlimited, we have shown, that the two standing waves can both enhance and hinder themselves in their coherent scattering effects. We have also shown, that the property of being symmetric will be transferred from the standing wave arrangement to the diffraction pattern. On the other hand, in the Bragg regime, where effectively only two momentum states are admissible by energy-momentum conservation, we saw quantum two-state dynamics, that is characterized as a Rabi-oscillation for both individual, as well as for the combined standing waves. Due to the strong ponderomotive potential in a standing wave, we concluded, that the oscillation in the bichromatic case is basically composed of the constituing monochromatic versions, because they are predominant compared to the impact of other conceivable photon combinations. Within this mindset, the lower frequency wave contributes with the four-photon Rabi frequency, scaling like $\sim \xi_1^4$, to the process, while the second harmonic adds the two-photon Rabi frequency with scaling $\sim \xi_2^2$. In combination, the resulting Rabi frequency shows distinct interference from maximal amplification to total extinction. The most strongly marked interference can be expected, when $\xi_1^2 \approx \xi_2$.

In the second part, we changed the original monochromatic standing-wave setup by doubling the frequency of one beam, resulting in bichromatic counterpropagating waves,

which we examined in the Bragg regime. By ruling out the aforementioned monochromatic effects from the ponderomotive potentials that way, three-photon processes can become dominant. Especially for the combined interaction of an electron with two low and one high frequency photons, we calculated the transition amplitude. On top of that, we extended the concept of the ponderomotive potential in a way suitable. We found, that the electron spin as well as the photon helicity play a crucial role here. This interaction has also been predicted to exist for other charged particles with spin, like i.e. protons. Its diffraction probability would be appropriately scaled due to the different mass-to-charge ratio and g-factor [DAM16]. Additionally the now dominant interactions can be separated in two categories. The first being, when one of the three photons contributes through the $\vec{p} \cdot \vec{A}$-term, throwing its orbital angular momentum in the ring. In [Smi+04] they are called 'two-color Kapitza-Dirac effects', and their transition amplitude scales with $\sim \frac{p_x}{mc}\xi_1^2\xi_2$. The other category consists of interactions, where one photon couples to the electron spin. In [McG+15] they are called 'spin Kapitza-Dirac effects' having a scaling $\sim \frac{\hbar\omega}{mc^2}\xi_1^2\xi_2$. The details of all these three-photon processes depend heavily on the polarization of both counterpropagating waves. This dependence is nicely condensed in (8.21), and was exemplified for several polarization combinations. A very special combination of elliptically polarized lower frequency with circularly polarized second harmonic, that is spin-dependent and simultaneously robust to transverse momentum, could be identified therein. It can possibly lead to future sources of briliant and short spin-polarized electron beams. These processes discussed in part II have another property in common. Due to the asymmetry with respect to the propagation direction, the electron experiences different dressing effects from both lasers in its two momentum states satisfying the Bragg condition. A relative shift in the kinetic energies emerges. This field-induced detuning leads to reduced Rabi amplitudes and accordingly increased oscillation frequencies. The actual amount of detuning was characterized to be dependent on the laser frequencies and amplitudes, forming a dyke-like structure.

Combining Bragg scattering processes of the second and the first part of this thesis, a three-stage spin sensitive interferometer for free electrons was demonstrated. We showed that, with suitable fine tuning, it acts as a spin-polarizing beam splitter. Since it does not change the spin of already polarized electron beams, it resembles in effect a Stern-Gerlach device for electrons. That way, it is not only a proposal for a scheme to create spin-polarized electrons, but also gives a positive theoretical answer to the longstanding, yet recently lively discussed question of Bohr and Pauli, whether is was possible at all to spatially separate charged elementary particles by their spin.

In summary, we have shown that momentum and spin of free electrons can be coherently controlled in Kapitza-Dirac scattering by exploiting suitable combinations of bichromatic laser fields.

Appendix A

Adiabatic Switching

In this appendix we want to show, that the switching time as implemented by the function $f(t)$ throughout this thesis distinguishes three different regimes. Similar considerations have been made in [DM15b].

Investigation of the monochromatic ($\alpha^2 = 1$) Kapitza-Dirac effect with the methods of Sec. 6.1 allows us, to include a detuning p_z from the resonant momenta. The electron is now scattered from momentum $-\hbar k + p_z$ to $\hbar k + p_z$ by virtue of the vector potential

$$\vec{A}(t,z) = a_0 \vec{\epsilon} \cos(\omega t)\cos(kz) = \frac{a_0}{2}\vec{\epsilon}\cos(\omega t)\sum_n \left(|n\rangle\langle n-1| + |n\rangle\langle n+1|\right) . \tag{A.1}$$

For the Dyson-expansion to the first order we obtain

$$\begin{aligned}\langle 1|\, U_\mathrm{m}(T+\tau)\,|-1\rangle &= \frac{e^2 a_0^2}{8i\hbar m c^2}\int dt \exp\left(-\frac{i}{\hbar}E_1'(T+\tau-t)\right) f(t)^2\cos^2(\omega t)\exp\left(-\frac{i}{\hbar}E_{-1}' t\right) \\ &= \frac{e^2 a_0^2}{8i\hbar m c^2}\exp\left(-\frac{i}{\hbar}E_1'(T+\tau)\right)\int dt \exp\left(\frac{i}{\hbar}\delta t\right) f(t)^2\cos^2(\omega t)\end{aligned} \tag{A.2}$$

where the detuning amounts to $\delta := E_1' - E_{-1}' = \frac{2\hbar k p_z}{m}$ in energy.*

In order to obtain easy-to-interpret results, we introduce a very simple model of the switching function

$$f(t)^2 = \begin{cases} \frac{t}{\tau} & \text{if } 0 < t \le \tau \\ 1 & \text{if } \tau < t \le T \\ \frac{T+\tau-t}{\tau} & \text{if } T < t \le T+\tau \\ 0 & \text{elsewhere} \end{cases} . \tag{A.3}$$

It satisfies the relation $\int dt f(t)^2 = T$ for the effective interaction time used in the numerical simulations, independently of the adjustable switching time τ. An illustration of $f(t)^2$ is shown in Fig. A.1. This tool allows us to evaluate the transition amplitude

*In Sec. 6.4 other states and the existence of the field induced detuning Δ led to another expression for δ.

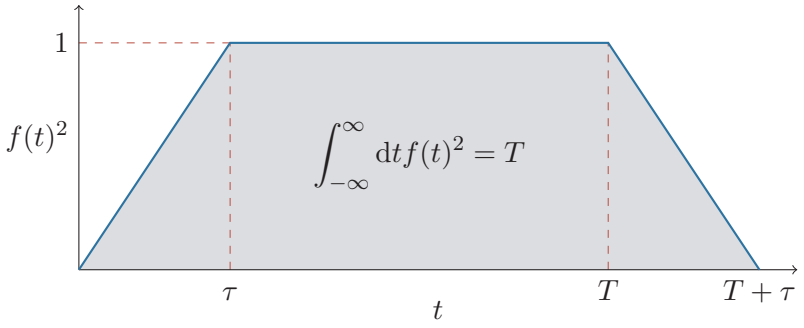

Figure A.1: Plot of the switching function used for the analytical considerations in this appendix. The area under the curve equals the effective interaction time T.

in equation (A.2) analytically with the absolute value

$$\begin{aligned} I &:= |\langle 1|\, U_{\mathrm{m}}(T+\tau)\, |-1\rangle| \\ &= \Bigg| -\frac{\hbar^2\Omega_R}{2\delta^2\tau}\left(1-e^{\frac{i}{\hbar}\delta T}\right)\left(1-e^{\frac{i}{\hbar}\delta\tau}\right) + \frac{\hbar^2\Omega_R}{2\left(4\hbar^2\omega^2+\delta^2\right)^2\tau}\times \\ &\quad \Big\{ \left[\left(4\hbar^2\omega^2+\delta^2\right)\cos(2\omega t) - 4i\hbar\omega\delta\sin(2\omega t)\right] \mathrm{e}^{\frac{i}{\hbar}\delta t}\Big|_{t=0}^{\tau} \\ &\quad - \left[\left(4\hbar^2\omega^2+\delta^2\right)\cos(2\omega t) - 4i\hbar\omega\delta\sin(2\omega t)\right] \mathrm{e}^{\frac{i}{\hbar}\delta t}\Big|_{t=T}^{T+\tau} \Big\} \Bigg| \end{aligned} \tag{A.4}$$

with the monochromatic Rabi frequency $\Omega_R = \frac{e^2 a_0^2}{8\hbar m c^2}$. The second term describes fast oscillations, that are suppressed by $\frac{1}{\tau}$. The first term, however, behaves differently for the resonant and the detuned case. In the resonant limit $\delta \to 0$, the first term reduces

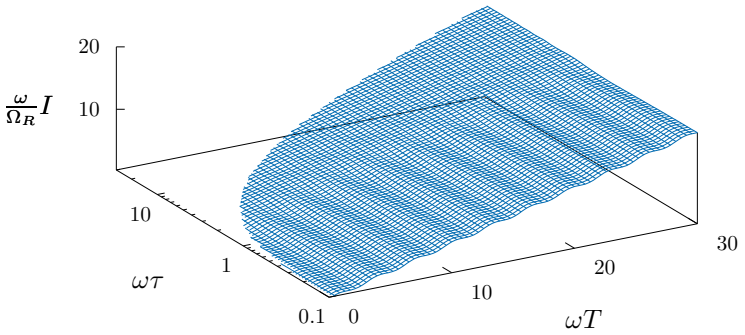

Figure A.2: Plot of the general appearance of (A.4) for the resonant case ($\delta = 0$). One can see bounded oscillating features on the right front edge, and the linearly growing term, that is independent of the switching time τ. Only points with $\tau \leq T$ are plotted.

to $\frac{\Omega_R}{2}T$ in accordance to the resonant Rabi oscillation in the monochromatic case. For

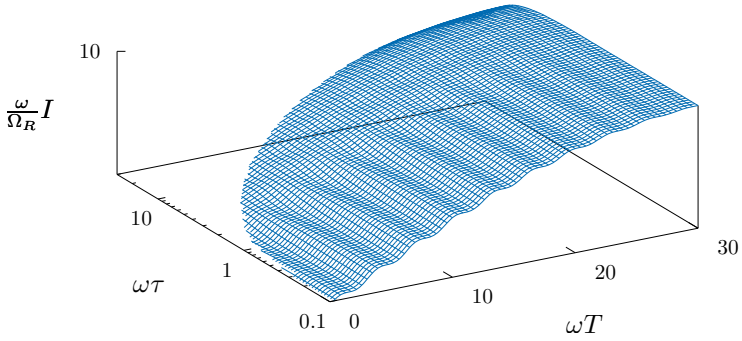

Figure A.3: The same plot as in Fig. A.2 for the detuned case with $\delta = 0.1\hbar\omega$. In contrast to there, one can see that the scattering probability is suppressed for adiabatic switching times (i.e. large τ).

$\delta \neq 0$, however, it is bounded by $\frac{2\hbar^2\Omega_R}{\delta^2\tau}$. That means, the resonance peak narrows down for longer switching time. For really adiabatic switching ($\tau \gtrsim \frac{1}{\Omega_R}$) the scattering can happen only for momenta fulfilling the Bragg condition exactly [Fed74].

In combination with the field induced detuning, the following picture arises from a parameter scan: For too short switching time ($\tau \lesssim \frac{6\pi}{\omega}$) the simulated vector potential abberates too much from a solution of the Maxwell equations, and the results are non-physical. For moderate switching times ($\frac{6\pi}{\omega} \lesssim \tau \lesssim \frac{1}{\Omega_R}$) we obtain the resonance peak from (6.33) and Fig. 6.4. Only when approaching the magnitude of the inverse Rabi frequency, the interaction becomes adiabatic. The resonance peak becomes sharper and its center moves to the exact Bragg condition ($\delta = 0$). However, the increased oscillation frequency remains unchanged.

We note that for laser fields with a Gaussian temporal profile, the 'effective switching time' is always of the order of the effective interaction time and therefore several Rabi cycles long (for the interactions of interest here).

Danksagung

Herrn Prof. Dr. Dr. Carsten Müller danke ich für die Überlassung des Themas und ganz besonders herzlich für seine stets ausgesprochen freundliche und hilfsbereite Unterstützung bei der Durchführung der Arbeit.

Für die freundliche Übernahme des Korreferates gilt mein persönlicher Dank Frau Prof Dr. Dagmar Bruß.

Allen Kollegen, die mich auf dem Weg begleitet haben, danke ich ganz herzlich, insbesondere Martin Jansen für die zahlreichen anregenden Diskussionen. Nicht zuletzt danke ich Eugen Bleile für die Unterstützung in technischen Fragen und Herrn Prof. Dr. Karl-Heinz Spatschek und Frau Elvira Gröters, die meine Arbeit von Anfang an begleitet haben.

Bibliography

[LCLS] https://lcls.slac.stanford.edu/.

[ASM94] C. S. Adams, M. Sigel, and J. Mlynek. "Atom optics". In: *Phys. Rep.* 240.3 (May 1994), p. 143.

[Ahr16] S. Ahrens. *Electron spin filter and polarizer in a standing light wave*. Apr. 21, 2016. arXiv: `1604.06201v3 [quant-ph]`. URL: `https://arxiv.org/abs/1604.06201`.

[Ahr+12] S. Ahrens et al. "Spin Dynamics in the Kapitza-Dirac Effect". In: *Phys. Rev. Lett.* 109.4 (July 2012), p. 043601.

[Ahr+13] S. Ahrens et al. "Kapitza-Dirac effect in the relativistic regime". In: *Phys. Rev. A* 88.1 (July 2013), p. 012115.

[AVM14] I. Akal, S. Villalba-Chávez, and C. Müller. "Electron-positron pair production in a bifrequent oscillating electric field". In: *Phys. Rev. D* 90.11 (Dec. 2014), p. 113004.

[AM13] S. Augustin and C. Müller. "Interference effects in Bethe-Heitler pair creation in a bichromatic laser field". In: *Phys. Rev. A* 88.2 (Aug. 2013), p. 022109.

[Aww16] H. M. Awwad. "Spin effects in Kapitza-Dirac scattering". B. Sc. thesis. Heinrich Heine University Düsseldorf, 2016.

[Ban+97] A. D. Bandrauk et al. "Enhanced harmonic generation in extended molecular systems by two-color excitation". In: *Phys. Rev. A* 56.4 (Oct. 1997), R2537.

[BGS97] H. Batelaan, T. J. Gay, and J. J. Schwendiman. "Stern-Gerlach Effect for Electron Beams". In: *Phys. Rev. Lett.* 79.23 (Dec. 1997), p. 4517.

[Bat07] H. Batelaan. "*Colloquium* : Illuminating the Kapitza-Dirac effect with electron matter optics". In: *Rev. Mod. Phys.* 79.3 (July 2007), p. 929.

[BLP96] V. B. Berestetskii, E. M. Lifshitz, and L. P. Pitaevskii. *Quantum Electrodynamics*. Elsevier Science & Technology, Aug. 5, 1996.

[BD64] J. D. Bjorken and S. D. Drell. *Relativistic quantum mechanics*. Mcgraw-Hill College, 1964.

[BDF12] M. Boca, V. Dinu, and V. Florescu. "Spin effects in nonlinear Compton scattering in a plane-wave laser pulse". In: *Nucl. Instrum. Methods Phys. Res., Sect. B* 279 (May 2012), p. 12.

[BSB88] P. H. Bucksbaum, D. W. Schumacher, and M. Bashkansky. "High-Intensity Kapitza-Dirac Effect". In: *Phys. Rev. Lett.* 61.10 (Sept. 1988), p. 1182.

[Cor+04] M. Cornacchia et al. "Future possibilities of the Linac Coherent Light Source". In: *Journal of Synchrotron Radiation* 11.3 (Apr. 2004), p. 227.

[Dat+91] G. Dattoli et al. "Theory of generalized bessel functions.-II". In: *Il Nuovo Cimento B* 106.1 (Jan. 1991), p. 21.

[DAM16] M. M. Dellweg, H. M. Awwad, and C. Müller. "Spin dynamics in Kapitza-Dirac scattering of electrons from bichromatic laser fields". In: *Phys. Rev. A* 94.2 (Aug. 2016), p. 022122.

[DM15a] M. M. Dellweg and C. Müller. "Kapitza-Dirac scattering of electrons from a bichromatic standing laser wave". In: *Phys. Rev. A* 91.6 (June 2015), p. 062102.

[DM15b] M. M. Dellweg and C. Müller. "Influence of laser pulse shape and spectral composition on strong-field Kapitza-Dirac scattering". In: *J. Phys.: Conf. Ser.* 594 (Mar. 2015), p. 012015.

[DM17a] M. M. Dellweg and C. Müller. "Controlling electron spin dynamics in bichromatic Kapitza-Dirac scattering by the laser field polarization". In: *Phys. Rev. A* 95 (Apr. 2017), p. 042124.

[DM17b] M. M. Dellweg and C. Müller. "Spin-Polarizing Interferometric Beam Splitter for Free Electrons". In: *Phys. Rev. Lett.* 118.7 (Feb. 2017), p. 070403.

[DP80] J. R. Dormand and P. J. Prince. "A family of embedded Runge-Kutta formulae". In: *J. Comput. Appl. Math.* 6.1 (Mar. 1980), p. 19.

[EF00] M. A. Efremov and M. V. Fedorov. "Wavepacket theory of the Kapitza-Dirac effect". In: *J. Phys. B: At., Mol. Opt. Phys.* 33.20 (Oct. 2000), p. 4535.

[EZE14] S. Eilzer, H. Zimmermann, and U. Eichmann. "Strong-Field Kapitza-Dirac Scattering of Neutral Atoms". In: *Phys. Rev. Lett.* 112.11 (Mar. 2014), p. 113001.

[EB15] R. Erhard and H. Bauke. "Spin effects in Kapitza-Dirac scattering at light with elliptical polarization". In: *Phys. Rev. A* 92.4 (Oct. 2015), p. 042123.

[FB04] F. H. M. Faisal and S. Bhattacharyya. "Spin Asymmetry in an Intense-Field Ionization Process". In: *Phys. Rev. Lett.* 93.5 (July 2004), p. 053002.

[Fed67] M. V. Fedorov. "The Kapitza-Dirac Effect in a Strong Radiation Field". In: *Sov. Phys. JETP* 25 (1967), p. 952.

[Fed74] M. V. Fedorov. "Stimulated scattering of electrons by photons and adiabatic switching on hypothesis". In: *Opt. Commun.* 12.2 (Oct. 1974), p. 205.

[Fed81] M. V. Fedorov. "Free-electron lasers and multiphoton free-free transitions". In: *Prog. Quantum Electron.* 7.2 (Jan. 1981), p. 73.

[FM80] M. V. Fedorov and J. K. McIver. "Multiphoton stimulated compton scattering". In: *Opt. Commun.* 32.1 (Jan. 1980), p. 179.

[FW50] L. L. Foldy and S. A. Wouthuysen. "On the Dirac Theory of Spin 1/2 Particles and Its Non-Relativistic Limit". In: *Phys. Rev.* 78.1 (1950), p. 29.

[FAB01] D. L. Freimund, K. Aflatooni, and H. Batelaan. "Observation of the Kapitza–Dirac effect". In: *Nature* 413.6852 (Sept. 2001), p. 142.

[FB02] D. L. Freimund and H. Batelaan. "Bragg Scattering of Free Electrons Using the Kapitza-Dirac Effect". In: *Phys. Rev. Lett.* 89.28 (Dec. 2002), p. 283602.

[FB03] D. L. Freimund and H. Batelaan. "A Microscopic Stern-Gerlach Magnet for Electrons?" In: *Laser Phys.* 13.6 (2003), p. 892.

[Fre+99] M. Freyberger et al. "Atom Optics in Quantized Light Fields". In: *Advances In Atomic, Molecular, and Optical Physics*. Elsevier BV, 1999, p. 143.

[GS22] W. Gerlach and O. Stern. "Das magnetische Moment des Silberatoms". In: *Zeitschrift für Physik* 9.1 (Dec. 1922), p. 353.

[GRP86] P. L. Gould, G. A. Ruff, and D. E. Pritchard. "Diffraction of atoms by light: The near-resonant Kapitza-Dirac effect". In: *Phys. Rev. Lett.* 56.8 (Feb. 1986), p. 827.

[HA75] V. M. Haroutunian and H. K. Avetissian. "An analogue of the Kapitza-Dirac effect". In: *Phys. Lett. A* 51.6 (Apr. 1975), p. 320.

[IKS04] D. Y. Ivanov, G. L. Kotkin, and V. G. Serbo. "Complete description of polarization effects in emission of a photon by an electron in the field of a strong laser wave". In: *The European Physical Journal C* 36.1 (July 2004), p. 127.

[IKS05] D. Y. Ivanov, G. L. Kotkin, and V. G. Serbo. "Complete description of polarization effects in e+ e- pair production by a photon in the field of a strong laser wave". In: *The European Physical Journal C* 40.1 (Mar. 2005), p. 27.

[JM13] M. J. A. Jansen and C. Müller. "Strongly enhanced pair production in combined high- and low-frequency laser fields". In: *Phys. Rev. A* 88.5 (Nov. 2013), p. 052125.

[Jar+05] A. Jarre et al. "Two-Dimensional Hard X-Ray Beam Compression by Combined Focusing and Waveguide Optics". In: *Phys. Rev. Lett.* 94.7 (Feb. 2005), p. 074801.

[KJE95] J. Z. Kamiński, A. Jaroń, and F. Ehlotzky. "Filtering resonance processes by bichromatic laser fields". In: *J. Phys. B: At., Mol. Opt. Phys.* 28.22 (Nov. 1995), p. 4895.

[KD33] P. L. Kapitza and P. A. M. Dirac. "The reflection of electrons from standing light waves". In: *Math. Proc. Cambridge Philos. Soc.* 29.02 (May 1933), p. 297.

[Kar+12] E. Karimi et al. "Spin-to-Orbital Angular Momentum Conversion and Spin-Polarization Filtering in Electron Beams". In: *Phys. Rev. Lett.* 108.4 (Jan. 2012), p. 044801.

[Kim+05] I. J. Kim et al. "Highly Efficient High-Harmonic Generation in an Orthogonally Polarized Two-Color Laser Field". In: *Phys. Rev. Lett.* 94.24 (June 2005), p. 243901.

[Kla+14] M. Klaiber et al. "Spin dynamics in relativistic ionization with highly charged ions in super-strong laser fields". In: *J. Phys. B: At., Mol. Opt. Phys.* 47.6 (Mar. 2014), p. 065603.

[KK12] K. Krajewska and J. Z. Kamiński. "Phase effects in laser-induced electron-positron pair creation". In: *Phys. Rev. A* 85.4 (Apr. 2012), p. 043404.

[KK13] K. Krajewska and J. Z. Kamiński. "Spin effects in nonlinear Compton scattering in ultrashort linearly-polarized laser pulses". In: *Laser Part. Beams* 31.03 (July 2013), p. 503.

[Mag54] W. Magnus. "On the exponential solution of differential equations for a linear operator". In: *Comm. Pure Appl. Math.* 7.4 (Nov. 1954), p. 649.

[Mar+88] P. Martin et al. "Bragg scattering of atoms from a standing light wave". In: *Phys. Rev. Lett.* 60.6 (Feb. 1988), p. 515.

[Mar13] K.-P. Marzlin. "Ramsey-Bordé interferometer for electrons". In: *Phys. Rev. A* 88.4 (Oct. 2013), p. 043621.

[Mau+06] J. Mauritsson et al. "Attosecond Pulse Trains Generated Using Two Color Laser Fields". In: *Phys. Rev. Lett.* 97.1 (July 2006), p. 013001.

[MBB11] S. McGregor, R. Bach, and H. Batelaan. "Transverse quantum Stern–Gerlach magnets for electrons". In: *New J. Phys.* 13.6 (June 2011), p. 065018.

[McG+15] S. McGregor et al. "Spin-dependent two-color Kapitza-Dirac effects". In: *Phys. Rev. A* 92.2 (Aug. 2015), p. 023834.

[MBK00] D. B. Milošević, W. Becker, and R. Kopold. "Generation of circularly polarized high-order harmonics by two-color coplanar field mixing". In: *Phys. Rev. A* 61.6 (May 2000), p. 063403.

[MEP97] D. B. Milošević, F. Ehlotzky, and B. Piraux. "Inelastic electron - atom collisions in a bichromatic laser field". In: *J. Phys. B: At., Mol. Opt. Phys.* 30.19 (Oct. 1997), p. 4347.

[Mor+99] C. F. de Morisson Faria et al. "Time-frequency analysis of two-color high-harmonic generation". In: *Phys. Rev. A* 60.2 (Aug. 1999), p. 1377.

[MM65] N. F. Mott and S. H. S. W. Massey. *The Theory of Atomic Collisions*. (3rd ed). Clarendon, Oxford, 1965.

[NF00] N. B. Narozhny and M. S. Fofanov. "Quantum processes in a two-mode laser field". In: *J. Exp. Theor. Phys.* 90.3 (Mar. 2000), p. 415.

[PBW95] G. G. Paulus, W. Becker, and H. Walther. "Classical rescattering effects in two-color above-threshold ionization". In: *Phys. Rev. A* 52.5 (Nov. 1995), p. 4043.

[Rei80] H. R. Reiss. "Effect of an intense electromagnetic field on a weakly bound system". In: *Phys. Rev. A* 2.5 (Nov. 1980), p. 1786.

[Ros04] L. Rosenberg. "Extended theory of Kapitza-Dirac scattering". In: *Phys. Rev. A* 70.2 (Aug. 2004), p. 023401.

[RG98a] G. H. Rutherford and R. Grobe. "Spin dynamics of electrons in a unidirectional, inhomogeneous magnetic field". In: *J. Phys. A: Math. Gen.* 31.46 (Nov. 1998), p. 9331.

[RG98b] G. H. Rutherford and R. Grobe. "Comment on "Stern-Gerlach Effect for Electron Beams"". In: *Phys. Rev. Lett.* 81.21 (Nov. 1998), p. 4772.

[SK92] K. J. Schafer and K. C. Kulander. "Phase-dependent effects in multiphoton ionization induced by a laser field and its second harmonic". In: *Phys. Rev. A* 45.11 (June 1992), p. 8026.

[Sch+15] V. Schkolnik et al. "The effect of wavefront aberrations in atom interferometry". In: *Appl. Phys. B* 120.2 (June 2015), p. 311.

[SL05] C. G. Schroer and B. Lengeler. "Focusing Hard X Rays to Nanometer Dimensions by Adiabatically Focusing Lenses". In: *Phys. Rev. Lett.* 94.5 (Feb. 2005), p. 054802.

[Sch+94] D. W. Schumacher et al. "Phase Dependence of Intense Field Ionization: A Study Using Two Colors". In: *Phys. Rev. Lett.* 73.10 (Sept. 1994), p. 1344.

[SZ97] M. O. Scully and M. S. Zubairy. *Quantum Optics*. Cambridge University Press, Sept. 4, 1997.

[SB00] M. Shapiro and P. Brumer. "Coherent Control of Atomic, Molecular, and Electronic Processes". In: *Advances In Atomic, Molecular, and Optical Physics*. Elsevier BV, 2000, p. 287.

[Smi+04] O. Smirnova et al. "Kapitza-Dirac Diffraction without Standing Waves: Diffraction without a Grating?" In: *Phys. Rev. Lett.* 92.22 (June 2004), p. 223601.

[Spe+11] P. Sperling et al. "Two-color Thomson scattering at FLASH". In: *High Energy Density Phys.* 7.3 (Sept. 2011), p. 145.

[STM98] C. Szymanowski, R. Taïeb, and A. Maquet. "Laser-Assisted Scattering of Polarized Electrons at High Field Intensities". In: *Laser Phys.* 8.1 (1998), p. 102.

[TPW12] W. X. Tang, D. M. Paganin, and W. Wan. "Proposal for electron quantum spin Talbot effect". In: *Phys. Rev. B* 85.6 (Feb. 2012), p. 064418.

[TWC95] D. A. Telnov, J. Wang, and S.-I. Chu. “Two-color phase control of high-order harmonic generation in intense laser fields”. In: *Phys. Rev. A* 52.5 (Nov. 1995), p. 3988.

[VE93] S. Varrò and F. Ehlotzky. “Free-free transitions in a bichromatic laser field”. In: *Phys. Rev. A* 47.1 (Jan. 1993), p. 715.

[VTM95] V. Véniard, R. Taïeb, and A. Maquet. “Two-Color Multiphoton Ionization of Atoms Using High-Order Harmonic Radiation”. In: *Phys. Rev. Lett.* 74.21 (May 1995), p. 4161.

[VC15] P. Vidil and B. Chalopin. “Controllable blazed grating for electrons using Kapitza-Dirac diffraction with multiple-harmonic standing waves”. In: *Phys. Rev. A* 92.6 (Dec. 2015), p. 062117.

[WK01] M. W. Walser and C. H. Keitel. “Narrow high-frequency spectral features via laser-induced slow spin flips”. In: *Opt. Commun.* 199.5-6 (Dec. 2001), p. 447.

[WBK15] A. Wöllert, H. Bauke, and C. H. Keitel. “Spin polarized electron-positron pair production via elliptical polarized laser fields”. In: *Physical Review D* 91.12 (June 2015), p. 125026.

[Yin+92] Y.-Y. Yin et al. “Asymmetric photoelectron angular distributions from interfering photoionization processes”. In: *Phys. Rev. Lett.* 69.16 (Oct. 1992), p. 2353.